SOLID STATE INTERACTION BETWEEN THIN METAL FILMS AND SiO_2 SUBSTRATES.

By

QINISILE Y. HLATSHWAYO

Dissertation presented in partial fulfilment of the requirements for the degree of

MASTER OF SCIENCE

to the

DEPARTMENT OF PHYSICS
UNIVERSITY OF ZULULAND

Promoter: Prof. R. Pretorius
Department of Physics, University of Stellenbosch

Co-promoter: Prof. O. M. Ndwandwe
Department of Physics, University of Zululand

FEBRUARY 2000

ACKNOWLEDGEMENTS

My heartfelt gratitude goes to all who supported me be it spiritually, materially or physically over the period that I tussled with this dissertation project. Special mention goes to the following individuals without whom this work would never have seen the light of day:

- Prof. R. Pretorius who supervised this work. Your vast experience and depth of knowledge in the domain of thin film analysis does not hamper your ability to introduce the uninitiated into what would otherwise be a daunting field.
- Prof. O.M. Ndwandwe who as co-supervisor set the ball rolling and facilitated this exercise to which he devoted his quality time that he would otherwise have spent with his family. You slogged with me by day and night as you took me through the paces in the solid state lab cutting, cleaning, conditioning, depositing etc. not forgetting the time we spent in the control room nor the numerous visits we paid to the Geology departments of Cape Town and Stellenbosch University to gather XRD data on our samples. As if this was not enough, you also guided me through the ultimate process of documenting all the data and information we had gathered. As words fail me, I can only say–ZWIDE!
- Dr. V. Prozesky the incumbent head of the MRG for availing the facilities and providing for our comfort at all times.
- The NRF board for the financial and material support availed. Your involvement will forever remain pivotal in the advancement of the scientific and technological development of this country.
- The technical team as comprised of:
    1. Karl who always reminded me of the wise men from the east, a technician par excellence. Your patience and willingness to help with such tasks as beam focussing, setting up of the electronics, collecting and collating of data, troubleshooting; truly a seasoned campaigner.
    2. Niel and Collin, always at hand whenever things seemed to go haywire with computers, printers, the photocopier and any related support systems.
    3. Lawrence, softspoken but endowed with such versatility and craftsmanship. You simply named it and he would contrive and construct it. One therefore had no excuse of not working due to a state of disrepair of the evaporator, furnace, machinery nor accesory required as Lawrence deftly saw to these within a twinkle of an eye.
- Chris and Cecil who I regularly fell back on when genplot and latex had me at sixes and sevens.

- Ginny for her almost impeccable efficacy, forever bursting with energy whilst smoothly operating the nerve centre of the MRG, relentlessly commited to our well being, be it in providing stationery, booking of meals, taking messages, compiling the monthly editions of NAC news with an added touch of humour.

- Oom Stan, a shrewd man indeed always advocating the use of common sense. "Problems are simply challenges" he would always say, watching over you as you went about with your lab tasks, offering advice and a helping hand unobtrusively at all times, as he was forever wary of "interfering".

- William for his accommodating nature and selfless attitude, safely transporting virtually everybody at the MRG to whatever destination.

- Joan for dilligently keeping our surroundings spruced up at all times and ensuring that all the commodities in the staff tea-room were always readily available and neatly laid out.

- The entire MRG staff and students for the warmth and the cheerfulness they always exuded and for all their support.

- Everyone at home

    1. My mother who always taught me to trust in the Lord and instilled a work ethic in me from a very tender age.
    2. My father who blooded me in the field of science and always insisted on "clarity"and the "use of common sense". Your efforts have not been in vain – MHAYISE!
    3. My siblings Nompumelelo, Mzwandile and Kukhanyakwezwe who were always beside me through thick and thin.

- The apple of my eye Thabile who inspite of my regular sojourns in the Cape was always appreciative of the prevailing state of affairs. With this task completed, is it not time for me to make up for all the days you spent alone with Nomaswazi and Nselelo? – NGIBA!

- Mazwendoda, who for the past 25 years has been a friend-cum-confidant. We have always teased, joked, motivated one another, discussed ideas that shape mankind and the world.

- Linda Thela who always ferried me to and from Durban whenever I so requested.

- The University of Zululand under whose auspices this dissertation was conducted.

- Last but not least, the Lord Almighty *"In everything give thanks, for this is the will of God"* 1 Thess.5:18

ABSTRACT

Thin films of Cu, Ir, Mo, Pt, Re, Y, Yb and Zr were vacuum deposited onto SiO_2 substrates of thermally oxidized Si< 100 > wafers and were annealed in a vacuum tube furnace. Samples were then analysed using Rutherford Backscattering Spectrometry (RBS) and X-Ray Diffraction (XRD) to determine whether solid state reactions took place and to identify the compound phases formed. It was found that Y, Yb and Zr reacted with the SiO_2, while none of the other metals reacted even after heating for hours at high temperatures of up to 900°C. These results as well as all the other metal-SiO_2 interaction studies that could be found in the literature were summarized and extensively analysed. In all the cases where the metal reacted with the SiO_2 (Hf, Nb, Ta, Ti, V and Zr) with the exception of the rare-earth metals Y, Tb and Yb, it was found that a thin layer of metal silicide formed sandwiched between the SiO_2 substrate and a top layer of metal oxide. From this configuration the following model for the diffusion process could be formulated. Metal atoms diffuse to the SiO_2/silicide interface where interaction with and dissociation of SiO_2 takes place. The released oxygen atoms then diffuse through the silicide layer to form a metal oxide on top of the silicide. It could therefore be concluded that oxygen diffuses more readily through the silicide than silicon through the metal oxide. If the opposite was true the sample configuration after reaction would have been $SiO_2/MO_x/MSi_y$. In the case of the rare-earth metals, solid-state reaction always took place, but with all the elements M, Si and O being present throughout the reaction region. In the case of Yttrium ternary phases were identified, whereas XRD showed that a mixture of silicides and oxides formed in the case of Ytterbium.

In this study an extensive table of heats of formation for the silicides and oxides was compiled, from which heats of reaction could be calculated. The theoretical thermodynamic predictions were found to be consistent with experimental observations. This study also showed that the results could be correlated with the mean electronegativity of the metal which offers a convenient empirical method of predicting whether a metal will react with SiO_2 or not. It is found that metals with an average electronegativity (average of Allred-Rochow, relative compactness and Pauling electronegativities) of less than 1.45 on the Pauling scale react with SiO_2. An even better correlation with electronegativity could be obtained when using the Miedema electronegativity parameter (ϕ^*). Metals with ϕ^* values of less than 4.45 V were found to react with SiO_2 and those with values equal to or greater than 4.45V were found not to react.

It has also been shown how ternary phase diagrams can be used to predict solid-state interaction between metal films and SiO_2.

ISIFINGQO

Izingwengwezi ze Cu, Ir, Mo, Pt, Re, Y, Yb ne Zr ziye zahwamukiselwa phezu kwe SiO_2 yona ebihlunyiswe phezu kwamacwecwe eSi< 100 >. Lamacwecwe abe esefakwa kuhavini oshisayo. Ukuhwamukisa nokushisisa kwenziwe emva kokugeqa wonke umoya kusihwamukisi kanye nakuhavini. Lamacwecwe abe esecwaningwa nge Rutherford Backscattering Spectrometry (RBS) kanye ne X-Ray Diffraction (XRD) ukuthola ukuthi ngabe kube khona yini ukulumbana ngaphansi kwesimo sobuduli nokuthola ukuthi ngabe izale nkomoni. Kuhlaluke ukuthi i Y, Yb ne Zr ziye zalumbana ne SiO_2 ekanti lezi ezinye izingwengwezi azivezanga kulumbana ne SiO_2 kuze kuyofinyelela emazingeni okushisa angu 900°C. Lemiphumela kanye naleyo eminye eshicilelwe emayelana nokulumbana kwe SiO_2 nokusansimbi ibe isifingqwa ihlaziywa. Kuhlaluke ukuthi uma kube khona ukulumbana njengesibonelo se SiO_2 ne Hf, Nb, Ta, Ti, V ne Zr (ngaphandle kwalezonsimbi mhlaba ezingandile njenge Y, Tb ne Yb) ungwengwezi lwensimbi ehlangene nesilikhoni (MSi_y) lufunyanwa njalo luphahlwe yi SiO_2 kanye nongwengwezi lwensimbi ehlangene nomoyampilo (MO_x). Lokhu kuhleleka kwalezingwengwezi kusinika lesisithombe mayelana nokuhamba sakuchusha kwama athomu: Ama athomu alokho okusansimbi achusha aze ayofika emngceleni weSiO_2 ne MSi_y. Okulandelayo kuba wukuhlakazeka kwe SiO_2, ebese kuthi ama athomu omoyampilo achushe ku MSi_y aze ayolumbana nama athomu alokho okusansimbi kwakheke i MO_x. Lokhu kusiholela ekuthini sithi ama athomu omoyampilo achusha kalula ku MSi_y kunokuba kuchusha isilikhoni ku MO_x. Uma isilikhoni ibichusha kalula kunomoyampilo, ukuhleleka kwalezingwengwezi bekuyoma kanje: $SiO_2/MO_x/MSi_y$. Ucwaningo lwensimbi mhlaba engandile luveze ukuthi ukulumbana kwayo ne SiO_2 esimweni sobuduli kwenzeka khathi zonke ekanti ama athomu esilikhoni, nawokusansimbi nawomoyampilo atholakala kuzo zonke izingwengwezi ezakhekayo. Imiphumela yohlaziyo nge XRD iveze ukuthi ulumbano olwenzeka uma sisebenza nge Ytterbium lukhipha ingxube ye MO_x ne MSi_y ekanti ulumbano olwenzeka uma sisebenza nge Yttrium luveza ubukhona bama athomu esilikhoni, awokusansimbi kanye nawomoyampilo (ongxubentathu) atholakala ekhona kuzo zonke izingwengwezi ezakhekayo.

Kulomsebenzi sididiyele uhla lwemidlandla kushisa yalokho okusansimbi nxa kulumbene nesilikhoni (MSi_y) kanye nohla lwemidlandla kushisa yalokho okusansimbi nxa kulumbene nomoyampilo (MO_x). Sibe sesisebenzisa lezinhla ukubala izinga lomdlandla kushisa uma lokho okusansimbi kulumbana ne SiO_2. Ukubikezela kwethu ukulumbana (nokungalumbani) kwalokho okusansimbi ne SiO_2 okuncike ezibalweni kanye nasolwazini olumaqondana nomdlandla kushisa sikuthole kuhambisana nemiphumela yocwaningo lwethu. Lomsebenzi (uhlangene neminye imiphumela eshicilelwe) ubuye uveze ubudlelwano phakathi kokulumbana kwalokho okusansimbi ne SiO_2 kanye namandla ama athomu okudonsa ama elektron. Lokho okusansimbi okunamandla angaphansi kuka 1.45 (atholakala ngokudidiyela indlela yokubala ka Allred Rochow, eka Pauling neqhathanisa ukuqoqeka) ngokwesilinganiso sika Pauling, kuhlaluka ukuthi khona kuyalumbana ne SiO_2. Sithe uma sibheka amandla ama athomu okudonsa ama elektron ngokwezibalo zikaMiedema (ϕ^*) sawathola eqhathiniseka kangcono nemiphumela yethu yokulumbana kunalapho besisebenzise amandla ngokwezibalo zika Allred Rochow, Pauling kanye nendlela eqhathanisa ukuqoqeka. Lokho okusansimbi okunani lakho lika ϕ^* lingaphansi kuka 4.45V kutholakale ukuthi kuyalumbana ne SiO_2 ekanti lokho okunani lakho lika ϕ^* lilingana noma lingaphezulu kuka 4.45V akulumbani.

Imidwebo engonxantathu eveza nokulumbana okungxubentathu ingasetshenziswa nayo ukubikezela ukuthi ukulumbana phakathi kwalokho okusansimbi ne SiO_2 ngaphansi kwesimo sobuduli kungenzeka yini noma qha.

Contents

CHAPTER 1

BACKGROUND AND SCOPE OF INVESTIGATION.

1.1 Technological importance of thin films.

A silicon chip of $1cm^2$ can accomodate more than 1 million individual devices. By reducing the interconnecting paths and the size of the device features (miniaturization), the speed of operation is increased. The computing power (density of data storage) of a chip is also increased by miniaturization.

Most of the silicon chips contain metal oxide semiconductor (MOS) devices since these prove easy to fabricate. Fabrication problems of semiconductor devices fall into two categories viz:

(a)Practicability - Control over processes like alignment of lithographic masks, etching of metallic and insulating layers and the maintenance of scrupulous cleanliness at all stages. Lattice defects near the surface of the conductor must be avoided as this may impact on the operation of the devices.

(b)Efficiency of device - Obtaining materials that are better conductors (or insulators) to improve the perfomance of devices. - Preventing leakages of current between adjacent devices - Connecting each device into the circuit via a network of thin film metallic conductor tracks. The metallic conductor tracks will often need to be superimposed with a layer of insulator separating them to obtain the desired

interconnection. These arrays of metal and insulator which form the "wiring" on the chip are called metallization.

Metallization of semiconductors is desirable to provide electrical circuitry. It is important therefore to understand the ability of the metal to adhere to the substrate. Deposition of a metal on a semiconductor has been shown to result in dissolution of the semiconductor, even if there is no chemical reaction taking place. Such dissolution is a result of the weakening of bonds of the semiconductor and formation of a new "pseudo alloy" (of poorly defined stoichiometry) because of indiffusion of the metal or outdiffusion of the semiconductor. This process greatly affects the electrical properties of the contact.

One of the limiting factors in achieving high reliability on integrated circuit devices is a poor choice of the metallization schemes. The problem is due to a requirement for a controlled contact at the metal-semiconductor interface and for a low resistance metal that does not lead to a voltage drop across the contact. The metallization must also be compatible with the processing temperature, have good adhesion, high resistance to corrosion and low electrical resistance. A general requirement for any contact (i.e. good adhesion) is that there must be a uniform and limited reaction between the two materials in contact. Advanced integrated circuit metallization requires materials with both low resistivity and high thermal stability. Materials that meet these requirements include refractory metals, silicides and nitrides. During circuit fabrication, these metallization layers may come into contact with various solids and gases at elevated temperatures. Consequently the chemical stability of the metallization layer is a critical factor in choosing the material.

Interest in silicides is due to their usefulness in integrated circuits as Schottky barriers, ohmic contacts, low resistivity gate and interconnects and high temperature stability [**1**]. This interest has been aroused by the fact that with the scaling down of device sizes, the line widths get narrower and the resistance contribution to the RC delay increases. Besides the desired low resistivity, the usefulness of the silicide metallization schemes depends on the ease with which the silicides can be formed

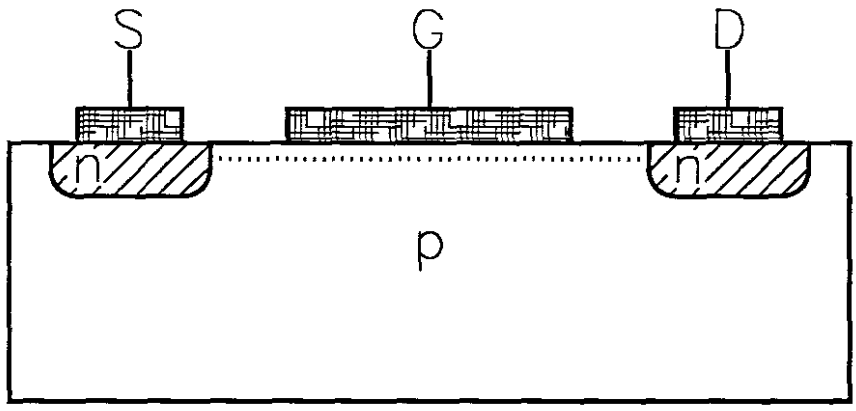

FIGURE 1.1: Schematic illustration of a simple semiconductor device e.g. an n-channel field effect transistor [2] showing the Source, the Gate and the Drain.

and patterned and on the stability of the silicides throughout the device processing and usage. In the fabrication of metal oxide silicon (MOS) devices, very thin layers of the metal (say of the order of 100 atoms in thickness) need to be deposited on the Si substrate. Layers deposited by these growth techniques can be used successfully as gate oxides in highly efficient MOS devices (see **Fig. 1.1**).

SiO_2 is useful as an interlayer dielectric and protective capping in integrated circuit technology. It is however in competition with other materials such as polyimides whose dielectric properties are very similar to those of SiO_2. Polymeric films have been proven to be depositable by simple techniques. In some ways, polymers may have definite advantages, including low temperature processing, cheapness and low stress levels. Their disadvantage lies in the fact that the purity of the precursor material (the polyamic acid from which the polyimides are derived) is not as good as is required in proximity to semiconductor integrated circuits and the diffusion of contaminants through the fully cured layers is considered unacceptably fast. The diffusion rate of water through cured polyimide is rapid and can thus lead to moisture reaching the metallic conductors and causing corrosion. On the contrary, the diffusion rate of contaminants through silicon oxide is very slow indeed. The adhesion of silicon oxide to most metals supercedes that of the polyimides.

In order for a material to be a useful interlayer dielectric, it should satisfy most

of the following properties, viz,

1. The barrier layer should be thermodynamically stable when in contact with the two materials which it separates.

2. There should be no rapid diffusion of any of the two materials it separates along the grain boundaries in the barrier film.

3. It should form low-resistance contacts with both materials.

4. The barrier must adhere well to all the materials with which it is in contact.

5. The material of the barrier layer should not have an electrochemical potential very different from that of the two materials it is separating, otherwise galvanic corrosion cells can be set up in the metallization layers.

Table 1.1 compares the dielectric properties of silicon oxide with certain other materials.

The structure and electronic properties of the interface produced when a metal is deposited on a semiconductor will determine if the contact is ohmic or Schottky. There is as yet no generally accepted model which predicts the type of contact produced since the mechanism by which the electrical properties are developed is not yet fully understood. Hence, the experimental results do not concur fully with any given model.

1.2 Solid-State interaction.

When two solid films of dissimilar elements are brought together with each other (e.g. by sequential evaporation of one film on top of the other) and their temperature raised sufficiently, a reaction may or may not take place. There is a large body of knowledge as regards to which materials may or may not react. We review here some of the methods used to predict whether an interaction may or may not take place and which products may result.

TABLE 1.1: A comparison of the dielectric properties of a selection of barrier layers used at Al-Si contacts.

	Advantages	Disadvantages	Applications
SiO_2	Low dielectric constant LPCVD layers are highly conformal	High intrinsic stress levels	Interlayer dielectric Thermal gate oxide
Si_3N_4	Low diffusion rates for contaminants Low oxidation rates	High dielectric constant High intrinsic stress	Capacitor dielectric Annealing cap Diffusion barrier Oxidation mask
AlN	Low dielectric constant Thermal expansion coefficient same as GaAs	Deposition process not well developed	Annealing cap
Polyimide	Cheap Conformal Low dielectric constant	Stable only below 400^0C Rapid indiffusion of water	Interlayer dielectric (especially on GaAs devices) Protective coatings on device surfaces
PSG	Flows at high temperatures Traps sodium ions	Corrosion problems due to HPO_3	Passivation layers

1.2.1 Thermodynamics.

The reason for the transformation of the two films put together into a new phase is the fact that the initial state is unstable relative to the final state. If the initial state is stable relative to any other possible state, no transformation will take place i.e. the solid films will not react chemically [3]. For the case of transformations that occur at constant temperature and pressure, the relevant thermodynamic potential

to look at is the Gibb's free energy (G) viz

$$G = H - TS \tag{1.1}$$

where H is the enthalpy, T the temperature and S the entropy.

Enthalpy is in turn given by

$$H = E + PV \tag{1.2}$$

where E is the internal energy of the system, P the pressure and V the volume. A system is in equilibrium if it is in its most stable state i.e. the one corresponding to a minimum in G. Changes occuring while in this state are such that

$$dG = 0 \tag{1.3}$$

In **Fig. 1.2**, state G_2 would be the lowest state (most stable), while state G_1 is a metastable state (local minimum). If the system is in state G_1 and thermal energy is added to the system, then depending on how much energy is applied, the system may move to state G_2. Transformations that occur to the system therefore tend to lower G.

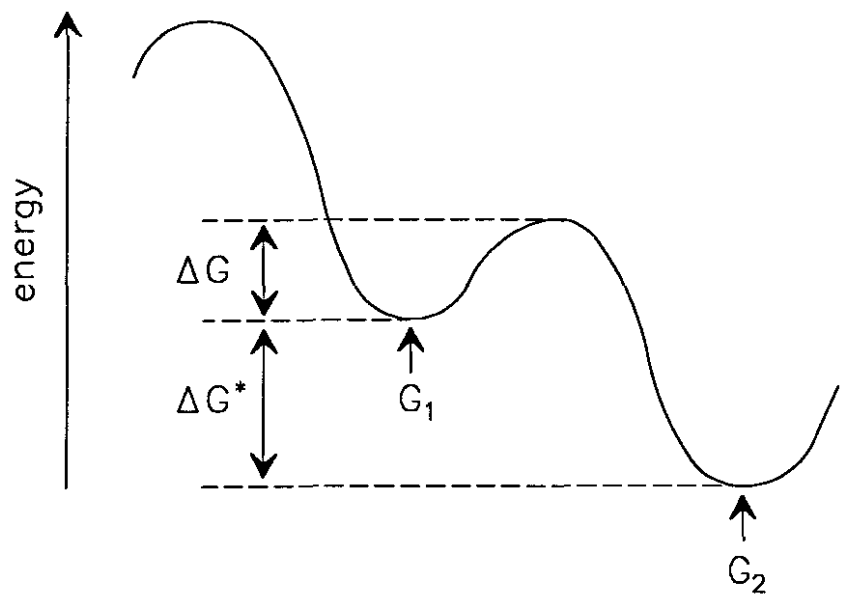

FIGURE 1.2: A hypothetical Gibb's function, showing metastable state G_1 and a stable state G_2. It also shows a barrier that must be overcome by an atom that changes it's Gibbs function value from G_1 to G_2. The Gibbs barrier height is ΔG and the overall change in the Gibbs function value is ΔG^*.

$$\Delta G^{*} < 0 \tag{1.4}$$

Thermodynamics does not provide answers as to how fast this transformation will take place, but only that it may happen or not.

For the case of solids (solid film in contact with another solid film), the $T\Delta S^{\circ}$ term is small and the Gibb's free energy may be approximated by

$$\Delta G^{\circ} \approx \Delta H^{\circ} \tag{1.5}$$

which is known as the Neumann and Kopp's rule. Furthermore we may in most cases approximate ΔG°_{T} by ΔH°_{298} where ΔG°_{T} is the Gibb's free energy at a higher temperature (e.g. 900°C) and $\Delta \mathrm{H}^{\circ}{}_{298}$ is the enthalpy at room temperature i.e.

$$\Delta G^{\circ} \approx \Delta H^{\circ}_{298} \tag{1.6}$$

1.2.2 The Miedema model.

The "macroscopic atom" model of Miedema [5] was formulated to predict the enthalpy of formation ΔH with varying atomic concentration in both binary liquids and solid phases (see **Fig. 1.3**). The model uses qualitative experimental information derived from the general appearance of binary phase diagrams. Positive enthalpy as given by the model values correspond to non-existing alloys whereas negative enthalpy values correspond to possible stable alloys or compounds. The model uses properties of pure metals like the electron density at the boundary of the Wigner-Seitz atomic cell, n_{ws} and the chemical potential for electronic charge, ϕ^{*}.

The model uses the readily available values of n_{ws} for non-transition metals but estimates n_{ws} for transition metals by assuming that the relationship between n_{ws} and the experimental ratio of bulk modulus κ and molar volume V for pure metals is reasonably represented by

$$(n_{ws})^{2} = \frac{\kappa}{V} \tag{1.7}$$

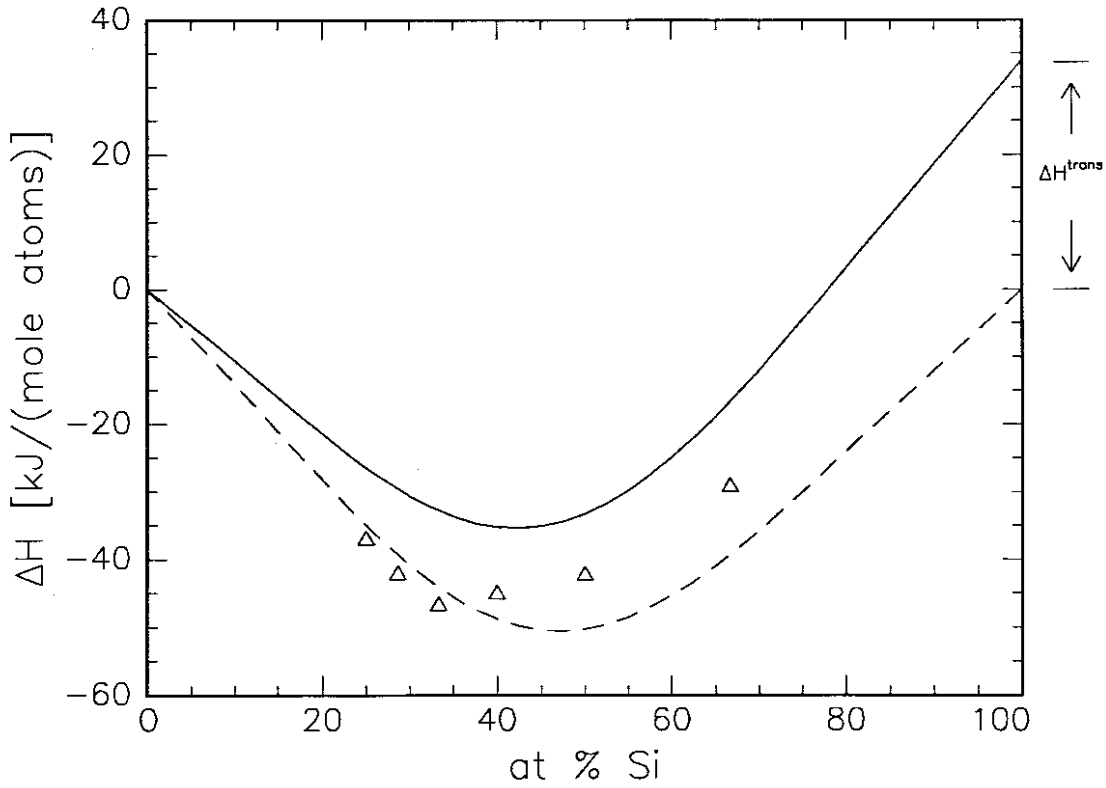

FIGURE 1.3: The dotted line gives the values of the heats of formation for the Ni-Si system calculated according to the semi empirical model of Miedema. By introducing a correction factor ΔH^{trans} which is 34kJ/(mol.at) for Si, the semiconducting element is converted into a hypothetical metallic one and values corresponding to the solid line are obtained. The triangles show the experimental values of the heats of formation [4].

The other property used to characterize metals by the model is the value of electronegativity parameter or the chemical potential for electronic charge. The model uses experimental values of work function as a starting point.

A recommended set of values of ϕ^* is given [5]. Similarities between ϕ^* and other values e.g. the Pauling scale are obvious. Compared to other scales, the scale used in the Miedema model is one referring specifically to solids.

According to the model,

$$\Delta H^{for} \propto [-P(\Delta\phi^*)^2 + Q(\Delta n_{ws}^{\frac{1}{3}})^2] \tag{1.8}$$

where P and Q are proportionality constants.

ϕ^* is given by

$$\phi^* = 5.2\left(\frac{Z}{V}\right)^{\frac{1}{3}} + 0.2 \text{ for transition metals} \tag{1.9}$$

$$\phi^* = 5.2\left(\frac{Z}{V}\right)^{\frac{1}{3}} + 0.7 \text{ for non-transition metals} \tag{1.10}$$

where Z is the number of valence electrons per atom.

For a third class of alloys, that of transition metals alloyed with polyvalent non-transition metals, a term R^* is introduced.

$$\Delta H^{for} \propto [-P(\Delta\phi^*)^2 + Q(\Delta n_{ws}^{\frac{1}{3}})^2 - R^*] \tag{1.11}$$

This term (R^*) is required when a non-transition metal (with conduction electron wave functions predominantly mixed with atomic p-type wave functions) is alloyed with a transition metal (admixture of atomic d-type wave functions).

Criteria used for choosing $\Delta H°$

Since there are many possible values, experimental plus empirical that one may use for $\Delta H°$, it is important to have a criterion for choosing them. $\Delta H°$ will be used in this study for calculation of heats of reaction. It is therefore noticed that their absolute values are unimportant - only their relative values count. We will therefore as much as possible use the Miedema model for values of $\Delta H°$ and obtain $\Delta H°$ from published experimental data where Miedema values are not given (e.g. for metal oxides).

1.2.3 The EHF Model.

The effective heat of formation (EHF) model predicts the sequence of compound formation in binary thin film systems [6]. It has been experimentally determined that for thin films (say $\leq 1\mu$m), only one compound phase is present at a time, contrary to the bulk case where most or all the compound phases given by the phase diagram may be observed. In the case of silicides for instance, only one compound phase forms between the thin metal and silicon films with no indication

of any other phase as long as the metal and silicon are still available. Knowledge of phase formation sequence is of interest to materials scientists since by controlling experimental parameters, specific phases may be formed.

One of the first rules for predicting phase formation was that of Walser and Bene' [7] which states that:

"The first compound nucleated in planar binary reaction couples is the most stable congruently melting compound adjacent to the lowest temperature eutectic on the bulk equilibrium phase diagram".

This rule was later extended by Tsaur "et al" [8] to subsequent phase formation in metal-silicon systems. According to their rule,

"the second phase formed is the compound with the smallest ΔT that exists in the phase diagram between the composition of the first phase and the unreacted element."

They defined ΔT as the temperature difference between the liquidus curve and the peritectic (or peritectoid) point for the system under consideration. Bene' subsequently extended the Walser-Bene' rule to metal-metal systems by relaxing the requirement that the first phase that forms needs to be congruent. A theory for simple phase growth in thin film complexes was put forth by Gosele and Tu in which they inferred interfacial reaction barriers and adopted a competitive kinetic growth model. It is predicted that the first compound phase must exceed a critical thickness before a second compound phase may form and grow simultaneously with the first one. Ronay proposed a rule for the first phase silicide formation taking into account the central eutectic, the diffusing species and interfacial free energy. This rule states that:

"The first nucleating phase in metal-silicon planar reaction couples is that congruently melting phase neighbouring the central eutectic in the phase diagram, which is closer in composition to the diffusing species. This phase must also have a low interfacial free energy with one of the elements constituting the phase diagram. The low interfacial free energy is indicated either by eutectic formation with, or

by epitaxial growth on, one of the elements."

None of these rules, however, makes use of thermodynamic data such as heat of formation($\Delta H°$) and entropy($\Delta S°$). Pretorius proposed the effective heat of formation (EHF) model which allows for the use of thermodynamic data to predict first phase formation and subsequent phase formation sequence. In this model an effective heat of formation($\Delta H'$) is defined which depends on the available concentration of the reacting atomic species at the growth interface.

The driving force for a process to take place is given by the change in the Gibb's free energy, $\Delta G°$. For solid state interaction,the change in the heat of formation $\Delta H°$ is a good measure of the change in free energy, $\Delta G°$ since the change in entropy, $\Delta S°$ is negligible. Heats of formation can thus be used to predict the phase formation sequence when nucleation barriers do not exist since a system would always want to go to its lowest possible free energy state. During solid state interaction, phase formation at an interface is a dynamic non-equilibrium process with usually one compound phase forming at the interface. This is contrary to equilibrium systems, where formation of a mixture of phases might lead to the lowest free energy for the system.

The heat of formation is expressible in kJ/mol e.g. $\Delta H°(Pd_5Ti_3) = -710.4kJ/mol$. If we divide the heat of formation by the number of atoms in the molecule, we obtain the value $\Delta H°(Pd_5Ti_3) = -88.8kJ/(mol.at)$. Since the heat of formation proves insufficient in predicting first phase formation at the interface, we then define the effective heat of formation, $\Delta H'$, which depends both on the heat of formation and the concentration of the reacting species at the growth interface

$$\Delta H' = \Delta H° \times \frac{\text{effective concentration of limiting element}}{\text{compound concentration of limiting element}} \qquad (1.12)$$

Consider the solid state interaction of Pd and Ti to form the compound phase PdTi, where an ensemble of 3 atoms of each element is present at the reaction zone (see **Fig. 1.4(a)**). The effective concentration of the atoms of each element is 50 at.%.

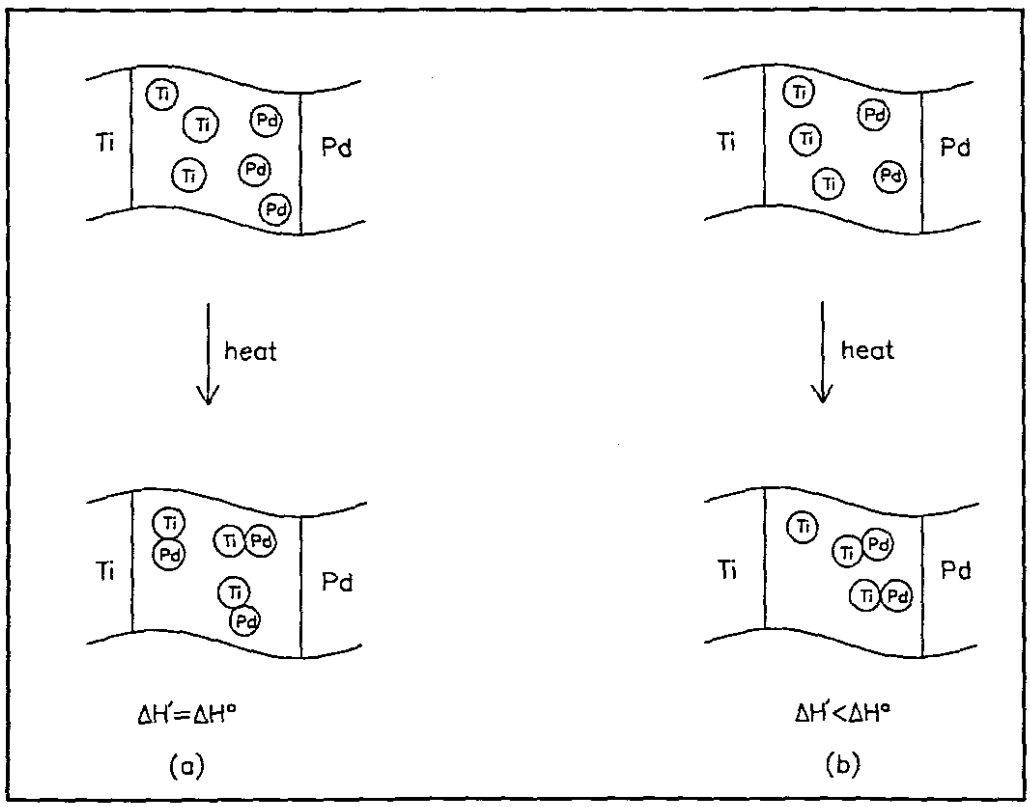

FIGURE 1.4: Schematic diagram of interaction between Pd and Ti atoms to form PdTi. (a) If there are three atoms of each element, three molecules of PdTi would be formed and the heat released would be equal to the standard heat of formation. (b) If there are two atoms of Pd and three atoms of Ti, Pd is the limiting element and the Effective Heat of Formation ($\Delta H'$) will be less than the Standard Heat of Formation, ($\Delta H°$).

The atomic concentration in the compound phase is also 50 at.% Pd and 50 at.% Ti. In this case, all the available atoms are used up to form PdTi molecules. Since all the available atoms are used up in the reaction, the total amount of heat released is equal to the standard heat of formation, i.e. 96.7kJ/(mol.at)$^{-1}$. For this case, the effective heat of formation is equal to the standard heat of formation i.e. $\Delta H'$ $=\Delta H°$.

Next consider a case where there are only two atoms of Pd and three atoms of Ti at the reaction interface (see **Fig. 1.4 (b)**). The effective concentration of atoms is thus 40 at.%Pd and 60 at.%Ti. In the formation of the PdTi compound phase, only two Pd and two Ti atoms would be used, the rest being in excess. Since phase formation at the growth interface is a dynamic non-equilibrium process, the atoms that are in excess would not contribute to the total heat released and would only be available for formation of the next increment of compound at the moving interface. In this particular case i.e. PdTi, Pd is the limiting element, while Ti is in excess. From equation **1.12** it follows that

$$\Delta H' = -96.7\left(\frac{0.40}{0.50}\right) = \text{-}77.4\text{kJ/(mol.at)} \tag{1.13}$$

From equation **1.12**, the effective heat of formation of any compound can be calculated as a function of the concentration of reacting species. **Fig. 1.5** shows a linear relationship between the effective heats of formation of various Pd-Ti binary phases and the concentration of the reacting species.

For each phase, the most negative effective heats of formation occur when the Pd and Ti concentrations match that of a particular compound, as the concentration ratio in equation **1.12** is then unity. Effective heats of formation diagrams are readily constructed by plotting the heats of formation of each compound at the compositional concentration (i.e. the effective heats of formation) and completing the triangulation by connecting these points to the end points of the concentration axis.

Equation **1.12**, defining the effective heat of formation can be derived as follows. Consider the formation of the compound A_xB_y at the interface between

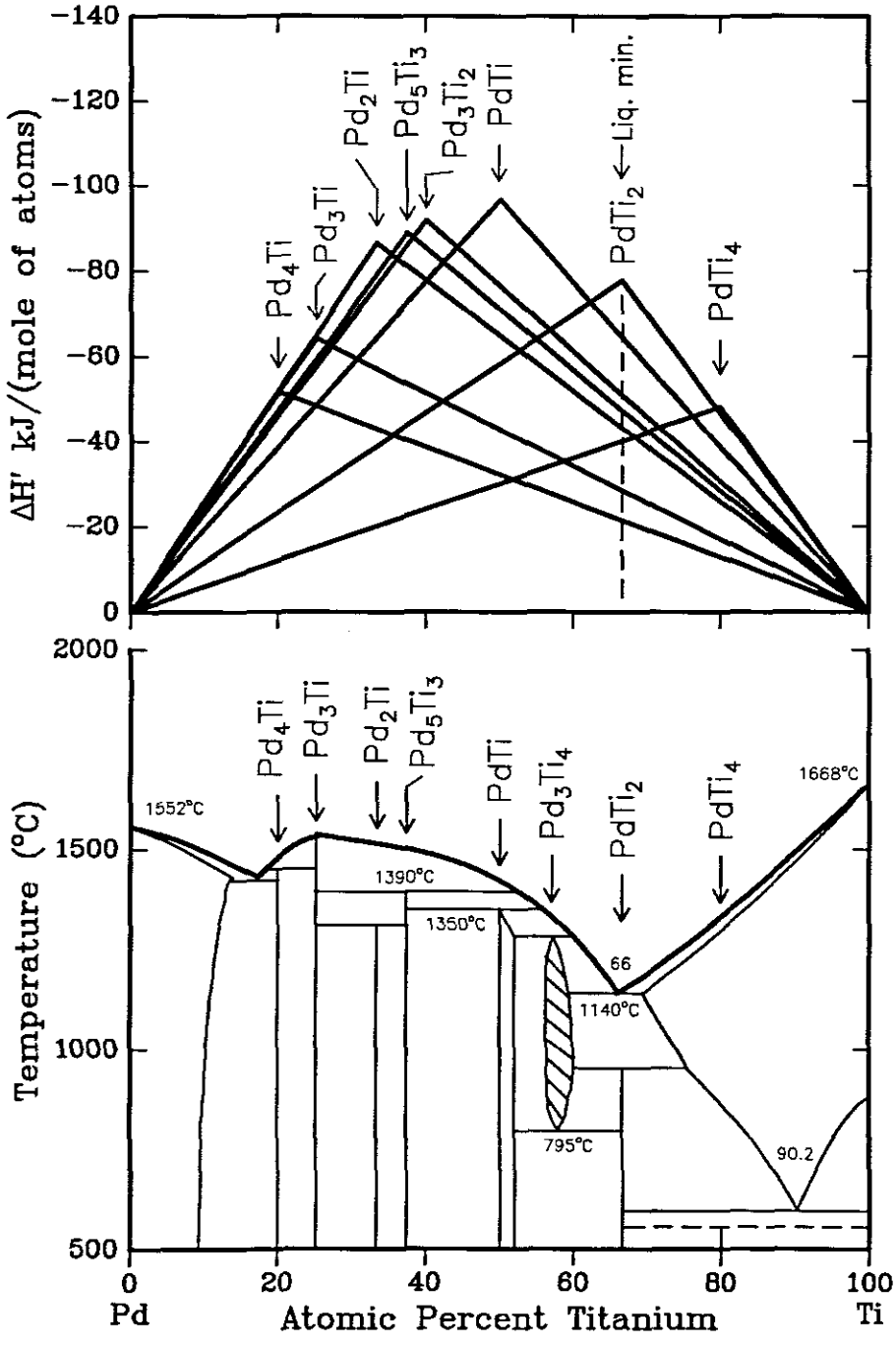

FIGURE 1.5: The phase diagram (bottom) and the EHF diagram (top) of the Pd-Ti system according to Moffat [9].

A and B to be given by the reaction

$$z(xA + yB) \rightarrow z(A_xB_y) \tag{1.14}$$

Let N be the total number of atoms available for reaction in the reaction zone where $N = N_A + N_B$ with N_A the total number of atoms of A and N_B the total number of atoms of B.

Let M be the total number of atoms consumed in the formation of A_xB_y ie

$$M = zx + zy = M_A + M_B \tag{1.15}$$

The effective (available) concentration of atom A is

$$C_e^A = \frac{N_A}{N} \tag{1.16}$$

The effective (available) concentration of atom B is

$$C_e^B = \frac{N_B}{N} \tag{1.17}$$

The compound concentration of A in A_xB_y is

$$C_c^A = \frac{x}{x+y} \tag{1.18}$$

The compound concentration of B in A_xB_y is

$$C_c^B = \frac{y}{x+y} \tag{1.19}$$

If A is the limiting element during the formation of A_xB_y, its atoms are fully consumed, whilst the atoms of B will be in excess. It follows that

$$M_A = N_A = NC_e^A \tag{1.20}$$

During formation of A_xB_y, atoms are consumed in the ratio

$$\frac{x}{y} = \frac{M_A}{M_B}$$
$$\Rightarrow M_B = \frac{y}{x} M_A \tag{1.21}$$

From eqns **1.15** and **1.21**, we have

$$M = M_A \left[1 + \frac{y}{x}\right]$$
$$= \frac{M_A}{C_c^A} \tag{1.22}$$

From **eq. 1.20** and **eq. 1.22**, we have

$$\frac{M}{N} = \frac{C_e^A}{C_c^A} \tag{1.23}$$

The heat of formation ΔH when expressed in J/(mol.at) is the heat released when Avogadro's number (A_v) of atoms is consumed during formation of A_xB_y. The consumption of M atoms releases $\frac{M}{(A_v)}\Delta$H. The number of moles of available atoms is $\frac{N}{(A_v)}$. Therefore, the heat released per mole of available atoms is

$$\Delta H \left(\frac{\frac{M}{(A_v)}}{\frac{N}{(A_v)}} \right) = \Delta H \frac{M}{N} \tag{1.24}$$

For a non-equilibrium reaction such as that described above, the effective heat of formation can be described as

$$\Delta H' = \Delta H \frac{M}{N} \tag{1.25}$$

From **eq. 1.23**, we have

$$\Delta H' = \Delta H \times \frac{C_e^A}{C_c^A}$$

or

$$\Delta H' = \Delta H \frac{\text{effective concentration of limiting element}}{\text{compound concentration of limiting element}} \tag{1.26}$$

1.2.4 Heats of reaction.

The heats of reaction may be calculated if the enthalpy of the products and reactants are known. It is given by the difference between the enthalpy of the products at temperature T and that of the reactants at the same temperature.

The standard enthalpy used in this case is the standard heat of formation at 298K and 1 atmosphere. We may find for example that when Ti is in contact with SiO_2 at room temperature it should undergo a reaction

$$Ti + SiO_2 \longrightarrow Ti_3Si + TiO$$

If the heat of reaction obtained is negative then it will mean that the reaction is possible. One finds that for Ti in contact with SiO_2 there are a number of such possibilities. Though it can be calculated that a reaction takes place, there is no way of predicting a particular resulting product.

A model that could be used to predict the resulting products is the Effective Heat of Formation model. This model however will in this case require a knowledge of ternary phase diagrams. There are very few known ternary phase diagrams and therefore the model cannot be used in this case.

1.3 Metal-SiO_2 interaction.

1.3.1 Importance.

Metal silicides find wide applications in advanced integrated circuit metallization because of their low resistivities (e.g. $TiSi_2$ has a resistivity of about $15\mu\Omega$cm) and high thermal stability. When an integrated circuit is being fabricated, a pure metal may come into contact with various dielectrics e.g. SiO_2. It is therefore important to understand the reactions between metals and SiO_2 so as to maintain stability of devices during fabrication.

1.3.2 Effect of metal thickness.

It is known that when two thin films in contact are heated, not all compound phases given in the equilibrium phase diagram are observed [**10**]. In the case of silicides,

where a large body of knowledge exists, it has been found in some cases that only one compound phase occurs during interaction between say silicon and a metal. When dealing with thick films (greater than about 10μm), it has been found that most or nearly all of the compound phases given by the equilibrium phase diagram are present. Gosele and Tu [10] have termed this the bulk case. They have termed the case where metal films are less than 10μm the thin film case. In our study, the metal films will in all cases be equal to or less than 4500Å and we will therefore be dealing with the thin-film case.

S. Q. Wang and J. W. Mayer [11] found that the rate of chemical reaction between a metal, e.g. Ti with SiO_2 depends on the thickness of the metal. The thicker the metal the larger the reaction rate, which is attributed to the fact that the remaining metal layer acts as a sink for the released oxygen. The argument is if there is oxygen incorporated in the metal layer then there are less metal atoms available for interaction at the metal/SiO_2 interface. Thinner films are expected to have a higher concentration of oxygen.

1.3.3 Prediction of interaction.

A method of predicting whether a metal will react with SiO_2 or not has been developed by Pretorius *et al.*[3]. It uses both the heats of reaction and electronegativities. According to the model and if it is assumed that the products are a metal silicide and a metal oxide, the reaction is written as

$$SiO_2 + M_x \longrightarrow M_ySi + M_{x-y}O_2 \tag{1.27}$$

where M is a metal. The reactions considered are those that happen at constant temperature and pressure, where the change in Gibb's free energy may be written as

$$\Delta G = \Delta H - T\Delta S$$

with ΔH the change in enthalpy (or heat of reaction). $\Delta S \approx 0$ since it is assumed that both reactants and products are solids. ΔG is therefore approximated by the enthalpy ΔH. If ΔH is less than zero, then the reaction between SiO_2 and the metal is thermodynamically possible.

The heat of reaction between Mn and SiO_2 is calculated as follows:

$$3\ Mn + SiO_2 \longrightarrow MnSi + 2MnO$$

$$3(0) + 3(-301.2) \longrightarrow 2(-41.5) + 4(-192.6)$$

$$-903.6 = \longrightarrow -83.0 - 770.4$$

$$\Delta H_R = +8.37\text{kJ/(mol.at)}$$

Working out other possibilities it is found that all heats of reactions for this system are positive. This would simply imply that Mn does not react with SiO_2.

Pretorius *et al.* [3] have also used electronegativity to predict whether a metal will react with SiO_2 or not. **Fig. 1.6** shows a plot of their calculated standard heats

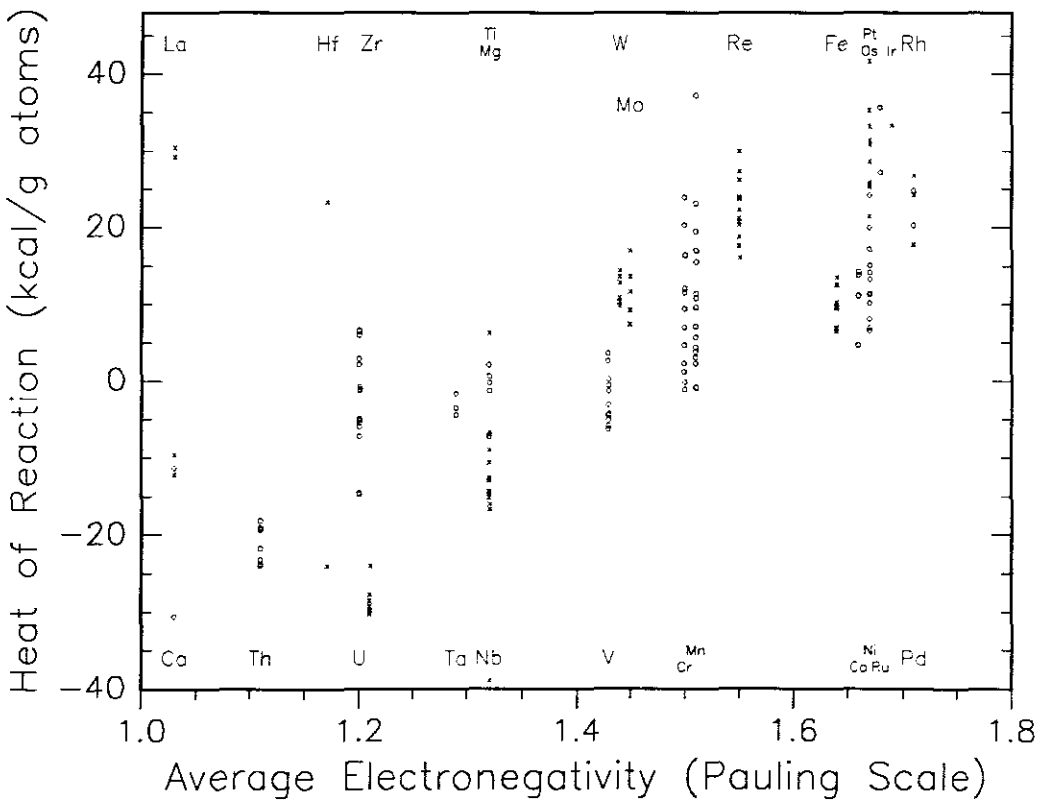

FIGURE 1.6: Heats of reaction for all possible combinations of various metals in interaction with SiO_2. Heats of reaction are plotted on the vertical axis whereas electronegativities are on the horizontal axis [3]. Crosses refer to elements at the top and open circles to elements at the bottom.

of reaction ΔH_R, plotted as a function of the average of three electronegativities (average of relative compactness, Pauling and Allred-Rochow electronegativities). A linear correlation between the calculated standard heats of reaction and the average electronegativities of the metals was found. They found that metals with average electronegativities of less than about 1.5 on the Pauling scale react with SiO_2 whereas those with average electronegativities greater than about 1.5 do not.

1.3.4 Prediction of reaction using ternary phase diagrams.

Beyers [12] has shown that ternary phase diagrams may be used to predict whether a compound involving three elements (or less) in contact with one of the three elements will be stable or not. The Gibb's phase rule predicts that there can only be a maximum of three phases in equilibrium in any portion of the phase diagram. Regions of three-phase equilibrium in these phase diagrams form triangles in isothermal sections of the diagram.

The corners in any such triangle contain phases that are thermodynamically stable when in contact with each other. Two phase tie lines are found at any temperature, by determining the Gibb's free energy of reaction (heat of reaction in our case because values of G are not easily obtainable) at the point where two possible tie lines would cross. This can be shown easily in the case of tungsten (W) (the ternary phase diagram is given in **Fig. 1.7**). The question to ask is whether WSi_2 is stable in contact with SiO_2, i.e. is there a tie line between WSi_2 and SiO_2?. To find this out, the values of the heat of reaction are calculated at the point where two tie lines would cross. For the case of WSi_2 and SiO_2, such points would be given by a reaction between WO_2 and Si as well as WO_3 and Si to give SiO_2 and WSi_2 (see **Table 1.2**).

Since all values of ΔH_R obtained are negative, then a tie line exists between WSi_2 and SiO_2 i.e. WSi_2 is stable when in contact with SiO_2 at room temperature (since values of $\Delta H°$ used are those at room temperature). Note that these stable tie lines do not cross. In a similar manner, a stable tie line between W and SiO_2 is established, thus showing that W will not react with SiO_2 at room temperature. It

TABLE 1.2: Heat of reaction calculations to show the presence of a tie line between WSi_2 and SiO_2

Tie line reactions	ΔH_R kJ/(mol.at)
$7\ Si + 2\ WO_3 \longrightarrow 2\ WSi_2 + 3\ SiO_2$	-80.7
$3\ Si + WO_2 \longrightarrow WSi_2 + SiO_2$	-67.8

is very likely that W will not react with SiO_2 even at high temperatures, the order of 1000°C. Actually, Brown *et al.* found that W does not interact with SiO_2 even

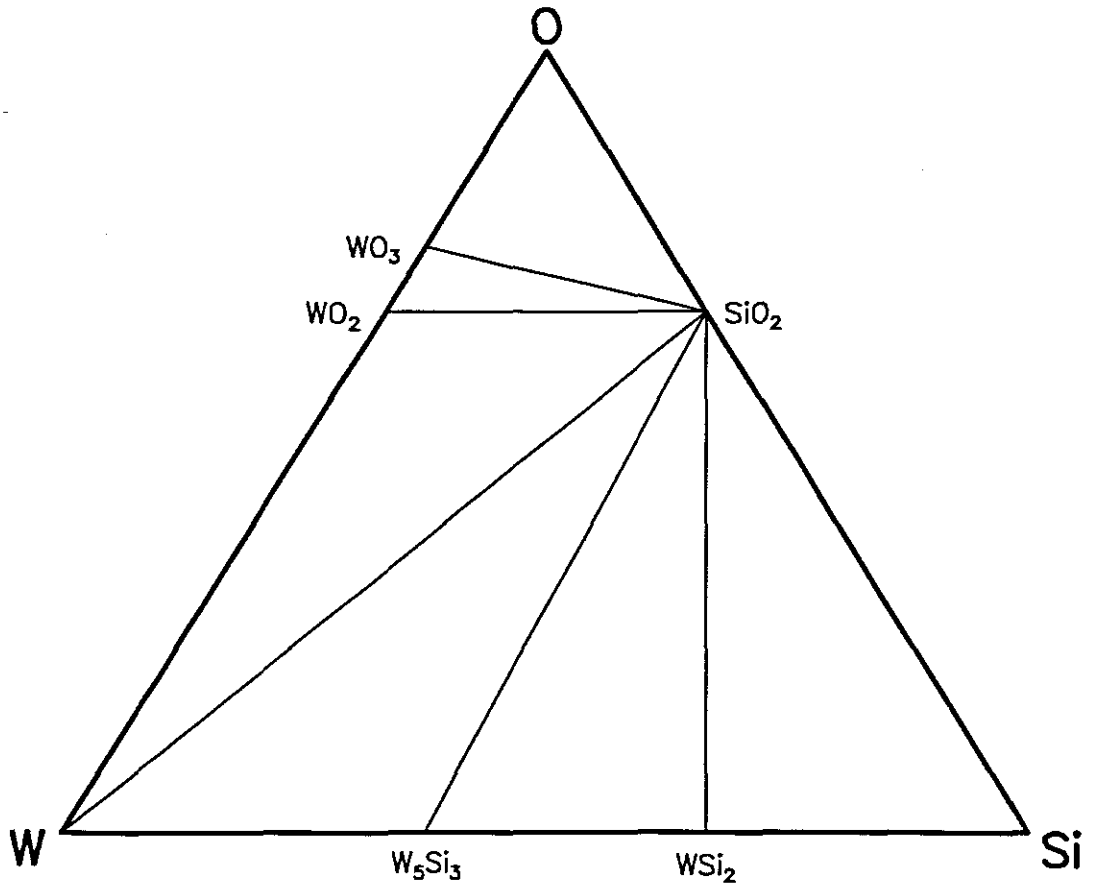

FIGURE 1.7: A ternary phase diagram of the W–Si–O system showing tie lines (solid lines within the large triangle) radiating from SiO_2 (the dominant phase) to W and to the oxides and silicides of W. A tie line between two phases indicates that the two phases are stable in contact with one another. Adapted from Beyers [13] .

at 1100°C [14].

1.4 Scope of this investigation.

Integrated circuit metallization schemes require materials with both low resistivity and high thermal stability. During circuit fabrication, the metallization schemes come into contact with other materials e.g. Si, Al, Ti, SiO_2, etc. at elevated temperatures. The knowledge of the chemical reactions that may result as well as the stability of the metallization is of great importance to the device technologist.

A study of SiO_2 in contact with metals will lead to a better understanding of the physics of solid-state reaction. This study concerns itself with the interaction between SiO_2 and thin metal films. The characterization methods used to find layer thicknesses of deposited materials and the resulting products after annealing are Rutherford Backscattering Spectrometry and X-Ray Diffraction Spectroscopy. The sample characterisation methods are described in chapter 2. Chapter 3 deals with the interaction between refractory metals (Zr, Mo) and SiO_2. Chapter 4 looks at the reaction between rare earth metals (Yb, Y) and SiO_2. Noble metals (Cu, Pt, Ir, Re) in contact with SiO_2 are dealt with in chapter 5. The experimental results found in this investigation and from the literature are then compared with theoretically calculated heats of reaction in Chapter 6 and a correlation with the electronegativity of the metal is investigated. R. Beyers and R. Sinclair [13] showed that ternary phase diagrams could be used to to explain the experimental results. Chapter 7 gives a summary and an overall view of this study of solid state interaction between metals in contact with SiO_2.

CHAPTER 2

EXPERIMENTAL TECHNIQUES.

2.1 Sample preparation.

2.1.1 Preparation and cleaning of wafers.

Commercially obtained silicon wafers of $< 100 >$ orientation were thermally oxidized. These wafers were about 280μm in thickness and 100mm in diameter. The oxide thickness on Si$< 100 >$ was in all cases more than 4000Å. This was done to ensure that after interaction with a metal, some SiO_2 would still be left unreacted. The substrates were cut into 13mm by 13mm squares. This large area ensured a reasonable XRD signal would be reflected from the exposed area of these square wafers. The wafers were then chemically cleaned first with methanol, followed by acetone, then trichloroethylene, acetone, methanol and lastly in deionised water. The stirring was carried out using an ultrasound bath. The resistivity of the deionised water was better than 12MΩcm. The wafers were then attached onto aluminium holders. These holders were then placed onto a rotatable sample holder which was then put inside a high vacuum system (see **Fig. 2.1**).

2.1.2 Vacuum deposition.

A high vacuum system with three crucibles was used. The system has one electron beam. The crucibles can be moved and each can be placed in the path of the electron beam thus allowing one to deposit three different elements sequentially one on top of

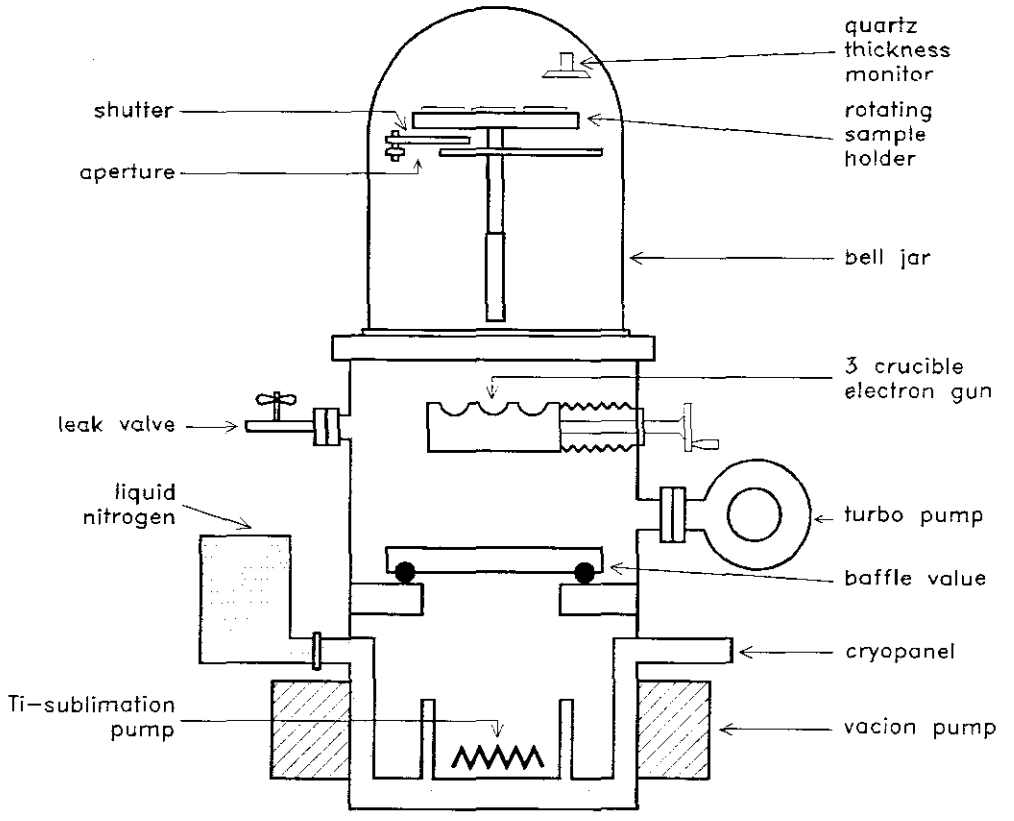

FIGURE 2.1: Sketch showing the high vacuum evaporation system

the other. Crucibles are cleaned before introducing the elements. A shield separates the crucibles from each other so as to avoid cross contamination from one crucible to the other.

The rate of deposition can be varied by changing the electron beam current. Atoms from the element being evaporated then impinge on the surface of the samples which were placed face down on a rotating sample holder. A quartz monitor was used to find the rate of deposition as well as the thickness of the deposited layer. All depositions were done in vacuum of better than 10^{-8}kPa. Vacuum was maintained by means of ion pumps, sublimation pumps, turbopump as well as a cryopanel.

The top part of the vacuum system can be isolated from the bottom part by a baffle valve. This allows vacuum to be maintained at the bottom part while the top is being cleaned and samples changed. The pressure at the bottom can reach 10^{-9}kPa. Pressure was measured by means of a Penning gauge.

The cryopanel at the bottom part helps to trap gases like H_2O and CO_2 thus reducing the pressure. Ion pumps consist of pumping elements surrounded by a

strong magnetic field. A pumping element has a multi-celled anode between two titanium cathode plates. Electrons accelerated between the cathode and the anode make helical paths in the magnetic field. They ionize gas atoms which then drift because of the electric field towards the titanium cathode. Atoms of Ti get sputtered as a result. They then getter the oxygen in the system, thus decreasing the pressure.

The samples onto which deposition had been done were allowed to cool in vacuum for more than five hours. Vacuum was in all cases broken by high grade dry nitrogen to prevent oxidation and contamination of the samples. Samples that oxidized easily were kept in a dessicator under vacuum before and after annealing.

2.1.3 Vacuum annealing.

The thin films were annealed so as to accelerate interaction between the metal film and the SiO_2 substrate. All anneals were done in vacuum at pressures of better than 10^{-7}kPa. Quartz boats in which samples were annealed were first preheated so as to drive out any gases from these boats. Up to eight samples could be annealed sequentially at different temperatures by inserting them in turn into the annealing oven from a rotating carousel. A platinel II thermocouple was used to monitor the temperature and stabilize it to any desired preset value.

Vacuum was maintained by means of a turbomolecular pump and a mechanical forepump. A cold nitrogen trap was used to reduce the pressure further. After annealing, samples were left in vacuum for up to five hours. Vacuum was broken by letting in dry nitrogen so as to minimize oxidation.

2.2 Sample characterisation.

Two characterisation methods were used to identify resulting compound phases after annealing.

2.2.1 Rutherford Backscattering Spectrometry

Backscattering spectrometry using a monoenergetic (2MeV) and collimated beam of $^4He^+$ particles together with a computer aided simulation of RBS were used to determine:

- the relative atomic composition i.e. stoichiometry of the compounds/phases of thin metal films deposited on SiO_2 before and after annealing them.

- the thickness of metal films (and their resultant compounds/phases) deposited on SiO_2 before and after annealing them.

Measurement of the number and energy of the $^4He^+$ particles backscattered from atoms in the near surface region allows for:

- identification of the atomic mass of the target element ie

$$E_\alpha \propto \text{mass}$$

.

- determination of the distribution of target elements as a function of depth below the surface i.e.

$$\frac{dE}{dx}$$

is the depth scale.

- the scattering cross section, σ where

$$\sigma \propto Z^2$$

.

Application of this technique is illustrated in **Fig. 2.2** for the ideal case of a two element thin film of uniform composition on a low mass substrate.

$^4He^+$ particles scatter elastically from target atoms with energies characteristic of the mass of the struck particle. They lose energy as they pass in and out of the material film. Energy analyses of the backscattered $^4He^+$ particles by the detection system yields the backscattering spectrum shown in the lower diagram in the form of counts per channel versus channel number. The channel number is linearly related to the backscattered energy E_1. Appearing in the spectrum is a nearly flat topped peak for each element present in the film. The peak widths are caused by the energy loss of the alpha particles.

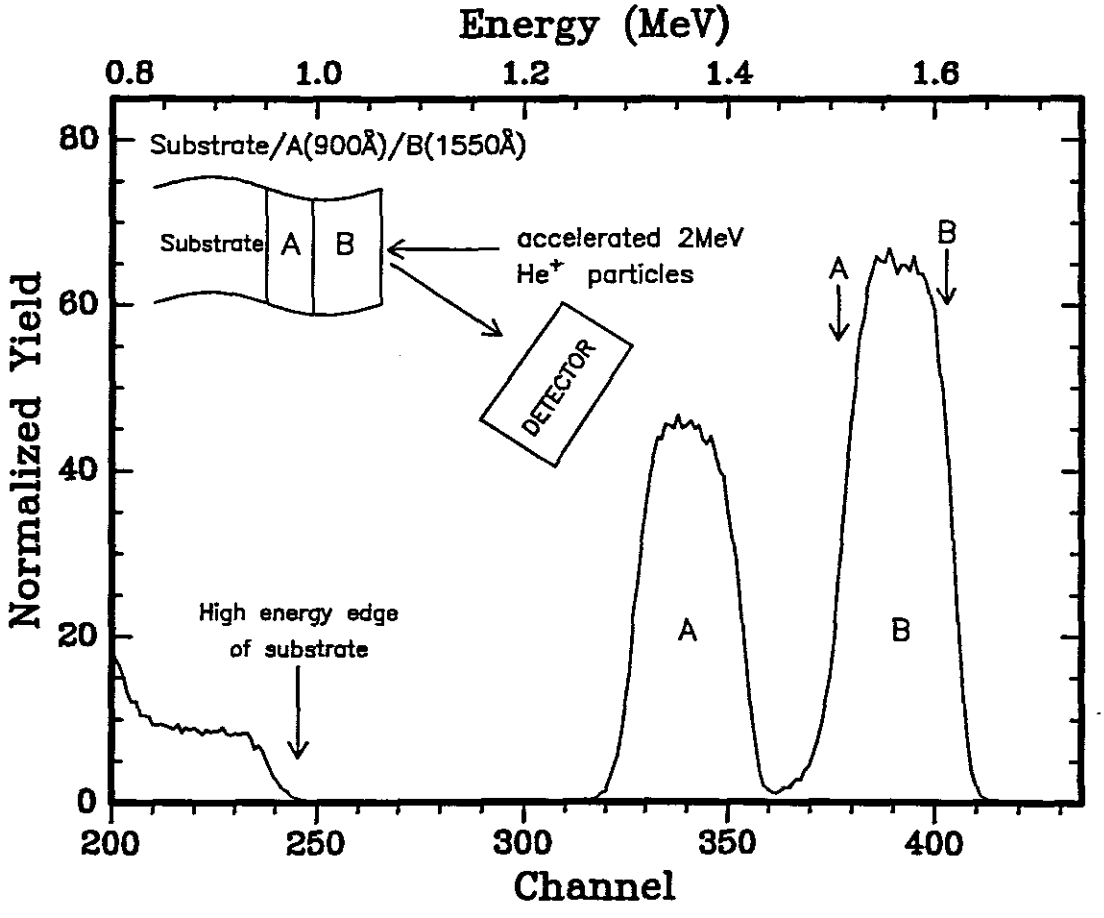

FIGURE 2.2: Backscattering spectrometry. The insert diagram shows a sample with the following profile: substrate/A(900Å)/B(1550Å). 2Mev He^+ particles scatter from the sample onto a detector. The spectrum shows a plot of the number of counts (or the yield) as a function of the energy of the scattered particles. The arrows indicate the surface position energies for elements A and B. These positions are dependent on the atomic mass, while the counts are dependent on the square of the atomic number i.e. Z^2.

The film elements may be identified by insertion of measured energies (E_1^A; E_1^B) of the high energy sides of the peaks into

$$K_i = \frac{E_1^i}{E_o} \tag{2.1}$$

to calculate the kinematic factor K for the i th element. E_o is the incident ion's laboratory kinetic energy. Application of conservation of energy and momentum leads to the kinematic factor K being given by

$$K = \left[\frac{(M^2 - m^2 \sin^2\theta)^{\frac{1}{2}} + m\cos\theta}{M+m}\right]^2 \tag{2.2}$$

where θ is the laboratory angle through which the incident ion is scattered, and m and M are the masses of the incident and target particles respectively. Since the parameters m, E_o and θ are usually known, M is determined and the target element is identified.

If t is the film thickness and N_i the atomic density of the i th element, then $(Nt)_i$ is the areal density, given by

$$(Nt)_i = \frac{A_i \cos\theta_1}{Q\Omega\sigma_i(E,\theta)} \tag{2.3}$$

A_i is the integrated peak count for the Q ions which are incident at angle θ_1. Ω is the detector solid angle and σ_i the cross section.

The average stoichiometric ratio for the compound film A_xB_y is given by

$$\frac{y}{x} = \frac{N_B}{N_A} = \frac{A_B}{\sigma_B}\frac{\sigma_A}{A_A} \tag{2.4}$$

In this equation, the hard to measure quantities Q and Ω have cancelled.

Given that the film density is ρ_{AB},

and that $M_{AB} = xM_A + yM_B$ is the molecular weight of compound A_xB_y, we have

$$N_A^{AB} = \frac{x\rho_{AB}A_v}{M_{AB}} \tag{2.5}$$

and

$$N_B^{AB} = \frac{y\rho_{AB}A_v}{M_{AB}} \tag{2.6}$$

where A_v is Avogadro's number and N_A^{AB} the atomic density of A in compound AB, N_B^{AB} the atomic density of B in compound AB. Thus

$$t = \frac{(Nt)_A}{N_A^{AB}} = \frac{(Nt)_B}{N_B^{AB}} \tag{2.7}$$

1-2 MeV ^{4}He ions have been used for the preceeding analysis for the following reasons

- data for the energy loss of ^{4}He ions in the elements are better known than for other ions.
- the silicon surface barrier detector energy resolution for ^{4}He is about 15keV.
- the backscattering cross section for ^{4}He ions incident on all elements more massive than Be are nearly all Rutherford in this energy region.

The principal strengths of Rutherford backscattering (RBS) with ^{4}He ions are

- it is an absolute method in that it does not require the use of standards.
- it is quick and easy; typical data acquisition is about 10 minutes.
- it is frequently non-destructive.
- it may be used for depth profiling, with 10-30nm depth resolution.

The principal failure of this technique is its failure to analyze trace elements.

For fixed θ, the energy separation ΔE, for beam particles scattered by target particles of mass M is

$$\Delta E = E_0 \left(\frac{dK}{dM}\right) \Delta M \tag{2.8}$$

If ΔE is set equal to δE, the minimum energy separation that can be experimentally resolved, then δM, the mass resolution of the system is

$$\delta M = \frac{\delta E}{E_0 \left(\frac{dK}{dM}\right)} \tag{2.9}$$

δE contains contributions from detector resolution, straggling, beam energy spread and various geometric effects.

The mass resolution at the sample surface is determined mainly by the detector resolution. For deeper layers, straggling dominates.

The average differential cross section, $\sigma(\theta; E)$ for scattering of beam particles of energy E by target particles in a thin film is defined by

$$\sigma(\theta; E) = \left(\frac{1}{Nt}\right) \frac{dQ(E)}{Q} \frac{1}{\Omega(\theta)} \tag{2.10}$$

where Nt is the number of target atoms/unit area perpendicular to the beam, and $\frac{dQ(E)}{Q}$ is the fraction of incident particles scattered into the small solid angle $\Omega(\theta)$ centred at the deflection angle θ.

If scattering is Rutherford (pure Coulomb), then the scattering cross section is

$$\sigma_R(E, \theta) = \left(\frac{Z_1 Z_2 e^2}{4E}\right)^2 \times \frac{4[(M^2 - m^2 \sin^2\theta)^{\frac{1}{2}} + M\cos\theta]^2}{M \sin^4\theta (M^2 - m^2 \sin^2\theta)^{\frac{1}{2}}} \tag{2.11}$$

where Z_1 and Z_2 are the atomic numbers of the incident and target atoms respectively. This equation is in cgs units with

$$e^2 \approx 1.44 \times 10^{-12} \text{MeVcm}$$

An accurate approximation for large backscattering angles and $\left(\frac{m}{M}\right) \ll 1$ is

$$\sigma_R(E, \theta) \approx 0.02073 \left(\frac{Z_1 Z_2}{4E}\right)^2 \left[\sin^{-4}\left(\frac{\theta}{2}\right) - 2\left(\frac{m}{M}\right)^2\right] \tag{2.12}$$

The IBM and Cornell geometries are the common experimental arrangemets. For both geometries the incident beam is horizontal and the sample surface is vertical. In the IBM geometry, the scattered beam (directed at the detector) and the incident beam are in the same horizontal plane.

In the Cornell geometry, the incident and the scattered beam are in the same vertical plane, with the detector directly below the incident beam. In both geometries the angle between the incident beam and the sample normal is θ_1, while the angle between the scattered beam and the sample normal is θ_2. The tilt axis is a vertical axis through the beam spot on the sample surface. θ_1 is the tilt angle.

For the IBM geometry, $\theta = \pi - \mid \theta_1 \pm \theta_2 \mid$. For the Cornell geometry $\cos\theta_2 = \cos(\pi - \theta)\cos\theta_1$. The geometry used in our case is the IBM geometry.

The mass resolution at the sample surface is determined mainly by the detector resolution. For deeper layers, straggling dominates.

The average differential cross section, $\sigma(\theta; E)$ for scattering of beam particles of energy E by target particles in a thin film is defined by

$$\sigma(\theta; E) = \left(\frac{1}{Nt}\right) \frac{dQ(E)}{Q} \frac{1}{\Omega(\theta)} \tag{2.10}$$

where Nt is the number of target atoms/unit area perpendicular to the beam, and $\frac{dQ(E)}{Q}$ is the fraction of incident particles scattered into the small solid angle $\Omega(\theta)$ centred at the deflection angle θ.

If scattering is Rutherford (pure Coulomb), then the scattering cross section is

$$\sigma_R(E, \theta) = \left(\frac{Z_1 Z_2 e^2}{4E}\right)^2 \times \frac{4[(M^2 - m^2 \sin^2\theta)^{\frac{1}{2}} + M\cos\theta]^2}{M \sin^4\theta (M^2 - m^2 \sin^2\theta)^{\frac{1}{2}}} \tag{2.11}$$

where Z_1 and Z_2 are the atomic numbers of the incident and target atoms respectively. This equation is in cgs units with

$$e^2 \approx 1.44 \times 10^{-12} \text{MeVcm}$$

An accurate approximation for large backscattering angles and $\left(\frac{m}{M}\right) \ll 1$ is

$$\sigma_R(E, \theta) \approx 0.02073 \left(\frac{Z_1 Z_2}{4E}\right)^2 \left[\sin^{-4}\left(\frac{\theta}{2}\right) - 2\left(\frac{m}{M}\right)^2\right] \tag{2.12}$$

The IBM and Cornell geometries are the common experimental arrangemets. For both geometries the incident beam is horizontal and the sample surface is vertical. In the IBM geometry, the scattered beam (directed at the detector) and the incident beam are in the same horizontal plane.

In the Cornell geometry, the incident and the scattered beam are in the same vertical plane, with the detector directly below the incident beam. In both geometries the angle between the incident beam and the sample normal is θ_1, while the angle between the scattered beam and the sample normal is θ_2. The tilt axis is a vertical axis through the beam spot on the sample surface. θ_1 is the tilt angle.

For the IBM geometry, $\theta = \pi - \mid \theta_1 \pm \theta_2 \mid$. For the Cornell geometry $\cos\theta_2 = \cos(\pi - \theta)\cos\theta_1$. The geometry used in our case is the IBM geometry.

RBS only gives the ratio of different atomic species and cannot tell whether a compound phase has formed. To confirm whether there is a compound phase or not, X-ray diffraction techniques are used.

2.2.2 X-ray diffraction spectroscopy.

To find out which compound phases were present in the samples after annealing, X-ray diffraction was done on the samples. The machine used was a Phillips vertical diffractometer employing the Bragg-Brentano geometry (see **Fig. 2.3**). Both the sample and the detector move, with the detector moving an angle of 2θ for each θ moved by the sample. This geometry is suitable for thin films since it gives reflections from atomic planes parallel to the surface of the sample.

Monochromatic X-rays from a Cu tube were used. These get reflected into an X-ray detector. Sample detector movements are controlled from an external computer. Signals from the detector are then fed to the computer for analysis. Step size and duration of data acquisition could be chosen at will. The JCPDS diffraction data files were used to identify the compound phases present in the sample.

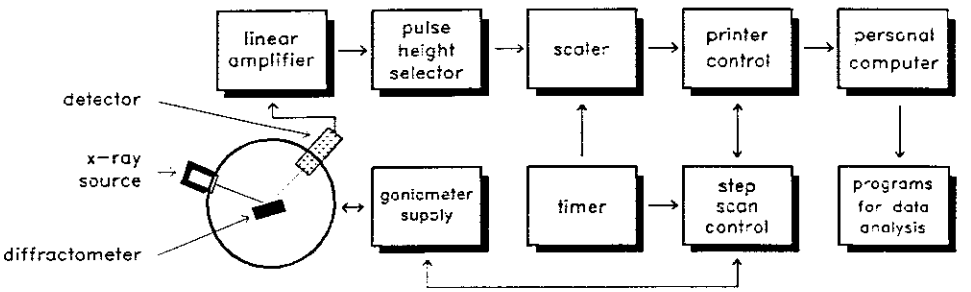

FIGURE 2.3: The essential features of an X-ray Diffractometer

CHAPTER 3

REFRACTORY METALS.

3.1 Introduction.

Silicides of refractory metals find wide application in integrated circuit metallization schemes. The interest in refractory metal silicides stems from their high thermal stability and low resistivities [12]. When a circuit involving pure refractory metals is being fabricated, the metals come into contact with SiO_2, hence a knowledge of the reaction between SiO_2 and the refractory metals is important in the understanding of the stability of devices.

In previous studies of the reaction between refractory metals and SiO_2, it was found that some refractory metals such as V, Ti and Nb react with SiO_2 [3], while others like Mo and W do not [12]. For those refractory metals that do react, it was found that a silicide layer formed next to the SiO_2 and an oxide near the surface region.

In this study we revisit the interaction between refractory metals and SiO_2 (this chapter): reaction between noble metals and SiO_2 (chapter 4) and reaction between SiO_2 and rare earth metals (chapter 5). The aim is to confirm those reactions that are known, to study systems that have not been studied before and to compare SiO_2 reactions involving SiO_2 and refractory metals, noble metals and rare earth metals.

3.2 Experimental.

Commercial silicon wafers of < 100 > orientation, covered with thermally grown SiO_2 were cut into 13mm by 13mm squares and then chemically cleaned and rinsed in de-ionised water (resistivity $\approx$ 12MΩcm) in an ultrasonic bath. The relatively large surface area of the samples made it possible to easily detect X-ray diffraction signals.

Thin layers of the refractory metals zirconim (Zr) and molybdenum (Mo) were then deposited on the wafers under vacuum by means of electron beam heating. The thickness of the SiO_2 layer was about 8000Å to ensure that after interaction with the metal some SiO_2 would be left. The samples were allowed to cool while remaining under vacuum to avoid thermal oxidation from the ambient. The Si< 100 >/SiO_2/metal samples were then put into pre-heated boats and annealed for various periods of time in an oil free vacuum system, with vacuum better than 10^{-7} kPa. The purpose of pre-heating the boats was to reduce sample contamination during annealing from the gases that they may have absorbed. All samples were analyzed by Rutherford Backscattering Spectrometry (RBS) using a beam of accelerated 2MeV α particles. RUMP (Rutherford Utilities and Manipulation Program) simulation was used to determine the thicknesses of the metal and SiO_2 layers as well as the thicknesses of the compound phases formed. Phase identification was carried out by means of X-ray diffraction (XRD) and the subsequent analysis of the X-ray spectra using JCPDS diffraction data files.

3.3 Results.

3.3.1 Zr-SiO_2.

A 1600Å layer of zirconium (Zr) was evaporated by means of an electron beam onto Si< 100 > wafers, covered with thermally grown SiO_2. The deposition was done under vacuum that was oil free and was about 3×10^{-8}kPa. The deposition rate was maintained at approximately 3.0Å/s. The Zr-SiO_2 samples were then annealed for 30 minutes at various preset temperatures in a vacuum furnace whose pressure was

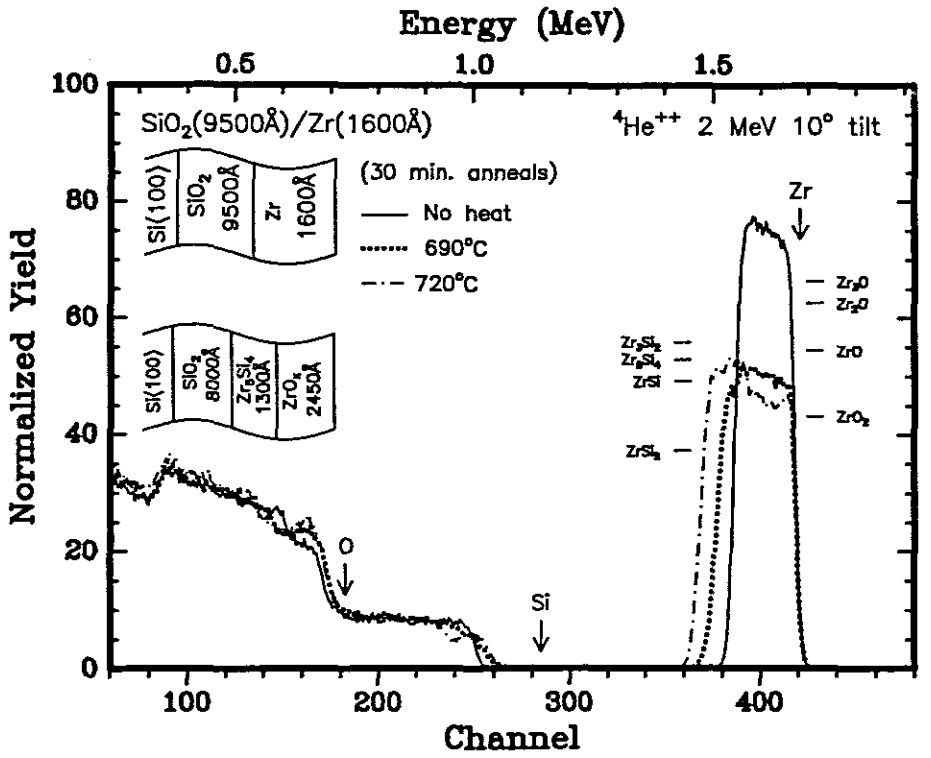

FIGURE 3.1: Backscattering spectra of Si< 100 >/SiO_2(9500Å)/Zr(1600Å) samples as-deposited and annealed for 30 minutes at various temperatures. The as deposited sample shows no interaction. The sample annealed at 690°C has Zr_5Si_4 next to the SiO_2 and ZrO_x with $x \simeq 1.8$ on the surface. The sample annealed at 720°C shows the presence of both Zr_5Si_4 and ZrO_2.

of the order of 10^{-8}kPa. Results of Rutherford Backscattering Spectrometry (RBS) for the as deposited (i.e. no heat) sample as well as samples annealed at 690°C and at 720°C are shown in **Fig. 3.1**. The thickness of the SiO_2 on top of the bulk Si< 100 > was 9500Å. Signal heights are shown next to the Zr signal. The as deposited sample shows no interaction between the Zr and the SiO_2. The signal height of the sample annealed at 690°C has been reduced showing that there has been an interaction between SiO_2 and Zr. The Si signal of the Si in SiO_2 has also moved forward. It has however not reached the surface position of Si, showing that there is no Si on the surface. The spectrum height on the front part of the Zr signal corresponds to ZrO_x with $x \simeq 1.8$, meaning that both ZrO and ZrO_2 may be present in the sample (see **Fig. 3.1**). The height of the back part of the Zr signal

corresponds to the formation of Zr_5Si_4. The sample annealed at 720°C shows the formation of ZrO_2 on the surface and Zr_5Si_4 next to the SiO_2. For both annealed samples there is no free Zr. **1997 JCPDS** International Centre for Diffraction Data files were used to identify compound phases resulting from the interaction of SiO_2 and Zr. **Fig. 3.2** is an X-Ray Difraction spectrum of Zr-SiO_2 samples annealed at various temperatures. The unannealed sample shows that the deposited Zr is already crystalline. It also shows that there has not been any interaction between Zr and SiO_2. This is in agreement with the RBS results. The spectrum of the sample annealed at 690°C shows the presence of Zr_5Si_4, ZrO_2 and ZrO. This is in agreement with the RBS observation. All the free Zr has been consumed on this sample. Note that the Zr_5O_4 signal overlaps with the ZrO_2 signal. A similar experiment **[15]** also showed that the silicide was Zr_5Si_4. These XRD results are consistent with the RBS results. The XRD spectrum of the sample annealed at 720°C shows the presence of Zr_5Si_4 and ZrO_2. There is no unique ZrO signal.

3.3.2 Mo-SiO_2.

Thermally oxidized substrates of Si< 100 > were chemically cleaned and loaded into a high vacuum evaporation system. Molybdenum (Mo) metal was then deposited onto the SiO_2 covered Si< 100 > substrates at an average rate of 2.4Å/s. Vacuum was maintained at about 1×10^{-7}kPa. The samples were allowed enough time to cool while remaining in vacuum before they were transferred into a vacuum annealing furnace and annealed at various temperatures. RBS was then carried out on the samples.

Fig. 3.3 is an RBS spectrum of the Mo on SiO_2 samples for the unheated sample and the samples annealed at 800°C and at 900°C for 3 hours respectively. The as deposited sample shows no interaction between the Mo and the SiO_2. The sample annealed at 800°C is similar to the unannealed sample. The sample annealed at 900°C also shows no interaction. We conclude therefore from the RBS results that there is no interaction between Mo and SiO_2 for temperatures of up to 900°C.

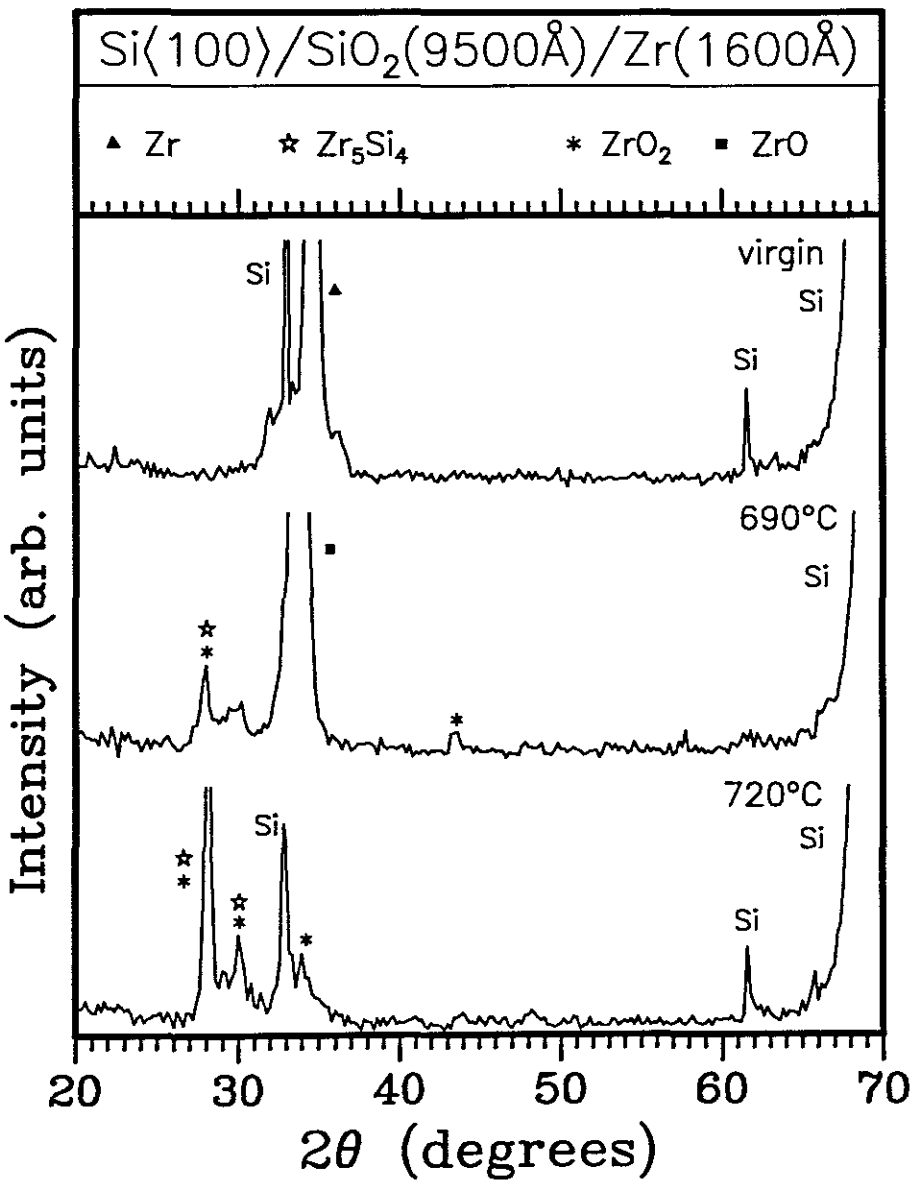

FIGURE 3.2: X-ray diffraction spectra of Si< 100 >/SiO_2(9500Å)/Zr(1600Å) samples annealed at different temperatures for 30 minutes. The sample annealed at 690°C indicates the presence of Zr_5Si_4, ZrO and ZrO_2. The sample annealed at 720°C shows the presence of Zr_5Si_4 and ZrO_2.

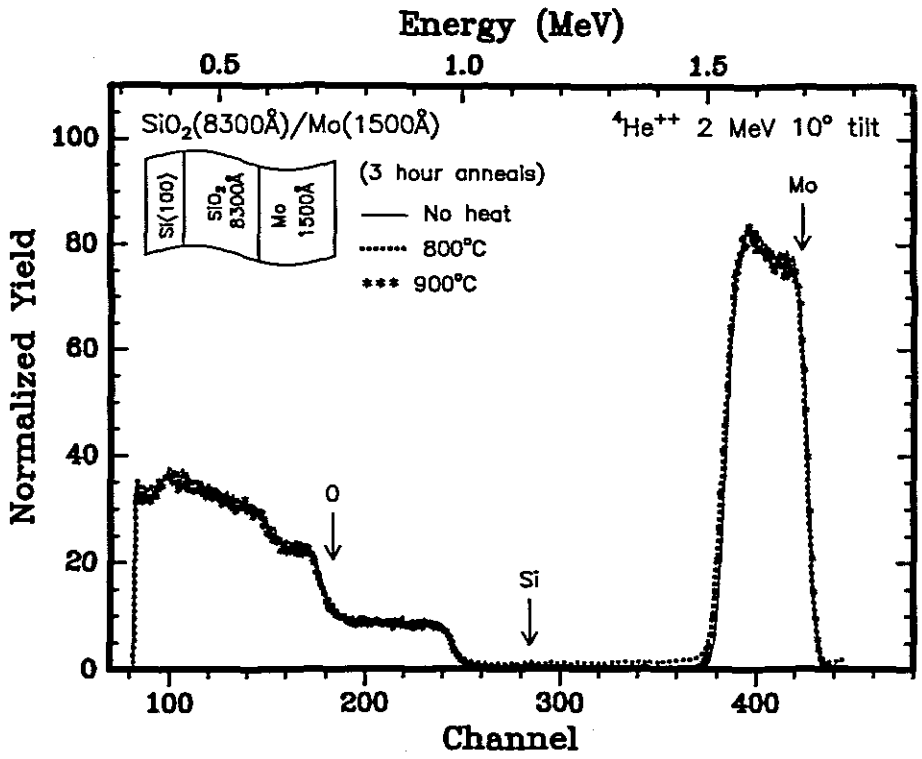

FIGURE 3.3: Backscattering spectra of Si< 100 >/SiO_2(8300Å)/Mo(1500Å) samples as-deposited and annealed for 3 hours at two different temperatures. The as deposited sample and the samples annealed at 800°C and 900°C show no interaction.

3.4 Summary and conclusion.

RBS experimental investigations done on thin film couples of Zr on thermally grown SiO_2 revealed that Zr reacts with SiO_2 at temperatures of about 700°C. The compound phases resulting from these interactions were revealed by RBS and X-ray diffraction to be Zr_5Si_4 and ZrO_2. The silicide Zr_5Si_4 was found to form adjacent to the unreacted SiO_2 whereas the oxide ZrO_2 formed on the surface. The resulting structure was $SiO_2/Zr_5Si_4/ZrO_2$. The XRD results were found to be in agreement with the RBS results. These results are in agreement with those obtained by other workers [3, 15, 16].

Our experimental investigations revealed that Mo does not react with SiO_2 when annealed in vacuum at temperatures of up to 900°C for 3 hrs. This observation shows that some refractory metals do not react with SiO_2.

CHAPTER 4

RARE EARTH METALS.

4.1 Introduction.

Rare earth metals find use as gate materials in solar cells and they also have been used in chemical sensors [17]. There is already a large body of scientific knowledge concerning the behaviour of refractory metals when in contact with SiO_2, but a lack of information with regards to the behaviour of rare earths. Available literature is sketchy at best and though it is mentioned that rare earths react with SiO_2 there is no mention of compound phases resulting from such chemical reactions [18].

In this work chemical reactivity between Yb and SiO_2 as well as between Y and SiO_2 has been investigated. Rare earths oxidize readily in air and in our study we have sandwiched rare earths with SiO_2 from both sides to prevent oxidation. The one side having thermally grown SiO_2 while the other had electron-beam deposited SiO_2. This also allowed a comparison between these two differently prepared layers. Thermodynamic data has also been used to explain the results obtained.

4.2 Experimental.

Thermally oxidized Si< 100 > wafers were cut into 13mm by 13mm squares, chemically cleaned and finally rinsed in deionized water ($\approx$12MΩcm resistivity). Thin layers of the rare earth metals Y and Yb were deposited on these Si< 100 >

wafers. The thickness of the oxide layer was about 9000Å to make sure that after interaction with the metal some SiO_2 is left. The Si/SiO_2/Metal samples were annealed in an oil free vacuum system, with vacuum better than 10^{-7} kPa. All samples were analyzed using RBS. The RBS results were used to determine the thicknesses of the metal and SiO_2 layers as well as the thicknesses of the compound phases formed. Phase identification was done by means of XRD spectrometry. JCPDS X-ray diffraction files were used to analyse the XRD spectra.

A 4000Å layer of Yb was electron-gun evaporated onto thermally grown and chemically cleaned SiO_2 substrates in vacuum. The deposition rate was maintained at an average of 3.0Å/s. The vacuum was oil free and better than 10^{-7}kPa. The thickness of the SiO_2 on top of the bulk Si< 100 > was 9000ÅThe ytterbium film was then covered with a 4500Å layer of SiO_2 electron-beam deposited at the same rate as the Yb, without breaking vacuum.The covering SiO_2 was obtained by evaporating ground quartz, using an electron beam. The covering layer of SiO_2 was intended to protect the ytterbium from possible surface oxidation during annealing. The Si< 100 >/SiO_2/Yb/SiO_2 samples were annealed for 30 minutes at specific preset temperatures in a vacuum furnace whose pressure was better than 10^{-7}kPa.

A 3000Å layer of yttrium (Y) was deposited by means of an electron beam on thermally oxidized silicon wafers at a rate of about 3.0Å/s. The deposition was done under a vacuum of the order of 10^{-8}kPa. The thickness of the SiO_2 substrate and the Y film were 9000Å and 3000Å respectively. The Y was then covered with a 5300Å layer of SiO_2. The overlying SiO_2 was obtained by evaporating ground quartz using electron beam heating. The vacuum was constantly monitored throughout the deposition. The overlying SiO_2 layer was intended to protect the Y film from oxygen contamination during annealing since Y oxidizes readily. The Si< 100 >/SiO_2/Y/SiO_2 samples were then placed in quartz boats and annealed at preset temperatures in a vacuum annealing furnace for 30 minutes. The vacuum was of the order of 10^{-8}kPa. The samples were then annalyzed using RBS and XRD techniques.

4.3 Results.

4.3.1 Yb-SiO_2.

Fig. 4.1 shows results of Rutherford Backscattering Spectrometry (RBS) for Yb deposited on an SiO_2 substrate and covered with an SiO_2 cap. The as deposited sample shows *no interaction*. The signal height of the sample annealed at 320°C has broadened showing that there has been interdiffusion between SiO_2 and Yb. The Si signals of the Si in the SiO_2 films on both sides of Yb have also moved forward and backwards due to interdiffusion between the various layers. The Si and O signals

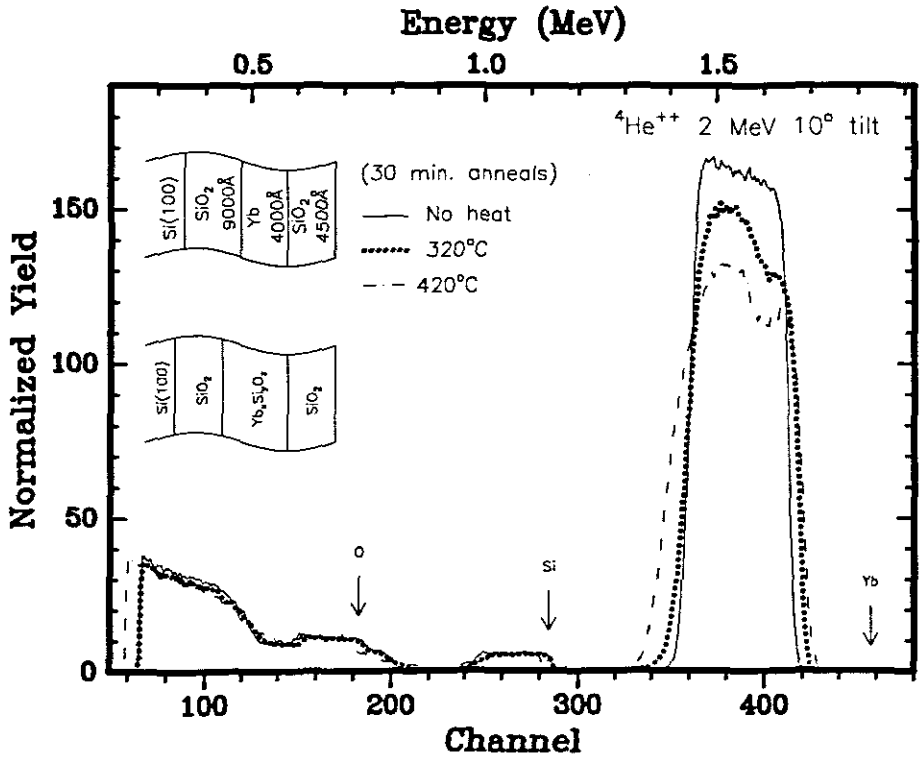

FIGURE 4.1: Rutherford backscattering spectra of three samples with original profile Si< 100 >/SiO_2(9000Å)/Yb(4000Å)/SiO_2(4500Å). Included is the as-deposited sample and two samples annealed for 30 minutes at different temperatures. The as deposited sample shows no interaction. The samples annealed at 320°C and at 420° shows asymmetry in the Yb signal. The ternary phases shown on the annealed sample gave the best fit on the RBS spectrum.

remain at the surface position thereby confirming the presence of SiO_2 on the surface of the sample.

It is clear from the RBS spectrum in **Fig. 4.1** that the interdiffusion or possibly interaction between the Yb and the two SiO_2 layers, thermally grown and deposited do not happen at the same rate. This can be seen from the fact that the Yb signals of the samples annealed at 320°C and 420°C are asymmetrical. A theoretical fit on the Yb spectrum revealed that the sample consisted of a ternary mixture of Yb, O and Si in the reaction region. The structure of the sample was found to be $Si< 100 >/SiO_2/Yb_xSi_yO_z/SiO_2$. It was difficult to determine the exact compound phases in the sample using RBS.

Fig. 4.2 shows the XRD spectra of samples annealed in vacuum at various temperatures. These samples have the profile $Si< 100 >/SiO_2/Yb/SiO_2$ before annealing. The spectrum of the unannealed sample shows that the deposited Yb has crystallized. Within the limits of the sensitivity of XRD, no oxidation was observed on the unannealed sample.

The XRD spectrum of the sample annealed at 320°C shows that a solid state reaction has taken place. It reveals that the compound phases Yb_5Si_3, Yb_3O_4 and Yb_2O_3 were present in the sample. It also shows that some crystalline Yb was still present (unreacted). Combining the information obtained from the RBS results and that obtained from the XRD analysis, it can be concluded that those phases present in the sample do not occur in discrete well defined layers. They must be a non-homogeneous mixture of various compositions, distributed in the reacted region. The **JCPDS** International Centre for Diffraction Data files showed that Yb has no ternary compound phases.

The XRD spectrum of the sample annealed at 420°C shows that this sample has the compound phases Yb_3Si_5, Yb_3O_4, Yb_2O_3 and Yb_5Si_3. The spectrum shows no unreacted Yb (in crystalline form).

Fig. 4.3 shows the RBS spectra of Yb on SiO_2 without an SiO_2 cap. The SiO_2 layer was found to be about 8000Å in thickness. The deposited Yb was 3700Å in thickness. The RBS spectrum of the unannealed sample shows no oxidation. The

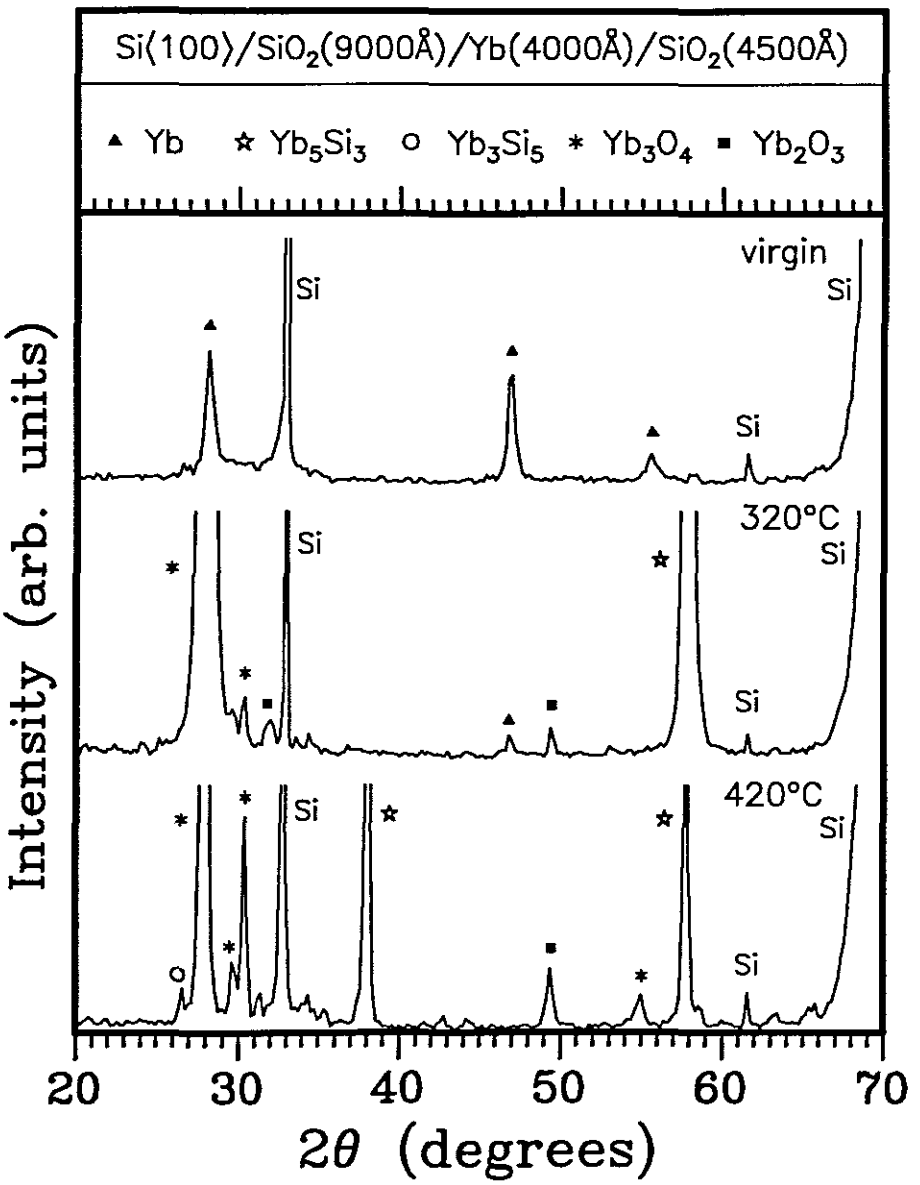

FIGURE 4.2: X-ray diffraction spectra of samples with original composition Si< 100 >/SiO_2(9000Å)/Yb(4000Å)/SiO_2(4500Å) samples showing a virgin sample, a sample annealed at 320°C and one annealed at 420°C for 30 minutes. The compound phases Yb_5Si_3, Yb_3Si_5, Yb_3O_4 and Yb_2O_3 were identified.

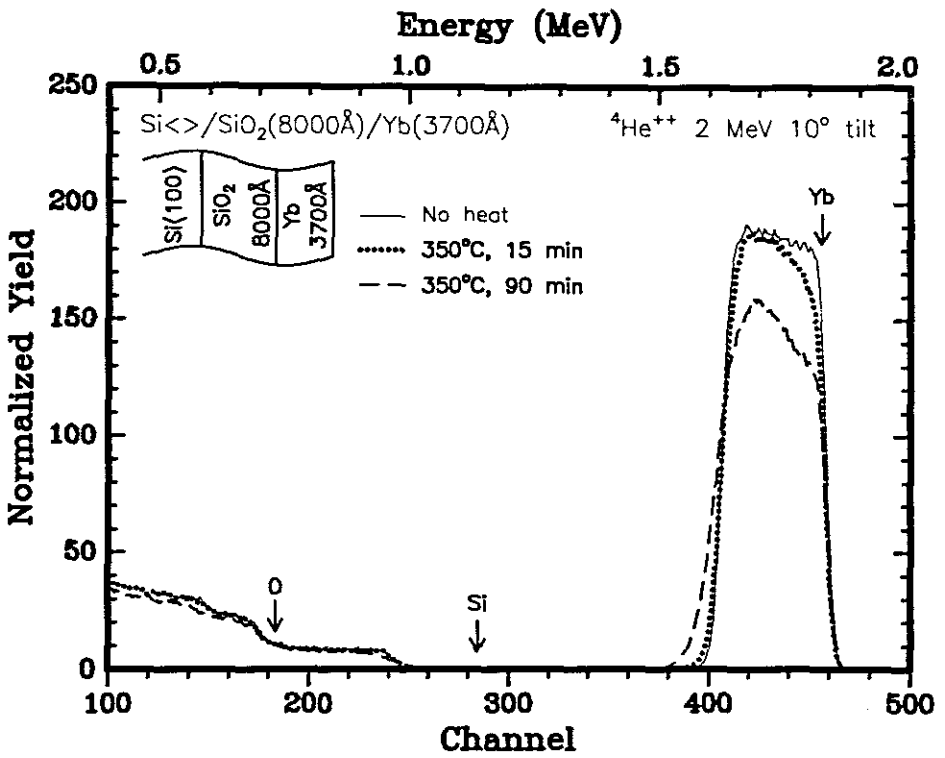

FIGURE 4.3: RBS spectra of Si< 100 >/SiO_2(8000Å)/Yb(3700Å)/) samples without an SiO_2 cap showing a virgin sample, a sample annealed at 350°C for 15 minutes and a sample annealed at 350°C for 90 minutes. The Yb peak gradually diminishes with an increase in annealing time, suggesting loss of material probably due to the formation of volatile oxides.

RBS spectrum of the sample annealed at 350°C for 15 minutes shows that there has been interdiffusion and possibly a chemical reaction between Yb and SiO_2. Looking at the spectrum of the sample annealed at 350°C for 90 minutes, it can also be seen that the surface area of the Yb signal has been reduced in size. It is suspected that there may be some volatile phases formed during annealing. This effect is more pronounced on those samples annealed at higher temperatures (not shown here).

4.3.2 Y-SiO_2.

Fig. 4.4 shows an RBS spectrum of an as deposited Si< 100 >/SiO_2/Y/SiO_2 sample (see the solid line) as well as that of two other samples of the same compo-

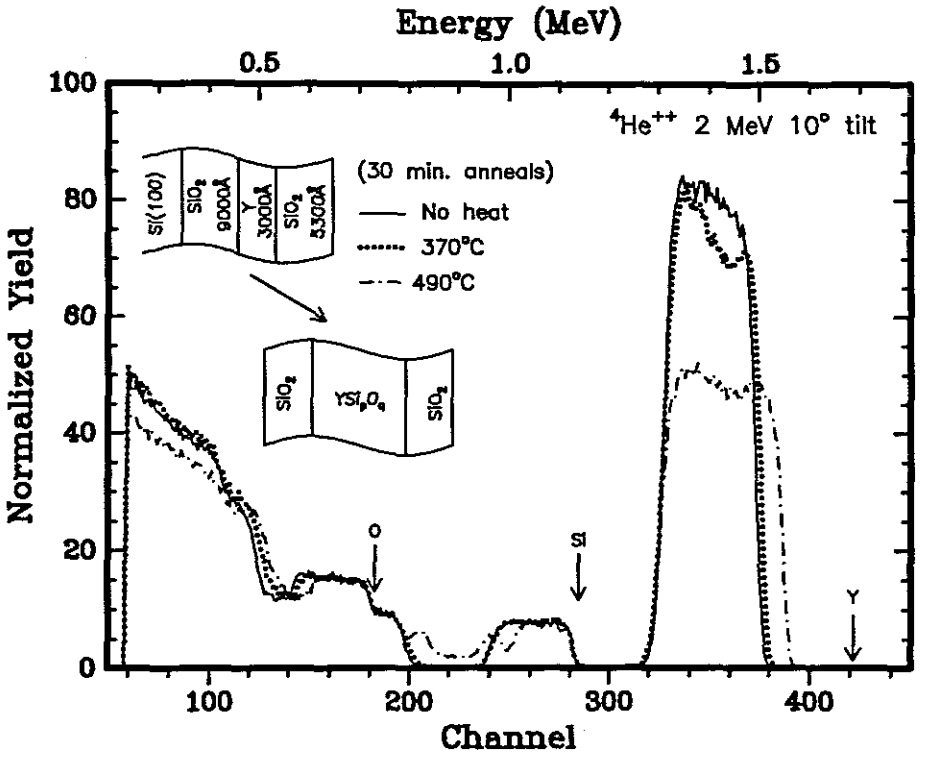

FIGURE 4.4: The diagram shows the backscattering spectra of Si< 100 >/SiO_2(9000Å)/Y(3000Å)/SiO_2(5300Å) samples as-deposited and annealed for 30 minutes at various temperatures. The as deposited sample show no interaction. The sample annealed at 370°C shows that a reaction has started. The sample annealed at 490°C shows a composition YSi_pO_q where p and q vary with distance from the thermally grown SiO_2 interface.

sition annealed at 370°C (see the dotted line) and at 490°C (see the broken line) for 30 minutes each. The RBS spectrum of the as deposited sample clearly shows the elements O and Si to be occupying surface positions (see arrows) thus confirming that the deposited SiO_2 film is indeed at the surface. The Y signal lies at an energy less than its surface position energy (see arrow), due to the top SiO_2 layer.

The Y signal in the RBS spectrum of the sample annealed at 370° has developed a step and has moved slightly towards the surface position of Y. As the change is so small, we conclude that interdiffusion and/or interaction between Y and SiO_2 has just begun at this temperature. For the RBS spectrum of the sample annealed at a higher temperature i.e. 490°C, the effects observed in the RBS spectrum of the

sample annealed at 370°C are more pronounced. The height of the Y signal has been further reduced whilst its width has broadened. However, the area of the signal does not appear to have decreased. We conclude that no loss of Y has occured. The lower energy edge of the Si signal from the overlying SiO_2 has shifted backwards whilst the higher energy edge of the Si signal due to the SiO_2 substrate has moved forward. We conclude that the SiO_2 in both the top and bottom layers reacts with Y. By using the RUMP simulation to obtain a fit on the RBS spectrum corresponding to 490°C, a ternary mixture was obtained, with SiO_2 layers on either side of it, i.e. $Si< 100 >/SiO_2/YSi_pO_q/SiO_2$. However, the ternary phase could not be identified from our RBS results.

XRD was done on an unannealed sample with structure $Si< 100 >/SiO_2/Y/SiO_2$. No oxidation could be detected on this sample (see **Fig. 4.5**). Samples of the same structure annealed at temperatures below 300°C for 30 minutes were found using XRD techniques to have not reacted. This result is in agreement with our RBS results. A sample annealed at 370°C for 30 minutes was however found to have reacted resulting in compound phases γ-$Y_2Si_2O_7$, Y_2SiO_5 and α-$Y_2Si_2O_7$. It was also found that there was still unreacted Y at this stage. The sample annealed at 490°C for 30 minutes was found to have compound phases, Y_2SiO_5, $YO_{1.335}$ and γ-$Y_2Si_2O_7$. Within the detection limits of XRD no unreacted Y could be found at this temperature.

4.4 Summary and conclusion.

Rutherford backscattering spectroscopy done on a Yb/SiO_2 thin film couples revealed that Yb interacts with SiO_2. This is in agreement with the results obtained by other workers [18]. The chemical reaction starts at about 320°C. In the case of uncovered Yb there is a loss of material (Yb) suggesting the formation of volatile compound phases. For Yb sandwiched between layers of SiO_2, RBS suggested the presence of all three elements (Yb, Si and O) throughout the layer resulting from the reaction. Yb does not have ternary phases (according to JCPDS files). The compound phases found to be present in the annealed samples were Yb_5Si_3, Yb_3Si_5,

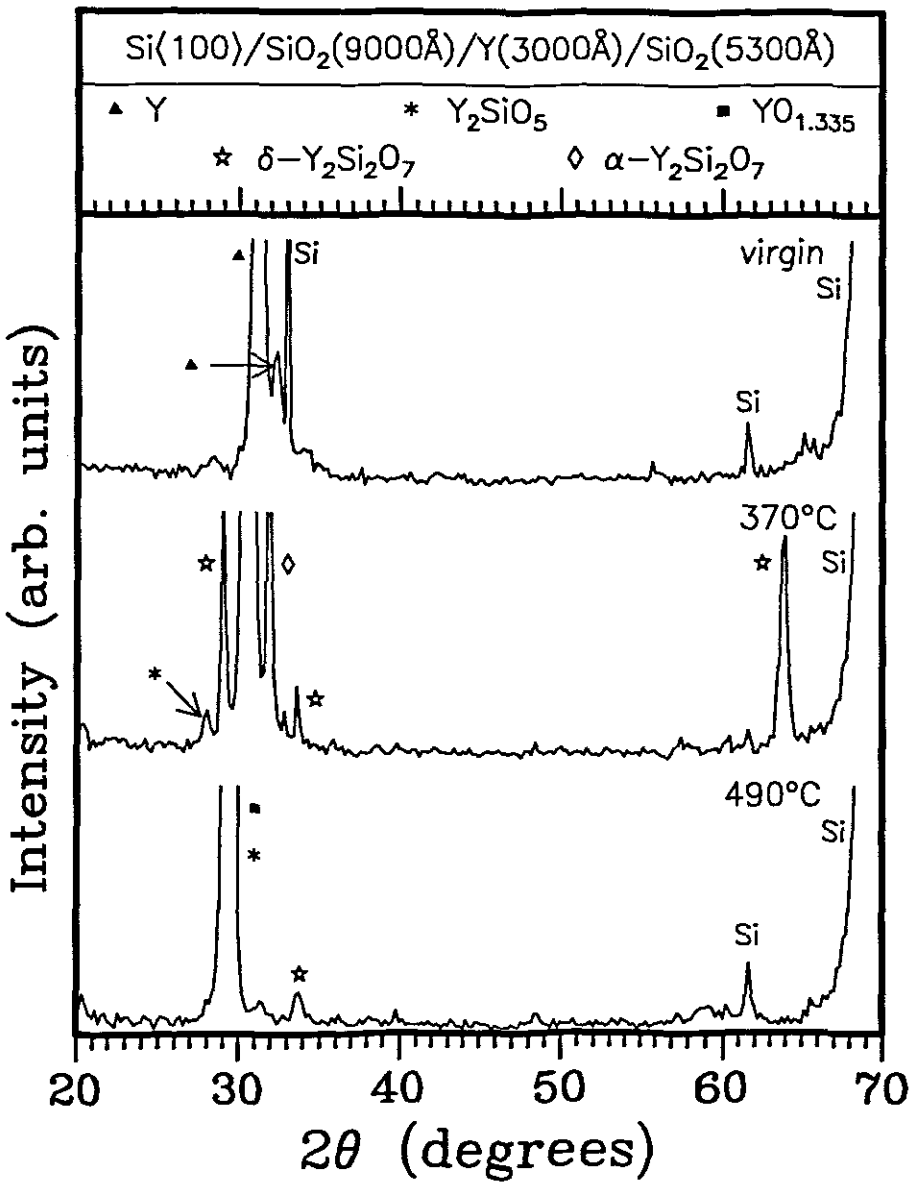

FIGURE 4.5: X-ray diffraction spectra of samples with structure Si< 100 >/SiO_2(9000Å)/Y(3000Å)/SiO_2(5300Å) samples showing a virgin sample, a sample annealed at 370°C and one annealed at 490°C for 30 minutes. Compound phases $\gamma Y_2Si_2O_7$ and $\alpha Y_2Si_2O_7$ were identified.

Yb_3O_4 and Yb_2O_3.

The RBS spectrum of the $SiO_2/Y/SiO_2$ thin film system showed the presence of interaction between the sandwiched Y film and both the capping and the thermally grown SiO_2 layers upon annealing (see **Fig. 4.4**). The interaction starts at about 370°C. Analysis of the RBS spectra using RUMP suggested the formation of a ternary phase i.e. YSi_pO_q. XRD analysis revealed the presence of the ternary phases γ-$Y_2Si_2O_7$ and α-$Y_2Si_2O_7$.

The general behaviour of the rare earth metals deduced from our experiments and from those of others [18] suggests that all those that have been investigated do react with SiO_2. The structures that result from such interactions are of the form Si/SiO_2/ternary mixture, even in cases where ternary compound phases do not exist. This is an effect dissimilar to refractory metals where clear discrete layers form.

CHAPTER 5

NOBLE METALS.

5.1 Introduction.

The elements Ni, Au and Ag as well as the elements of the platinum group viz Pt, Ir, Os, Re, Ru, Rh and Pd are collectively called the noble metals. Cu may be classified as a near noble metal. These metals find wide application in electronic devices such as transistors, capacitors and diodes. J. Y. Kim *et al* [19] have suggested the use of gold (Au) in metallization schemes since it has better electromigration resistance than aluminium. However, Au has has poor adherence on oxidized substrates. In their experimental investigations they have used copper (Cu) films of $\approx$130Å as an underlayer sandwiched between a quartz (SiO_2) substrate and a Au film, $\approx$ 750Å in thickness. They annealed the SiO_2/Cu/Au samples at temperatures of up to 500°C and their experimental data showed that a Au/Cu composite film was formed and that the Au developed holes during annealing.

R.R. Rye and A.J. Ricco [20] have studied palladium (Pd) in its use in Si< 100 >/SiO_2/Pd diodes and transistors. These diodes are used mainly in low-power electronic sensors as hydrogen detectors. This is a result of the high solubility of hydrogen in Pd. The hydrogen molecules dissociate on the catalytic metal surface and diffuse through the thin metal film to the metal-insulator interface. N.M. Davey and R.J. Seymour [21] have also suggested the use of platinum (Pt) as the gate metal

of a metal oxide semiconductor (MOS) transistor as an alternative to Pd. Detection limits for hydrogen in air are of the order of 0.5ppm and proposed applications include leak detectors and fire alarm systems.

5.2 Experimental.

Thermally oxidized silicon wafers (cut to 13mm by 13mm squares) were chemically cleaned and then rinsed in de-ionised water before being mounted onto aluminium holders. The thickness of the oxide layer in the wafers used was about 8000Å to make sure that after interaction with the metal some SiO_2 is left. The holders were then mounted in a vacuum chamber and the vacuum system was degassed down to a pressure of the order of 1×10^{-8}kPa. The vacuum was enhanced by pouring liquid nitrogen into the system when the pressure was about 1×10^{-7}kPa to assist in trapping gas molecules onto the walls of the cryo-panels.

An electron beam was targeted on lumps of Cu, Pt, Ir and Re metal placed in one of the crucibles in the vacuum deposition system to cause melting. The average pressure was 2×10^{-7}kPa. After deposition, the vacuum system was allowed to cool. The Si/SiO_2/Metal samples were annealed for various periods of time in an oil free vacuum system, with vacuum better than 10^{-7} kPa. The vacuum in the annealing furnace was also enhanced by feeding liquid nitrogen into the system. All samples were analyzed by RBS, using a beam of 2 MeV alpha particles, in vacuum of the order of 10^{-5}kPa. RUMP simulation was then used to determine the thicknesses of the various layers in the samples.

5.3 Results.

5.3.1 Cu-SiO_2.

A 2100Å layer of copper (Cu) was electron-gun evaporated onto thermally grown and chemically cleaned SiO_2 substrates in vacuum. Deposition was maintained at ≈4.8Å/s. The vacuum was oil free and better than 10^{-7}kPa. The thickness of the SiO_2 was 8200Å on top of bulk Si< 100 >. The Cu-SiO_2 samples were

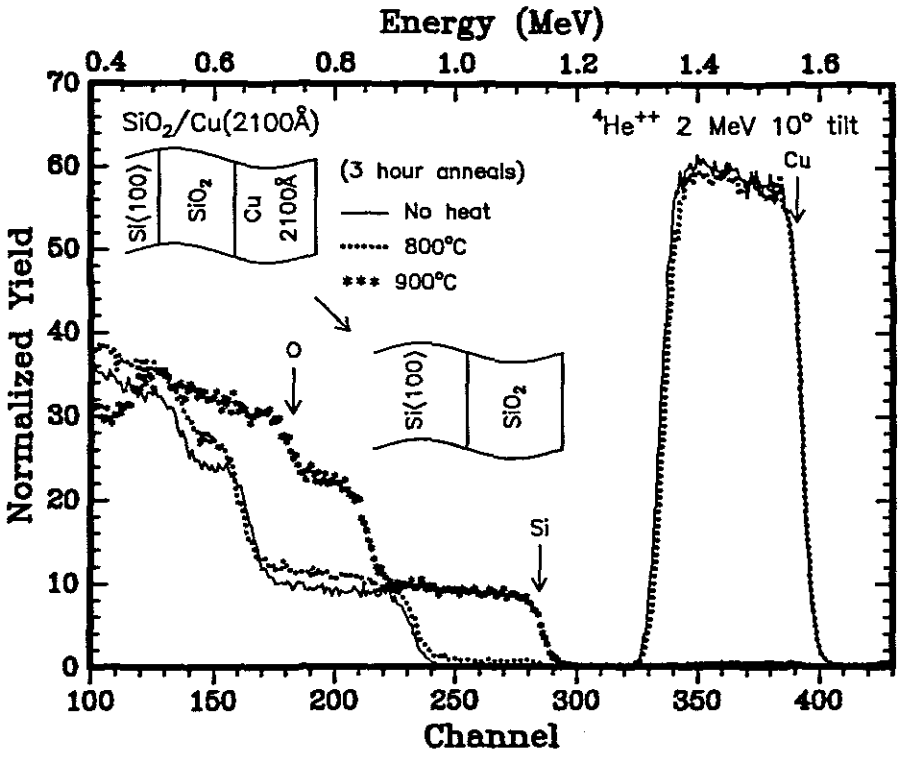

FIGURE 5.1: Backscattering spectra of Si< 100 >/SiO_2(8200Å)/Cu(2100Å) samples as-deposited and annealed for 3 hours at two different temperatures. The as deposited sample and the samples annealed at 800°C and 900°C show no interaction. The sample heated at 900°C shows no Cu signal indicating that the copper has been lost, either through evaporation or by formation of volatile copper oxides.

annealed for three hours at various temperatures in a vacuum furnace whose pressure was better than 10^{-7}kPa. Results of Rutherford Backscattering Spectrometry (RBS) are shown in **Fig. 5.1** for the as deposited sample and the samples annealed at 800°C and 900°C.

The as deposited sample shows no interaction. The sample annealed at 800°C for three hours also shows no interaction. The RBS spectrum of the sample annealed at 800°C coincides with that of the unannealed sample at all points. There has therefore been no interaction between Cu and SiO_2 according to this result. The spectrum of the sample annealed at 900°C has a missing Cu signal. Note also that for this RBS spectrum the Si and O signals are at their surface positions. This means that the SiO_2 of the sample annealed at 900°C is on the surface (i.e. not

covered with Cu anymore) and the Cu has been lost either by evaporation due to its relatively low melting point (1083°C) or the formation of volatile copper oxides.

5.3.2 Pt-SiO_2.

A layer of platinum (Pt) was deposited on SiO_2 substrates thermally grown on Si< 100 > by means of an electron beam at a rate of 2.6Å/s. Vacuum was maintained at about 3×10^{-8}kPa during deposition. The deposited Pt layer was about 1000Å in thickness. Two of the Pt on SiO_2 samples were annealed at 800°C and 900°C in vacuum of about 1×10^{-7}kPa for three hours.

Fig. 5.2 shows an RBS spectrum of the Pt on SiO_2 samples. The thickness of the SiO_2 was found to be 5500Å and that of the Pt was 1000Å. The RBS spectrum of the unannealed sample shows no interaction between Pt and SiO_2. The spectrum

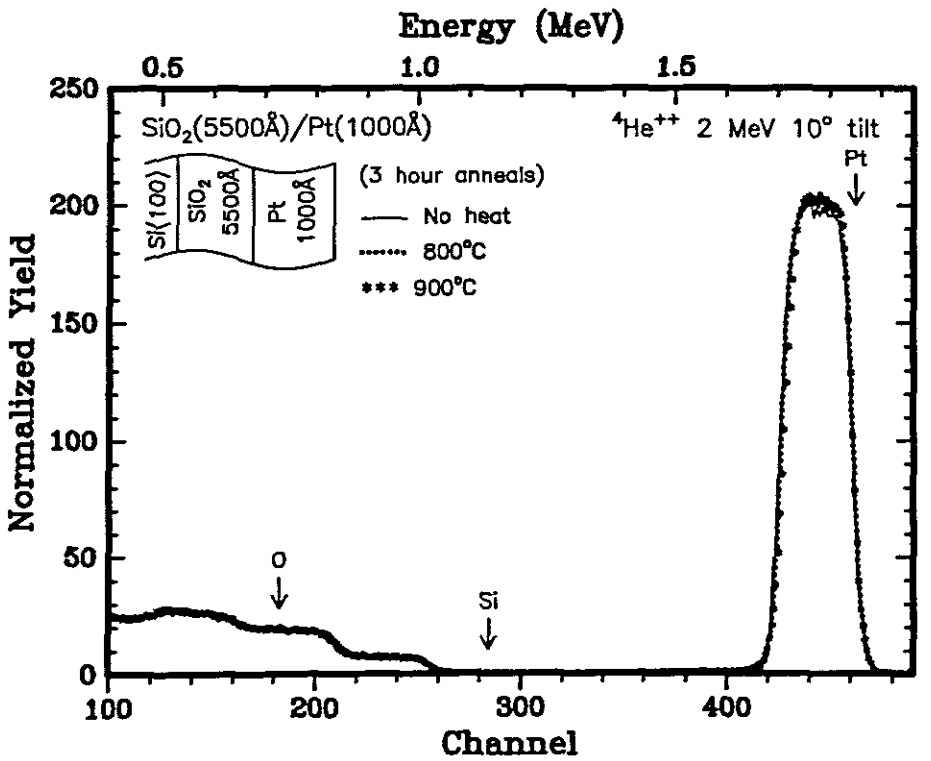

FIGURE 5.2: The RBS spectra of samples whose structure is Si< 100 >/SiO_2(5500Å)/Pt(1000Å) showed that there was no interaction. The annealed samples look the same as the unannealed sample. These samples were annealed at 800°C and 900°C for 3 hours.

of the sample annealed at 800°C for three hours coincides at all points with that of the unannnealed sample. There is therefore no interaction between Pt and SiO_2 on this sample according to our RBS results. There is also no observable interaction on the sample annealed at 900°C for three hours.

5.3.3 Ir-SiO_2.

A layer of iridium (Ir) was deposited under vacuum on SiO_2 substrates, thermally grown on Si< 100 > orientation wafers. The pressure was kept at approximately 1×10^{-7}kPa and the deposition rate at 4.4Å/s throughout the process.

Two of the Si< 100 >/SiO_2/Ir wafers were then placed into a vacuum annealing furnace and annealed at a pressure of 2×10^{-8}kPa at temperatures of 800°C and 900°C respectively, for 3 hours. After the furnace had been allowed sufficient time to cool so as to avoid thermal oxidation upon opening, the samples were removed and RBS was carried out on the annealed samples and on one of the as deposited samples using a beam of 2MeV alpha particles. The RBS spectra coincide at all points (see **Fig. 5.3**) both for the as deposited sample and the annealed samples indicating that no interaction between the SiO_2 and the Ir occured when annealing at 800°C and at 900°C for 3 hours. We also conclude that no interaction could have taken place at lower temperatures. By using RUMP simulation, the thickness of the SiO_2 layer was found to be 8000Å and that of the Ir found to be 600Å(see **Fig. 5.3**)

5.3.4 Re-SiO_2.

Rhenium metal (Re) was evaporated by means of an electron beam and deposited onto thermally grown SiO_2 on Si< 100 > substrates at a rate of 0.90Å/s. The pressure was maintained at an average of 2×10^{-7}kPa. The system was allowed sufficient time to cool thereby avoiding thermal oxidation of the samples on breaking vacuum. Two of the samples were placed in two separate pre-heated quartz boats which were then put into a high vacuum annealing furnace. The furnace was then pumped down to a pressure of less than 2×10^{-8}kPa and the samples annealed for 3 hours at 800°C and 900°C respectively.

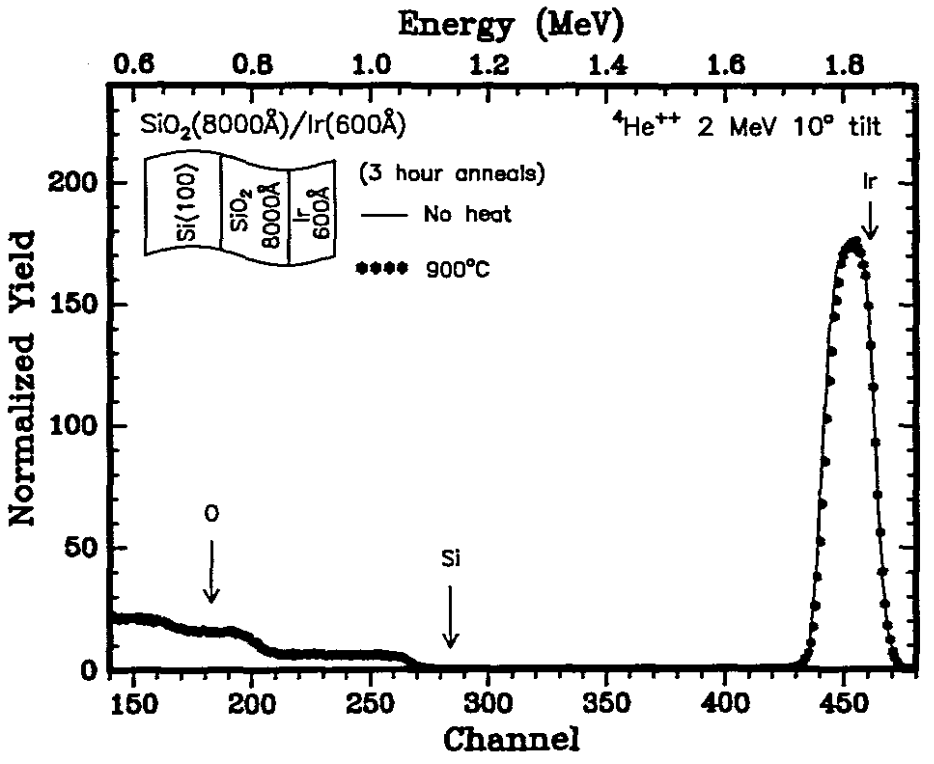

FIGURE 5.3: The RBS spectrum of the annealed samples show that there is no interaction between Ir and SiO_2. The samples were annealed in vacuum for 3 hours for 800°C and 900°C respectively. The structure of the samples is Si< 100 >/SiO_2(8000Å)/Ir(600Å).

The RBS spectrum of the as deposited Si< 100 >/SiO_2/Re sample coincides at all points with the RBS spectra of the Si< 100 >/SiO_2/Re samples annealed at 800°C and at 900°C for 3 hours (see **Fig. 5.4**). It is therefore concluded that no interaction occurred between the SiO_2 and the Re. Using RUMP simulation, the thicknesses of the SiO_2 and Re films was found to be 8800Å and 1500Å respectively. (see **Fig. 5.4**)

5.4 Summary and conclusion.

All the noble and near noble metals investigated in this work do not react chemically with SiO_2 for temperatures of up to 900°C when annealed for as long as 3hrs. Metals considered here were Cu, Pt, Mo, Ir and Re. In the case of Cu it was found that the metal is lost when annealing is done at temperatures above 800°C, possibly due to

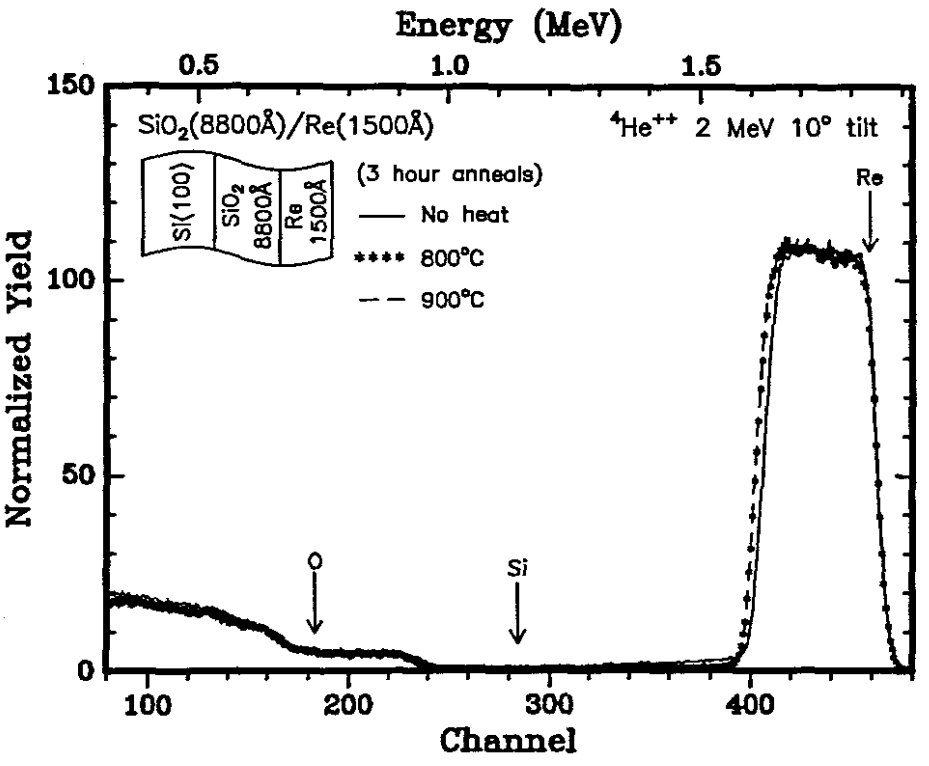

FIGURE 5.4: Backscattering spectra of Si< 100 >/SiO_2(8800Å)/Re(1500Å) samples as-deposited and annealed for 3 hours at two different temperatures. The virgin sample and the samples annealed at 800°C and 900°C show no interaction.

formation of volatile oxides of copper or due to the melting and evaporation of the metal. All the other metals are stable when in contact with SiO_2 up to 900°C. The characterisation method used in the sample analysis was RBS.

The experimental results obtained could be explained using thermodynamic data. Heats of formation were used to calculate heats of reaction for interaction between noble metals and SiO_2 leading to stable compound phases of metal oxide and metal silicides. These calculations gave heats of reaction which were positive, suggesting that noble metals are stable when in contact with SiO_2. This means, from a thermodynamic point of view that such noble metals should not react with SiO_2. This was found experimentally to be indeed the case i.e. our experimental observations are in agreement with our predictions based on thermodynamic calculations.

CHAPTER 6

PREDICTION OF METAL-SiO_2 INTERACTION.

6.1 Introduction.

Metal/silicon dioxide systems have received much attention due to their technological importance [3, 22]. Most of the work that has been done has concentrated on noble metals, near noble metals as well as on refractory metals. Low resistivity and high thermal stability makes refractory metal silicides useful in advanced integrated circuit interconnect schemes [12]. Good adhesion and uniformity of the resulting interface are therefore always desirable. The interaction of metal films with SiO_2 belongs to the class of ternary systems as opposed to interaction of metal films with Si, which belongs to binary systems. It has been suggested by Pretorius *et al* that strong adherence between the metals and the SiO_2 substrate indicates the occurrance of a reaction between the metal and the SiO_2 [3]. In cases where the metal film does not react with the substrate, they observed using scanning electron microscopy (SEM) that the metal tends to agglomerate and "ball-up" upon annealing. In cases where a reaction occurs, the result was a two layer structure of a metal rich silicide formed next to the SiO_2 substrate and a metal oxide layer on the surface.

6.2 Measured metal-SiO_2 interactions.

The results obtained in this study and those obtained by other workers on the interaction of metals with SiO_2 are summarised in **Table 6.1**. For refractory metals, the structure Si<>/SiO_2/silicide/metal oxide is found for cases where there is an interaction. We also found this same structure for the case of Zr which we investigated. There are refractory metals which do not react with SiO_2. We found that Mo does not react with SiO_2 when annealed in vacuum for temperatures of up to 900°C for 3 hours. Other workers have also found that there are refractory metals that do not react with SiO_2 e.g. Cr [**3, 16**]. Pretorius *et.al* found Cr to be a borderline case between those metals that react and those that do not. They found that under SEM observation metals that do not react do not adhere well on the SiO_2 substrate and tend to ball up. Those that reacted were found to form a uniform layer [**3**]. Cr is a strange case because it does not ball up and RBS shows that it does not react.

Very little work has been done on the reaction of SiO_2 with rare earth metals. Berning *et. al.* found that Tb reacts with SiO_2 to form alternating layers of silicide (with oxygen)/metal oxide/silicide (with oxygen)/metal oxide. He also found that the oxide contains Si [**23**]. No oxides or silicides were identified. We also found that the rare earth metals investigated by us (Y and Yb) react with SiO_2. We found using RBS that all three elements (Si, O and rare earth metal) were present throughout the reacted region. This is in agreement with Berning's results. We identified the compound phases in the resulting reacted region using XRD as Yb_5Si_3, Yb_3Si_5, Yb_3O_4 and Yb_2O_3 in the case of Yb and the γ and α phases of $Y_2Si_2O_7$ as well as Y_2SiO_5 for the case of Y. The oxide found was $YO_{1.335}$. The reacted regions according to our RBS results have varying concentrations of all three elements Si, Y or Yb with O - i.e. a ternary mixture of the elements.

An investigation to establish possible interaction between SiO_2 and the noble metals Cu, Pt, Re and Ir was conducted. Thin films of noble metals were deposited on thermally grown SiO_2 on Si< 100 > substrates. All annealing experiments were conducted in vacuum at temperatures of 800°C and 900°C for 3 hours. This

TABLE 6.1: Metal-SiO_2 interactions

Metal	Reaction ?	Reference
Co	No	[3]
Cr	No	[3,16]
Cu	No	This work
Dy	Yes	[23]
Fe	No	[3]
Hf	Yes	[3]
Ir	No	This work
Mn	No	[3]
Mo	No	This work
Nb	Yes	[11,3,24,25]
Ni	No	[3]
Pd	No	[3]
Pt	No	[3] This work
Re	No	This work
Ta	Yes	[12]
Tb	Yes	[23]
Ti	Yes	[11,3,24–27]
V	Yes	[3, 16, 24, 25, 28]
W	No	[14]
Y	Yes	This work
Yb	Yes	This work
Zr	Yes	[3,15,16] This work

investigation showed that there was no interaction between noble metals and SiO_2. Other workers [6] found the same results in the case of Cu and Pt annealed at 800°C for up to 4 hours. We found that in the case of Cu samples annealed at 900°C for 3 hours, all the Cu had been lost. The observed trend for all three metal classifications *viz.* refractory, rare earth and noble metals is summarized in **Fig. 6.1**. Refractory metals may or may not react with SiO_2. In cases where a reaction occurs the structure is Si< 100 >/SiO_2/metal silicide/metal oxide. All rare earth metals studied so far react with SiO_2. The resulting structure is Si< 100 >/SiO_2/ternary mixture.

6.3 Calculated heats of reaction.

The reaction of a thin metal film with an SiO_2 substrate resulting in the formation of a metal silicide and a metal oxide may be written as :

$$M_x + SiO_2 \longrightarrow M_ySi + M_{x-y}O_2 \qquad (6.1)$$

Possible reactions are those that lead to a lowering of the Gibb's free energy of the system i.e. $\Delta G<0$. This indicates that the metal-SiO_2 interface is thermodynamically unstable and that the reaction products are more stable than the metal in contact with the SiO_2.

If the reaction between the SiO_2 substrate and the thin metal layer occurs at constant temperature and pressure, the change in the Gibb's free energy is given by

$$\Delta G = \Delta H - T\Delta S$$

where ΔH is the change in enthalpy during the reaction (or the heat of reaction). ΔS the change in entropy and T the reaction temperature.

The annealing temperatures were kept well below the melting points of the reactants and products, hence the volume changes were negligibly small. For solid state reactions, $\Delta S \approx 0$ and so the change in the Gibb's free energy (ΔG) is thus approximated by the change in the enthalpy (ΔH). If ΔH is less than zero, the reaction is thermodynamically possible.

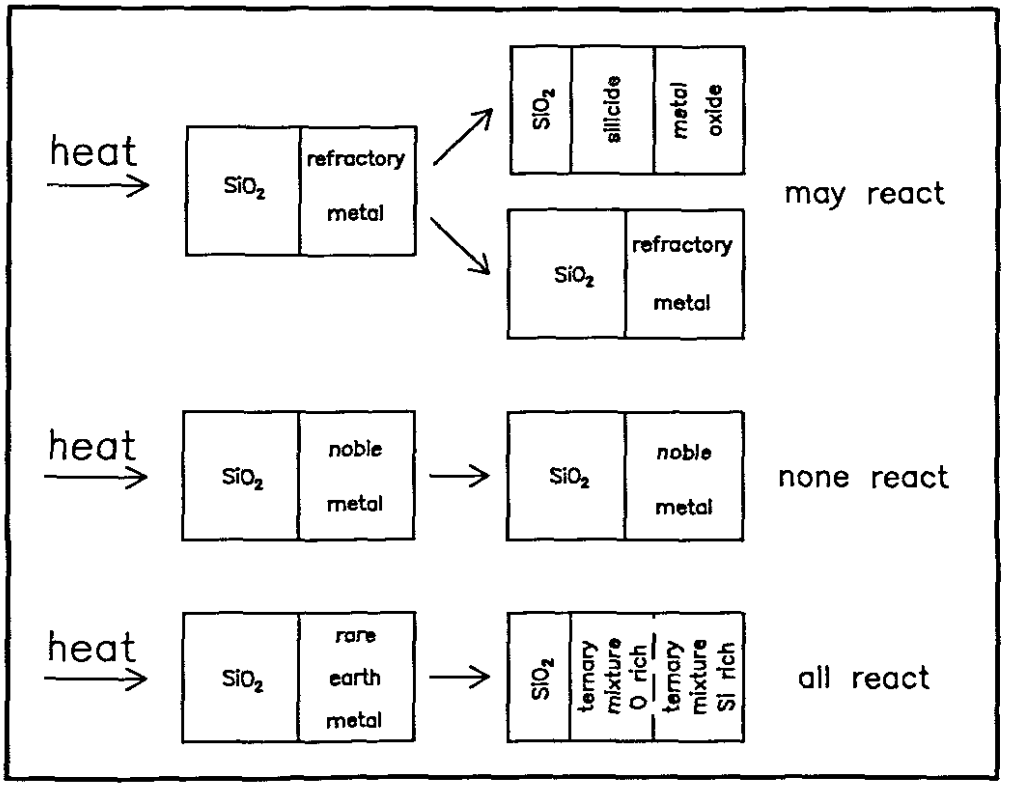

FIGURE 6.1: Clear trends are observed when SiO_2 is allowed to react with metals. For cases where a refractory metal reacts, a structure consisting of a silicide next to SiO_2 and a metal oxide away from SiO_2 develops. No known reactions are possible for noble metals. All cases where experiments were done react in the case of rare earths.

APPENDIX A gives values of the standard heats of formation ($\Delta H°$) of various metal oxides and metal silicides in kJ/(mol.atom) from which the heats of reaction ΔH_R may be obtained.

Consider the following reaction:

$$11Fe + 6SiO_2 \longrightarrow 3FeSi_2 + 4\ Fe_2O_3$$

Substituting the values of the heats of formation and multiplying by the total number number of moles of atoms yields:

$$11(0) + 18(-301.2) \longrightarrow 9(-30.6) + 20(-164.3)$$

$$0 + (-5421.6) \longrightarrow (-275.4) + (-3286.0)$$

$$\Delta H_R = \frac{[(-275.4) + (-3286.0)] - [0 + (-5421.6)]}{29}$$

$$= \frac{1860.2}{29}$$

$$\Delta H_R = +64.1\ \text{kJ/(mol.at)}$$

Since the heat of reaction (ΔH_R) is positive, the reaction is unlikely to proceed on its own.

Next consider the following reaction:

$$5Ti + 2SiO_2 \longrightarrow TiSi_2 + 4\ TiO$$

Substituting the values of the heats of formation and multiplying by the total number number of moles of atoms yields:

$$5(0) + 6(-301.2) \longrightarrow 3(-57.0) + 8(-271.3)$$

$$0 + (-1807.2) \longrightarrow (-171.0) + (-2170.4)$$

$$\Delta H_R = \frac{[(-171.0) + (-2170.4)] - [0 + (-1807.2)]}{11}$$

$$= \frac{-534.2}{11}$$

$$\Delta\ H_R = -48.6\ \text{kJ/(mol.at)}$$

Since the heat of reaction (ΔH_R) is negative, the reaction can occur on its own.

Table 6.2 gives calculated values of heats of reaction in kJ/(mol.at) for various interactions of the metal-SiO_2 type.

TABLE 6.2: Calculated heats of reaction (ΔH_R) for metal-SiO_2 interactions

Element	Silicides	Oxides	ΔH_R kJ/(mol.at)	Element	Silicides	Oxides	ΔH_R kJ/(mol.at)
Ca	Ca_2Si	CaO	−82.0	Dy	DySi	Dy_2O_3	−92.0
		CaO_2	5.9		$DySi_2$	Dy_2O_3	−91.6
	CaSi	CaO	−85.9		Dy_2Si_3	Dy_2O_3	−93.2
		CaO_2	18.8		Dy_3Si_5	Dy_2O_3	−92.8
	$CaSi_2$	CaO	−80.0		Dy_5Si_3	Dy_2O_3	−84.0
		CaO_2	37.6		Dy_5Si_4	Dy_2O_3	−92.0
Ce	Ce_5Si_3	CeO_2	−60.9	Er	Er_5Si_3	Er_2O_3	−75.6
		Ce_2O_3	−78.3		ErSi	Er_2O_3	−96.6
	Ce_3Si_2	CeO_2	−62.6		Er_3Si_5	Er_2O_3	−219.6
		Ce_2O_3	−80.3				
	Ce_5Si_4	CeO_2	−64.9	Fe	Fe_3Si	FeO	32.3
		Ce_2O_3	−83.3			Fe_3O_4	32.3
	CeSi	CeO_2	−66.9			Fe_2O_3	34.5
		Ce_2O_3	−86.1		FeSi	FeO	47.1
	Ce_3Si_5	CeO_2	−66.6			Fe_3O_4	48.5
		Ce_2O_3	−87.3			Fe_2O_3	52.0
	$CeSi_2$	CeO_2	−64.9		$FeSi_2$	FeO	57.3
		Ce_2O_3	−86.1			Fe_3O_4	59.9
						Fe_2O_3	64.1
Co	Co_2Si	CoO	44.3				
		Co_3O_4	51.6	Gd	Gd_5Si_3	Gd_2O_3	−78.5
	CoSi	CoO	54.2		Gd_5Si_4	Gd_2O_3	−83.6
		Co_3O_4	63.8		GdSi	Gd_2O_3	−85.9
	$CoSi_2$	CoO	68.0		Gd_2Si_3	Gd_2O_3	−86.9
		Co_3O_4	63.8		$GdSi_2$	Gd_2O_3	−85.2
Cr	Cr_3Si	CrO_2	26.2	Hf	Hf_3Si	HfO_2	−60.2
		CrO_3	56.9		Hf_2Si	HfO_2	−69.8
		Cr_2O_3	1.1		Hf_5Si_3	HfO_2	−73.3
		Cr_3O_4	0.03		Hf_3Si_2	HfO_2	−74.9
	Cr_5Si_3	CrO_2	40.2		Hf_5Si_4	HfO_2	−76.9
		CrO_3	79.5		HfSi	HfO_2	−77.9
		Cr_2O_3	9.5		$HfSi_2$	HfO_2	−71.6
		Cr_3O_4	7.2				
	CrSi	CrO_2	52.2	Ho	HoSi	Ho_2O_3	−93.8
		CrO_3	97.9		$HoSi_2$	Ho_2O_3	−93.6
		Cr_2O_3	16.9		Ho_5Si_3	Ho_2O_3	−85.7
		Cr_3O_4	14.1		Ho_5Si_4	Ho_2O_3	−91.0
	$CrSi_2$	CrO_2	62.8				
		CrO_3	114.8	Ir	Ir_3Si	IrO_2	78.5
		Cr_2O_3	23.2		Ir_2Si	IrO_2	92.4
		Cr_3O_4	19.8		Ir_3Si_2	IrO_2	102.2
					IrSi	IrO_2	116.2
Cu	$Cu_{56}Si_{11}$	CuO	57.1		Ir_2Si_3	IrO_2	129.9
		Cu_2O	45.6		$IrSi_2$	IrO_2	138.8
	Cu_4Si	CuO	64.0		$IrSi_3$	IrO_2	149.2
		Cu_2O	50.2				
	$Cu_{19}Si_6$	CuO	70.6	La	LaSi	La_2O_3	−78.3
		Cu_2O	54.3		$LaSi_2$	La_2O_3	−79.6

Cont...

Element	Silicides	Oxides	ΔH_R kJ/(mol.at)	Element	Silicides	Oxides	ΔH_R kJ/(mol.at)
Lu	Lu_5Si_3	Lu_2O_3	−87.2	Nb	$NbSi_2$	NbO	−0.8
	LuSi	Lu_2O_3	−95.1			NbO_2	8.5
	Lu_3Si_5	Lu_2O_3	−95.6			Nb_2O_5	17.4
Mg	Mg_2Si	MgO	−54.0	Nd	Nd_5Si_3	Nd_2O_3	−77.2
		MgO_2	33.7		Nd_5Si_4	Nd_2O_3	−82.1
					NdSi	Nd_2O_3	−84.6
Mn	Mn_6Si	MnO	0.8		Nd_3Si_4	Nd_2O_3	−85.9
		Mn_3O_4	8.1		Nd_2Si_3	Nd_2O_3	−85.8
		Mn_2O_3	13.6		Nd_5Si_9	Nd_2O_3	−84.9
		MnO_2	25.8				
		Mn_2O_7	59.6	Ni	Ni_3Si	NiO	34.2
	Mn_3Si_2	MnO	0.8			Ni_2O_3	58.4
		Mn_3O_4	9.4		Ni_5Si_2	NiO	36.6
		Mn_2O_3	7.2			Ni_2O_3	62.8
		MnO_2	30.3		Ni_2Si	NiO	40.2
		Mn_2O_7	70.6			Ni_2O_3	68.9
	Mn_3Si	MnO	1.2		Ni_3Si_2	NiO	47.6
		Mn_3O_4	11.4			Ni_2O_3	79.6
		Mn_2O_3	20.2		NiSi	NiO	56.3
		MnO_2	37.0			Ni_2O_3	92.3
		Mn_2O_7	86.9		$NiSi_2$	NiO	68.8
	Mn_5Si_2	MnO	1.5			Ni_2O_3	110.3
		Mn_3O_4	12.6				
		Mn_2O_3	21.0	Os	OsSi	OsO_2	110.2
		MnO_2	40.2			OsO_3	153.9
		Mn_2O_7	94.4			OsO_4	144.1
	Mn_5Si_3	MnO	3.4		Os_2Si_3	OsO_2	122.4
		Mn_3O_4	16.1			OsO_3	170.4
		Mn_2O_3	25.8			OsO_4	160.6
		MnO_2	48.1		$OsSi_3$	OsO_2	135.8
		Mn_2O_7	111.6			OsO_3	188.9
	MnSi	MnO	8.4			OsO_4	179.0
		Mn_3O_4	23.1				
		Mn_2O_3	34.2	Pd	Pd_5Si	PdO	55.8
		MnO_2	60.1		Pd_9Si_2	PdO	59.0
		Mn_2O_7	134.0		Pd_3Si	PdO	72.4
	$Mn_{11}Si_{19}$	MnO	15.8		Pd_2Si	PdO	86.3
		Mn_3O_4	32.5		PdSi	PdO	113.4
		Mn_2O_3	44.8				
		MnO_2	73.8	Pr	Pr_5Si_3	PrO_2	−41.0
		Mn_2O_7	156.7			Pr_2O_3	−79.1
					Pr_5Si_4	PrO_2	−43.3
Mo	Mo_3Si	MoO_2	28.5			Pr_2O_3	−84.2
		MoO_3	43.6		PrSi	PrO_2	−44.1
	Mo_5Si_3	MoO_2	37.4			Pr_2O_3	−86.9
		MoO_3	56.9		Pr_3Si_4	PrO_2	−43.4
	$MoSi_2$	MoO_2	55.5			Pr_2O_3	−88.2
		MoO_3	81.8		$PrSi_2$	PrO_2	−39.2
						Pr_2O_3	−86.7
Nb	Nb_5Si_3	NbO	−14.6				
		NbO_2	−9.6	Pt	Pt_3Si	PtO	76.7
		Nb_2O_5	−3.3			Pt_3O_4	89.9
						PtO_2	88.8

Cont...

Element	Silicides	Oxides	ΔH_R kJ/(mol.at)	Elements	Silicides	Oxides	ΔH_R kJ/(mol.at)
Pt	Pt_7Si_3	PtO	83.9	Ru	Ru_2Si	RuO_2	85.0
		Pt_3O_4	98.9			RuO_4	120.4
		PtO_2	98.4		RuSi	RuO_2	106.9
	Pt_2Si	PtO	88.3			RuO_4	152.5
		Pt_3O_4	104.5		Ru_2Si_3	RuO_2	119.2
		PtO_2	104.4			RuO_4	170.0
	Pt_6Si_5	PtO	102.9				
		Pt_3O_4	122.6	Sc	Sc_5Si_3	Sc_2O_3	−91.8
		PtO_2	124.2		ScSi	Sc_2O_3	−98.0
	PtSi	PtO	108.2		Sc_3Si_5	Sc_2O_3	−97.8
		Pt_3O_4	129.1				
		PtO_2	131.4	Si	-	SiO_2	−301.2
Pu	Pu_5Si_3	PuO_2	−57.4	Ta	Ta_9Si_2	Ta_2O_5	−7.7
	Pu_3Si_2	PuO_2	−58.5		Ta_2Si	Ta_2O_5	−6.5
	PuSi	PuO_2	−60.0		Ta_5Si_3	Ta_2O_5	−4.8
	Pu_3Si_5	PuO_2	−55.9		$TaSi_2$	Ta_2O_5	8.5
	$PuSi_2$	PuO_2	−53.3				
				Tb	TbSi	Tb_2O_3	−87.6
Re	Re_5Si_3	ReO_2	73.8			TbO_2	−44.0
		ReO_3	83.2		$TbSi_2$	Tb_2O_3	−86.7
		Re_2O_7	94.4			TbO_2	−38.2
		ReO_4	102.4		Tb_5Si_3	Tb_2O_3	−80.1
	ReSi	ReO_2	83.6			TbO_2	−41.2
		ReO_3	95.1		Tb_5Si_4	Tb_2O_3	−85.1
		Re_2O_7	108.1			TbO_2	−43.5
		ReO_4	117.5		Tb_3Si_5	Tb_2O_3	−88.2
	$ReSi_2$	ReO_2	94.6			TbO_2	−40.9
		ReO_3	108.3				
		Re_2O_7	123.2	Th	Th_3Si_2	ThO	−69.1
		ReO_4	134.1			ThO_2	−84.2
					ThSi	ThO	−72.6
Rh	Rh_2Si	Rh_2O	66.2			ThO_2	−89.8
		RhO	86.5		Th_3Si_5	ThO	−72.3
		Rh_2O_3	83.9			ThO_2	−91.0
	Rh_5Si_3	Rh_2O	69.3		$ThSi_2$	ThO	−71.8
		RhO	91.6			ThO_2	−90.8
		Rh_2O_3	89.3				
	Rh_3Si_2	Rh_2O	71.1	Ti	Ti_3Si	TiO	−49.2
		RhO	94.5			Ti_2O_3	−44.0
		Rh_2O_3	92.5			Ti_3O_5	−40.6
	RhSi	Rh_2O	78.2			TiO_2	−36.2
		RhO	105.9		Ti_5Si_3	TiO	−56.2
		Rh_2O_3	105.1			Ti_2O_3	−45.5
	Rh_4Si_5	Rh_2O	82.0			Ti_3O_5	−46.6
		RhO	112.0			TiO_2	−41.3
		Rh_2O_3	112.0		Ti_5Si_4	TiO	−58.2
	Rh_3Si_4	Rh_2O	82.2			Ti_2O_3	−52.4
		RhO	112.5			Ti_3O_5	−48.1
		Rh_2O_3	114.0			TiO_2	−42.5

Cont...

Element	Silicides	Oxides	ΔH_R kJ/(mol.at)	Elements	Silicides	Oxides	ΔH_R kJ/(mol.at)
Ti	$TiSi$	TiO	−56.5	V	V_5Si_3	VO	−17.2
		Ti_2O_3	−50.2			V_2O_3	−10.6
		Ti_3O_5	−45.6			V_3O_5	−4.1
		TiO_2	−39.7			V_4O_7	−0.9
	$TiSi_2$	TiO	−48.6			VO_2	6.3
		Ti_2O_3	−40.5			V_2O_5	23.5
		Ti_3O_5	−35.2		VSi_2	VO	−3.7
		TiO_2	−28.1			V_2O_3	6.3
						V_3O_5	14.9
Tm	Tm_5Si_3	Tm_2O_3	−87.2			V_4O_7	19.2
	$TmSi$	Tm_2O_3	−95.3			VO_2	28.9
	Tm_3Si_5	Tm_2O_3	−96.1			V_2O_5	51.9
U	U_3Si	UO_2	−38.9	W	W_5Si_3	WO_2	47.4
		U_4O_9	103.3			W_2O_5	53.5
		U_3O_7	−24.4			WO_3	55.6
		U_3O_8	−12.1		WSi_2	WO_2	59.4
		UO_3	−1.3			W_2O_5	67.7
	U_3Si_2	UO_2	−48.2			WO_3	70.9
		U_4O_9	133.3				
		U_3O_7	−30.0	Y	Y_5Si_3	Y_2O_3	−88.4
		U_3O_8	−14.3		Y_5Si_4	Y_2O_3	−94.1
		UO_3	−0.3		YSi	Y_2O_3	−97.1
	USi	UO_2	−52.9		Y_3Si_5	Y_2O_3	−98.6
		U_4O_9	147.0				
		U_3O_7	−33.0	Yb	Yb_5Si_3	Yb_2O_3	−66.2
		U_3O_8	−15.7		$YbSi$	Yb_2O_3	−73.3
		UO_3	−0.2		Yb_3Si_5	Yb_2O_3	−75.7
	U_3Si_5	UO_2	−54.5		$YbSi_2$	Yb_2O_3	−75.4
		U_4O_9	163.2				
		U_3O_7	−32.9	Zr	Zr_3Si	ZrO	−96.9
		U_3O_8	−14.0			ZrO_2	−59.2
		UO_3	3.0			ZrO_3	2.1
	USi_2	UO_2	−54.4		Zr_2Si	ZrO	−109.6
		U_4O_9	168.3			ZrO_2	−67.8
		U_3O_7	−32.2			ZrO_3	3.9
		U_3O_8	−12.9		Zr_5Si_3	ZrO	−112.4
		UO_3	4.5			ZrO_2	−68.7
	USi_3	UO_2	−51.6			ZrO_3	7.4
		U_4O_9	180.0		Zr_3Si_2	ZrO	−115.4
		U_3O_7	−28.4			ZrO_2	−70.8
		U_3O_8	−8.2			ZrO_3	7.5
		UO_3	10.0		Zr_5Si_4	ZrO	−117.2
						ZrO_2	−70.9
V	V_3Si	VO	−17.6			ZrO_3	11.4
		V_2O_3	−12.3		$ZrSi$	ZrO	−118.7
		V_3O_5	−7.0			ZrO_2	−70.4
		V_4O_7	−4.4			ZrO_3	16.4
		VO_2	1.3		$ZrSi_2$	ZrO	−115.9
		V_2O_5	15.1			ZrO_2	−61.5
						ZrO_3	36.4

6.4 Experimental results compared with calculations.

The reactions investigated took place at constant temperature and pressure. Since it is assumed that both reactants and products are in the solid state then a change in G may be approximated by a change in enthalpy (see chapter 1).

$$\Delta G \approx \Delta H.$$

Zr-SiO_2

From **Table 6.2**, we obtain values of the heats of reaction (ΔH_R) for the Zr/SiO_2 interaction resulting in the formation of silicides and oxides of Zr.

Consider the following reaction:

$$23Zr + 12SiO_2 \longrightarrow 3Zr_5Si_4 + 8ZrO_3$$

For this reaction, the heat of reaction is equal to +11.4kJ/(mol.at). The positive value indicates that such a reaction is not thermodynamically favourable and will therefore not proceed on its own.

Next consider the following reaction:

$$3Zr + SiO_2 \longrightarrow ZrSi + 2ZrO$$

From **Table 6.2**, the heat of reaction of this reaction is equal to −118.7kJ/(mol.at). Since the heat of reaction is negative, the reaction corresponding to it is thermodynamically favoured. The XRD spectrum of the sample annealed at 690°C (see **Fig. 3.2**) shows the presence of Zr_5Si_4, ZrO_2 and ZrO. From **Table 6.2**, the products Zr_5Si_4 and ZrO_2 have a heat of reaction of −70.9kJ/(mol.at) while Zr_5Si_4 and ZrO have a heat of reaction of −117.2kJ/(mol.at). In the case of the sample annealed at 720°C (see **Fig. 3.2**) the XRD spectrum shows the presence of Zr_5Si_4 and ZrO_2 only.

For each of the above pairs of products, the heats of reaction are negative indicating that the reactions leading to the formation of these products are ther-

modynamically favoured. Hence, the experimental results for zirconium are in agreement with the theoretical predictions.

Mo-SiO_2

A possible silicide and oxide formed in the Mo-SiO_2 reaction are given by the following reaction:

$$4Mo + SiO_2 \longrightarrow Mo_3Si + MoO_2$$

From **Table 6.2**, the value of the heat of reaction for the preceeding reaction is found to be +28.5kJ/(mol.at). It is also interesting to note that all the other combinations of silicides and oxides of Mo have also got positive values of (ΔH_R), indicating that none of these products will form spontaneously. Hence the observations made on the RBS spectrum showing no interaction between the Mo film and the SiO_2 substrate (see **Fig. 3.3**) are also confirmed by theoretical predictions.

Yb-SiO_2

The heats of formation of the ytterbium silicides are given in **APPENDIX A**. The only enthalpy that could be obtained for the oxides of ytterbium was that of Yb_2O_3. The results of the calculations of the heats of reaction resulting from the interaction between SiO_2 and Yb are summarized in **Table 6.2** and were all found to be negative. This suggests that the reaction between Yb and SiO_2 is thermodynamically possible. Experiment showed this to be the case i.e. Yb does indeed react with SiO_2. The heat of reaction between SiO_2 and Yb when the products were Yb_5Si_3 and Yb_2O_3 was found in particular to be negative. The thermodynamic calculations therefore agreed with our experimental results.

Y-SiO_2

The heats of formation of the silicides and the oxide of yttrium are given in **APPENDIX A**. The heats of reaction for the interaction between Y and SiO_2 were calculated (see **Table 6.2**) and were found to be negative, thereby suggesting that

Y is thermodynamically unstable in contact with SiO_2. Our experimental investigations confirmed that Y will interact with SiO_2 as shown by the RBS spectrum (see **Fig. 4.4**) as well as the XRD spectrum (see **Fig. 4.5**).

Cu-SiO_2

Using the values of the standard heats of formation ($\Delta H°$) as listed in **APPENDIX A**, the heats of reaction (ΔH_R) for all the combinations of the silicides and oxides of Cu were calculated and are given in **Table 6.2**. We observe that all the values of heats of reaction are positive. According to the thermodynamics, none of these reaction products will be formed spontaneously.

The RBS spectrum of the Si<>/SiO_2/Cu system shown on **Figure 5.1** shows no interaction between the Cu metal film and the SiO_2 substrate at temperatures of up to 800°C. At 900°C, all the Cu metal has been lost. Hence, experimental results support the theoretical predictions of no interaction between Cu and SiO_2.

Pt-SiO_2

The heats of reaction (ΔH_R) for all the combinations of silicides and oxides of Pt were calculated using the values of standard heats of formation ($\Delta H°$) listed in **APPENDIX A**. All the values obtained were found to be positive, as shown in **Table 6.2**. According to thermodynamics, the positive ΔH_R values indicate lack of interaction between the Pt metal film and the SiO_2 substrate.

The thermodynamic predictions are borne out by the RBS expermimental results shown in **Figure 5.2**. The Pt/SiO_2 samples were annealed at temperatures of up to 900°C for three hours with no observable interaction between the SiO_2 substrate and the overlying Pt metal film as shown by the RBS spectra which remained superimposed.

Ir-SiO_2

Calculations of heats of reaction (ΔH_R) for interactions between Ir and SiO_2

leading to the formation of all possible silicides and oxides of Ir were carried out and the values obtained were listed in **Table 6.2**. Values of heats of formation ($\Delta H°$) were obtained from **APPENDIX A**. For each reaction, the value of ΔH_R obtained was positive e.g. for the reaction

$$4Ir + SiO_2 \longrightarrow Ir_3Si + IrO_2$$

the value of ΔH_R was found to be +78.5 kJ/(mol.at), thereby suggesting no reaction occurs between the Ir metal and the SiO_2.

Experimental results also revealed an absence of interaction between the Ir and SiO_2 substrate as shown by the RBS results on **Fig. 5.3** for samples annealed at temperatures of up to 900°C for three hours. The RBS signals of the virgin and annealed samples coincided at all points for all temperatures up to 900°C leading to a conclusion that no interaction had occured between the Ir and SiO_2.

Re-SiO_2

The heats of reaction (ΔH_R) for the interaction between Re and SiO_2 are listed on **Table 6.2**. It is noticeable that the values obtained for all the different oxides and silicides of Re are positive, e.g. for the reaction

$$8Re + 3SiO_2 \longrightarrow Re_5Si_3 + 3ReO_2$$

the value of ΔH_R is +73.8kJ/(mol.at). According to thermodynamics, such a reaction will not occur on its own.

These theoretical predictions (based on thermodynamics) are in agreement with our RBS experimental results (see **Fig. 5.4**) which show no interaction between the SiO_2 substrate and the Re metal deposited on it when the samples were annealed for temperatures of up to 900°C for three hours. None of the signals on the RBS spectra was displaced thus confirming absence of any interaction.

6.5 Correlation with electronegativity.

TABLE 6.3: Metal-SiO_2 interaction results compared with calculated heats of reaction and the average electronegativity of the metal

Metal	Average Electronegativity Pauling scale	Heats of reaction range (ΔH_R) kJ/(mol.at)	Chemical reaction?
Yb	1.07	−75.7 to − 66.2	Yes
Tb	1.08	−88.2 to − 38.2	Yes
Y	1.10	−98.6 to − 88.4	Yes
Hf	1.17	−77.9 to − 60.2	Yes
Zr	1.21	−118.7 to + 36.4	Yes
Ta	1.29	−7.7 to + 8.5	Yes
Nb	1.32	−14.6 to + 17.4	Yes
Ti	1.32	−58.2 to − 28.1	Yes
W	1.41	+47.4 to + 70.9	No
V	1.43	−17.6 to + 51.9	Yes
Mo	1.45	+28.5 to + 81.8	No
Cr	1.50	0.0 to + 114.8	No
Mn	1.51	+0.8 to + 156.7	No
Re	1.51	+73.8 to + 134.1	No
Fe	1.64	+32.3 to + 64.1	No
Co	1.66	+44.3 to + 68.0	No
Ni	1.67	+34.2 to + 110.3	No
Pt	1.67	+76.7 to + 131.4	No
Ir	1.69	+78.5 to + 149.2	No
Pd	1.71	+55.8 to + 113.4	No
Cu	1.80	+45.6 to + 70.6	No

Values of electronegativity of the metals may also be used to predict whether a metal will react with SiO_2 or not [3]. Pretorius calculated electronegativity as an average of three electronegativities and based it on the Pauling scale. The three electronegativities used are the Allred-Rochow, the Pauling and the relative compactness electronegativities. **Table 6.3** give the results for metal-SiO_2 interactions, with the metals listed in increasing order of average electronegativity. The third column gives the range of the heats of reaction in kJ/(mol.at), calculated for each metal in reaction with SiO_2 to form a metal silicide and a metal oxide. It can be seen that vanadium is the metal with the highest value of average electronegativity, that reacts with SiO_2. The value of vanadium 's average electronegativity is 1.43. It means that roughly those metals with electronegativity equal to or less than 1.43 react with SiO_2 and those with electronegativity greater than 1.43 will not.
Tungsten is a curious case for two reasons. Its heats of reaction are positive and thus W is expected not to react with SiO_2. Experiment shows that it does not react with SiO_2 [14], in agreement with its calculated values of heats of reaction. The average electronegativity of W is however less than that of V, and is from this point of view expected to react with SiO_2. It does not.

Fig. 6.2 is a plot of average electronegativity (Pauling scale) versus heats of reaction (ΔH_R) in kJ/(mol.at) for various metals interacting with SiO_2, for all cases where data could be obtained. Elements listed at the top of the graph are shown as crosses and those listed at the bottom as circles. It is expected that for elements where all heats of reaction are positive there is no reaction and where there are some heats of reaction that are negative there will be a reaction. Ca for example is expected to react with SiO_2 since it has some negative values of ΔH_R whereas Ru should not react with SiO_2 since all values of ΔH_R corresponding to it are positive. The average electronegativity of Ca is below 1.45 (*viz.* 1.02) and that of Ru is above 1.45 (*viz.* 1.67). **Figure 6.2** also shows the position of rare earth metals in relation to other metals. All rare earth metals are expected to react with SiO_2 since they all have negative heats of reaction. All those that have been studied in this investigation (Yb and Y) as well as those studied by others (Tb) [23] react

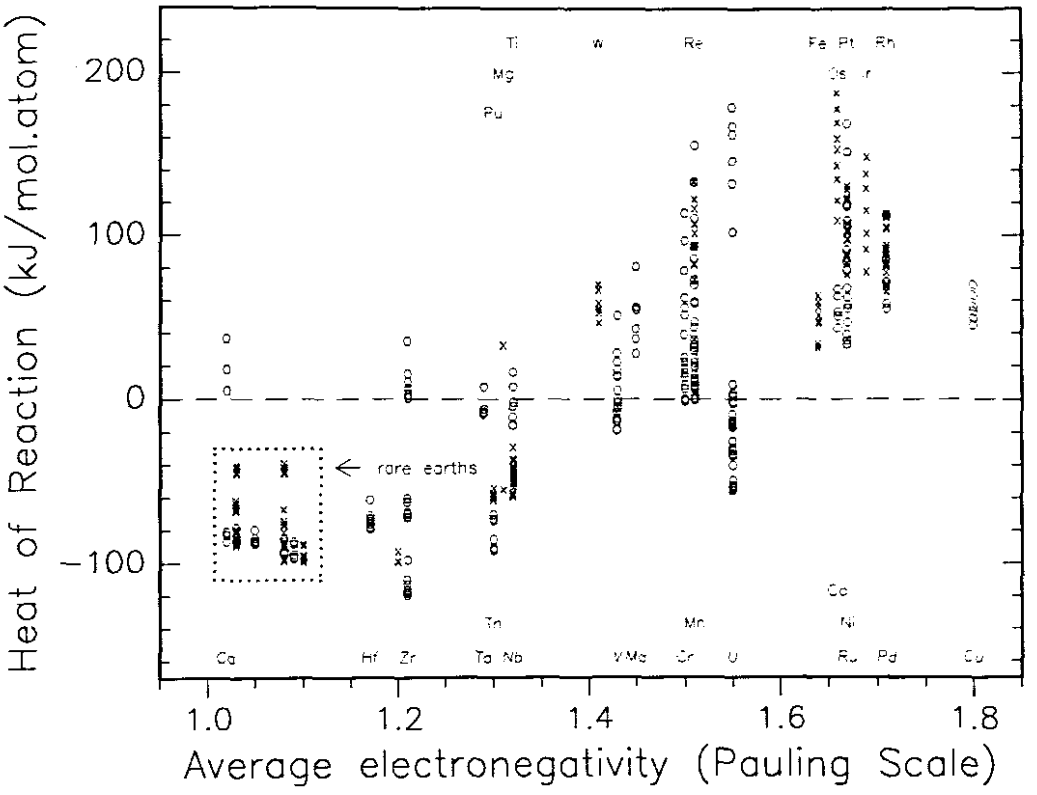

FIGURE 6.2: Heats of reaction for all possible combinations of various metals in interaction with SiO_2 (where data could be found). Heats of reaction are plotted on the vertical axis whereas electronegativities are on the horizontal axis. Heats of reaction of elements whose symbols are written at the top of the graph are indicated with crosses and those at the bottom with circles. The position where the rare earth metals lie is clearly shown.

with SiO_2. All rare earth metals have an average electronegativity of less than 1.45. **Fig. 6.3** shows values of average electronegativity (Pauling scale) plotted against heats of reaction (in kJ/(mol.at) for rare earth metals only. Heats of reaction are plotted on the vertical axis whereas average electronegativities are on the horizontal axis. It is seen that all rare earths considered here have a range of heats of reactions that fall in the negative region of the graph. They are therefore expected to react with SiO_2.

We would like to find out where the the crossover point is, as far as average electronegativity is concerned i.e. the value of elecronegativity above which metals do not react with SiO_2 and below which they react with SiO_2. **Figure 6.4** shows a

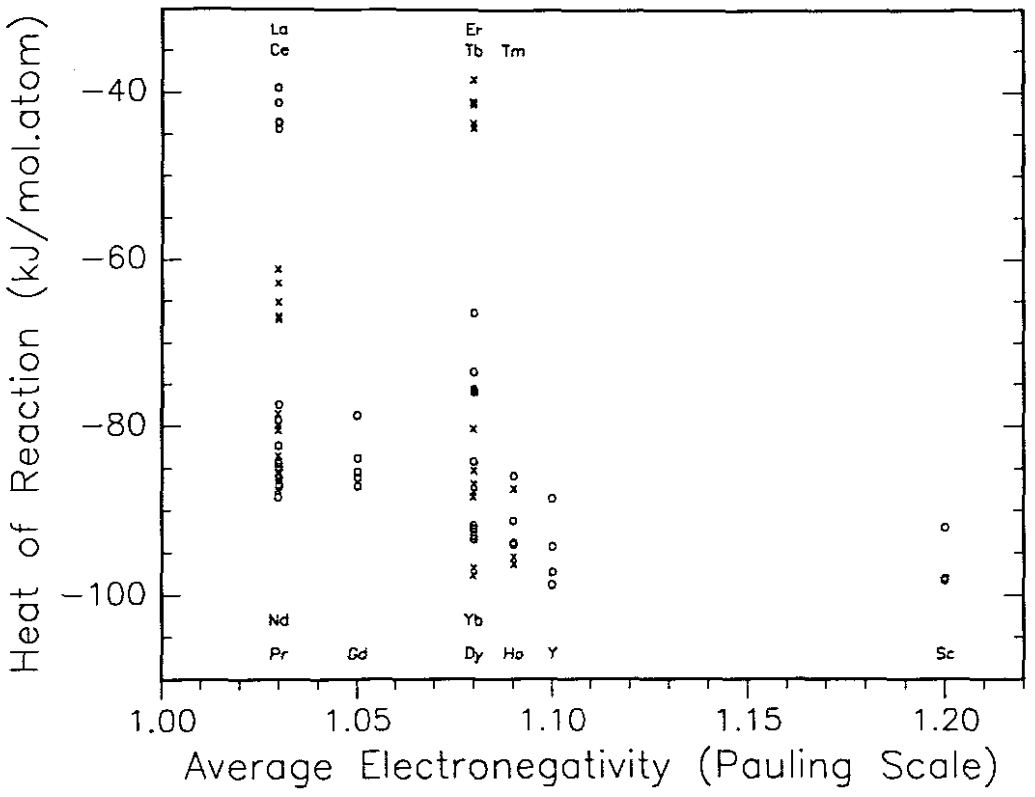

FIGURE 6.3: Heats of reaction for rare earth metals. Heats of reaction are plotted on the vertical axis whereas electronegativities are on the horizontal axis. All rare earths are expected to react with SiO_2.

plot of the most negative heat of reaction for each metal versus electronegativity. A straight line drawn through the points crosses the zero value of heat of reaction at about 1.45 suggesting that those metals with electronegativity less than 1.45 should react with SiO_2.

The average electronegativity of Yb is 1.07 on the Pauling scale. We note that this value of average electronegativity of less than 1.45 and Yb should therefore react with SiO_2. The reaction between Yb and SiO_2 is therefore expected, as has been shown by experiment to occur. It can be seen that the average electronegativities of all rare earths considered here are much less than 1.45. It is therefore expected that all of them will react with SiO_2. Y which is one of the rare earth metals we studied has an average electronegativity of 1.10 and experiment shows that it reacts with SiO_2.

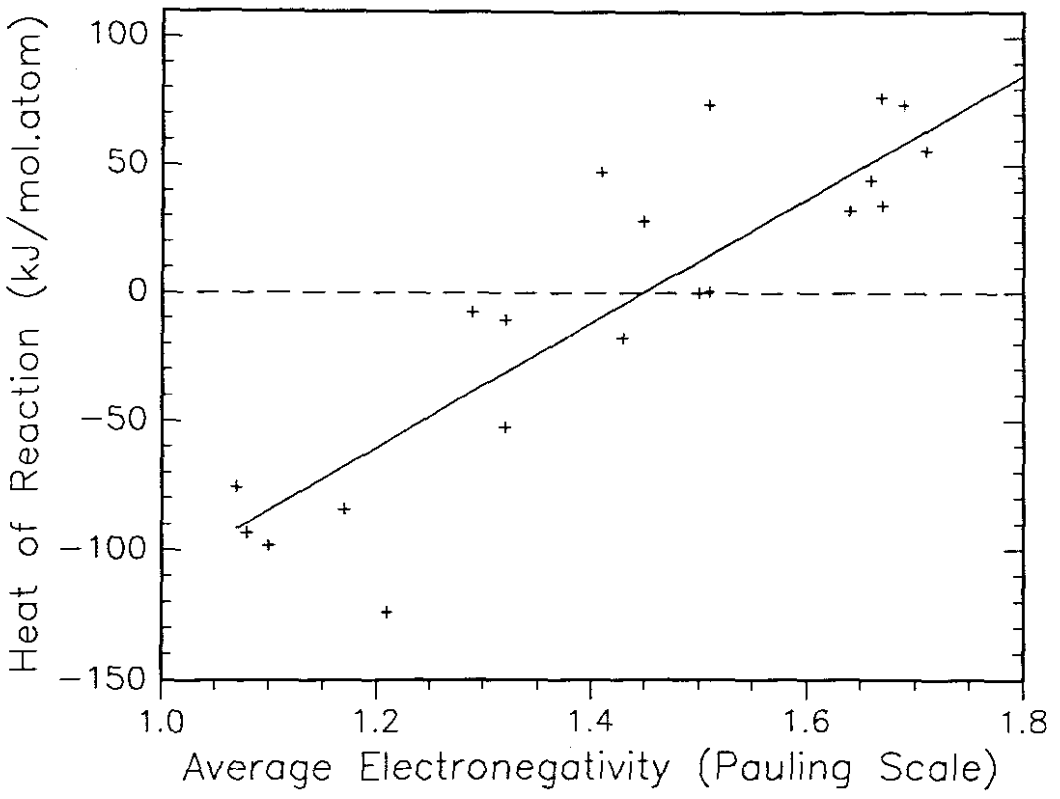

FIGURE 6.4: Average electronegativity according to the Pauling scale has been plotted against the most negative value of the Heat of Reaction in kJ/(mol.atom) and the best fit through the points obtained by means of the straight line passing through them. The straight line intercepts the electronegativity axis at a value of 1.45. Metals whose value of Electronegativity is less than 1.45 are expected to react with SiO_2

Based on the Pauling scale, copper has an average electronegativity of 1.80. This value is greater than 1.45 and Cu is therefore expected not to react with SiO_2. This is in agreement with our results for Copper. Platinum has an average electronegativity of 1.67. This is also greater than the changeover value of 1.45 and Pt would therefore be expected not to react with SiO_2. Our experimental results showed that it does not react with SiO_2.

Iridium has been shown through our experiments to be unreactive with SiO_2. The average electronegativity of Ir was found to be 1.69 on the Pauling scale. This value is greater than 1.45. As expected, Ir does not react with SiO_2.

Rhenium has an average electronegativity of 1.51 on the Pauling scale. This

value is greater than 1.45 and Rh should thus not react with SiO_2. This is in agreement with our experimental results for Rhenium.

A correlation may also be found between the electronegativity parameter ϕ^*, as defined in the Miedema model [5] and the heats of reaction. **Table 6.4** lists values of ϕ^* for metals, where experiments have been done, in increasing order. The units for ϕ^* are volts. Inspection of **Table 6.4** shows that metals with a value of ϕ^* of 4.25 V or less react with SiO_2 whereas those with a value of ϕ^* greater than 4.25 V do not. It is interesting to note from this same table that W which in the case of average electronegativity did not seem to fit the expected pattern now fits perfectly amongst those metals that do not react. **Figure 6.5** shows values of heats of reaction in kJ/(mol.at) for various metals in contact with SiO_2 versus the electronegativity parameter ϕ^*, as obtained from the Miedema model [5]. Crosses have been used to represent heats of reaction of the elements at the top and circles to represent the elements at the bottom. Values of the heats of reaction shown here were obtained from **Table 6.2**. A dashed line in **Figure 6.5** has been drawn along $\Delta H_R = 0$ kJ/(mol.at). Elements which have no points (heat of reaction) below the dashed line are expected not to react with SiO_2. We suspect that ϕ^* is a better parameter compared to average electronegativity to predict whether a reaction will or will not take place in the solid state.

We would like to determine the crossover point for ϕ^* graphically. A plot of ϕ^* versus the minimum of the values of the heats of reaction for each metal is shown in **Figure 6.6**. A straight line drawn through the points passes the zero value of minimum heat of reaction for each metal at ϕ^* equal to 4.45 V. We expect that metals with a value of ϕ^* less than 4.45 V will react whereas those whose value of ϕ^* is greater than or equal to 4.45 V will not react. Metals, in this study, with a value of ϕ^* which is less than 4.45 V are Yb, Y and Zr. We have found that all these metals react with SiO_2. Metals studied by other workers but not studied by us whose value of ϕ^* is less than 4.45 V are Tb Hf, Ti, Ta, Nb and V. In all these cases it was found that SiO_2 reacts with these metals. Metals with a value of ϕ^* of more than 4.45 V which were studied by us are Cu, Mo, Re, Ir and Pt. In all these

TABLE 6.4: Metal-SiO_2 interaction results compared with calculated heats of reaction ΔH_R and the electronegativity parameter ϕ^* as defined by Miedema [5]

Metal	ϕ^* Volts	Heats of reaction range (ΔH_R) kJ/(mol.at)	Chemical reaction?
Yb	2.58	−75.7 to − 66.2	Yes
Y	3.20	−98.6 to − 88.4	Yes
Tb	3.21	−88.2 to − 38.2	Yes
Zr	3.45	−118.7 to + 36.4	Yes
Hf	3.60	−77.9 to − 60.2	Yes
Ti	3.80	−58.2 to − 28.1	Yes
Ta	4.05	−7.7 to + 8.5	Yes
Nb	4.05	−14.6 to + 17.4	Yes
V	4.25	−17.6 to + 51.9	Yes
Cu	4.45	+45.6 to + 70.6	No
Mn	4.45	+0.8 to + 156.7	No
Cr	4.65	0.0 to + 114.8	No
Mo	4.65	+28.5 to + 81.8	No
W	4.80	+47.4 to + 70.9	No
Fe	4.93	+32.3 to + 64.1	No
Co	5.10	+44.3 to + 68.0	No
Ni	5.20	+34.2 to + 110.3	No
Re	5.20	+73.8 to + 134.1	No
Pd	5.45	+55.8 to + 113.4	No
Ir	5.55	+78.5 to + 149.2	No
Pt	5.65	+76.7 to + 134.4	No

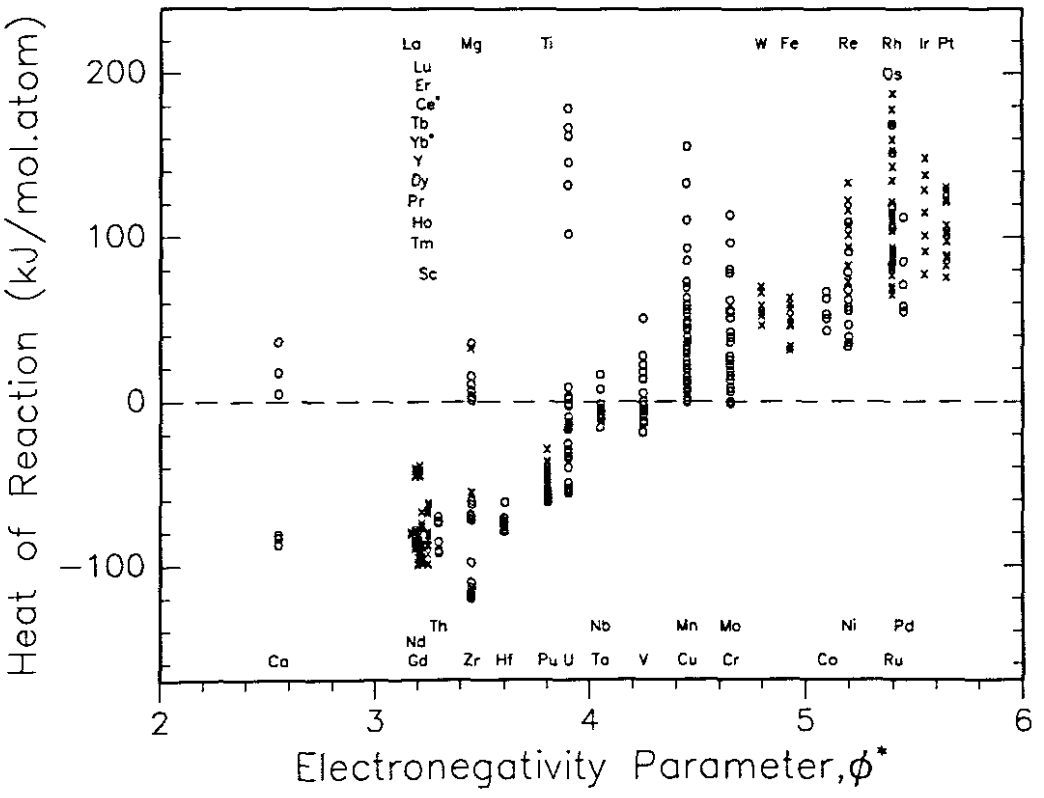

FIGURE 6.5: The electronegativity parameter ϕ^* as defined in the Miedema [5] model is shown on the horizontal axis while heats of reaction are on the vertical axis. Heats of reaction of elements whose symbols are written at the top of the graph are represented with crosses while the heats of reaction of elements whose symbols appear at the bottom are represented with circles.

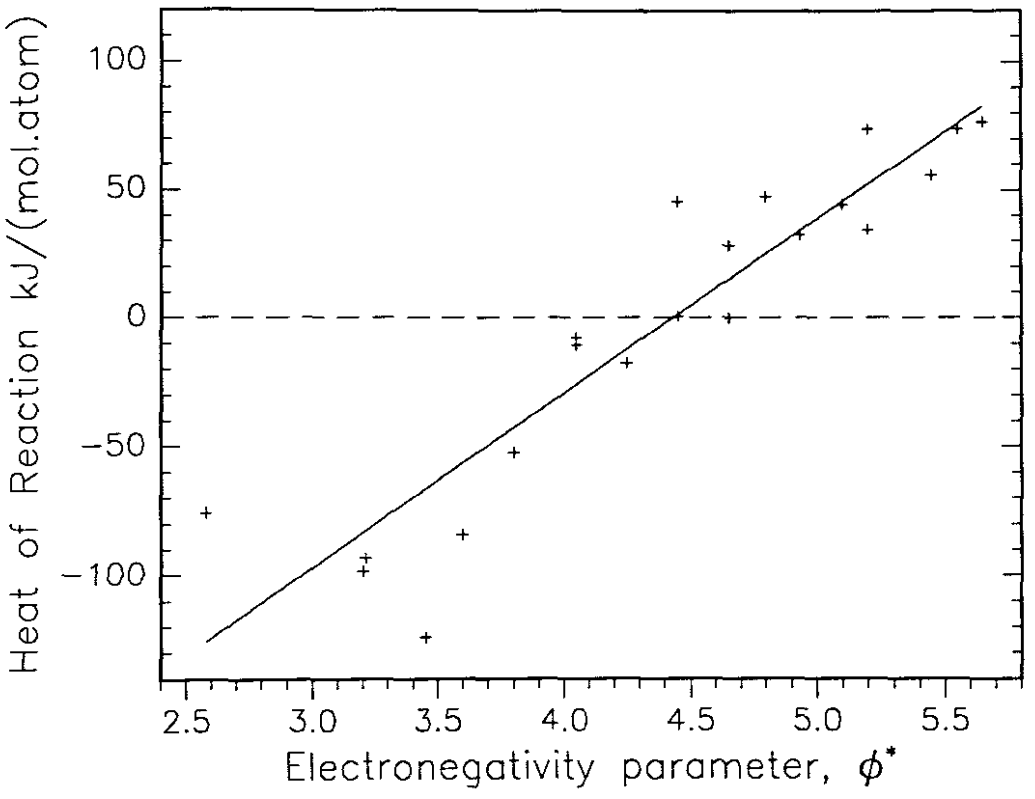

FIGURE 6.6: Values of ϕ^* as defined in the Miedema model [5] have been plotted against the minimum value of the Heat of Reaction in kJ/(mol.atom) and the best fit through the points obtained by means of the straight line passing through them. The straight line intercepts the electronegativity axis at a value of 4.45 V. Metals whose value of ϕ^* is less than 4.45 V will react with SiO_2

cases we found that the metals do not react with SiO_2. Other workers have also done experiments on metals whose value of ϕ^* is greater than 4.45 V. These metals (which were not studied by us) are Mn, Cr, W, Fe, Co, Ni and Pd. They found that these metals do not react with SiO_2.

6.6 Prediction using ternary phase diagrams.

Beyers *et al.*[12] have shown that thermodynamic considerations may be used to draw, at any temperature, a ternary phase diagram capable of predicting thin film reactions of a three element system involving a refractory metal, silicon and oxygen. A short discussion was given in **subsection 1.3.4** for the W-Si-O system. The

expected result of any possible chemical reaction between the refractory and noble metals on one hand and SiO_2 on the other can be described by means of ternary phase diagrams [12]. Since the experiments involve a ternary system and are done at fixed temperature and pressure, there should according to the Gibbs phase rule only be a maximum of three phases in equilibrium in any part of the phase diagram. The phase diagrams that follow are based on the method first conceived by R. Beyers, which is described in chapter 1. In these diagrams the solid tie lines connecting any phases mean that those phases can co-exist in equilibrium, without any chemical reaction between each other i.e. they are chemically stable when put into contact with each other.

Zr-SiO_2

Fig. 6.7 is a ternary phase diagram for the Zr-Si-O system. The figure is adapted from S. Q. Wang [15]. The solid line between the phases ZrO_2 and Zr_5Si_4 was established experimentally by S. Q. Wang and J. W. Mayer, whereas the broken tie lines are inferred from thermodynamic calculations and are based on the work of Beyers, Sinclair and Thomas [13].

Our own experimental investigation confirms the work of S. Q. Wang *et al.* [15] that the compound phases resulting from an interaction between SiO_2 and Zr are Zr_5Si_4 and ZrO_2. This means that the oxide ZrO_2 is stable when in contact with the compound phase Zr_5Si_4 in equilibrium up to 900°C. Put differently Zr will react with SiO_2 to produce ZrO_2 and Zr_5Si_4 at suitable temperatures.

The Zr-Si-O stability phase diagram (see **Fig. 6.7**) belongs to the "metal oxide dominant"category since all the tie lines radiate from the metal oxide viz ZrO_2.
In his Ph.D thesis, Beyers [29] has noted that when a co-sputtered $ZrSi_2$ film containing excess silicon is oxidized at 900°C, the metal oxide ZrO_2 was identified (using TEM) as the product and not SiO_2. Thus, the reaction is given by

$$ZrSi_2 + O_2 \longrightarrow ZrO_2 + 2Si$$

This is a consequence of the ZrO_2-Si tie line in the phase diagram. If the reaction

were given by

$$ZrSi_2 + O_2 \longrightarrow SiO_2 + Zr,$$

then a tie line would occur between SiO_2 and Zr, thereby cutting the existing tie lines between ZrO_2 and the metal silicides, resulting in a violation of the Gibb's phase rule.[12]

Mo-SiO_2

Fig. 6.8 is a ternary stability phase diagram involving the elements Si, O

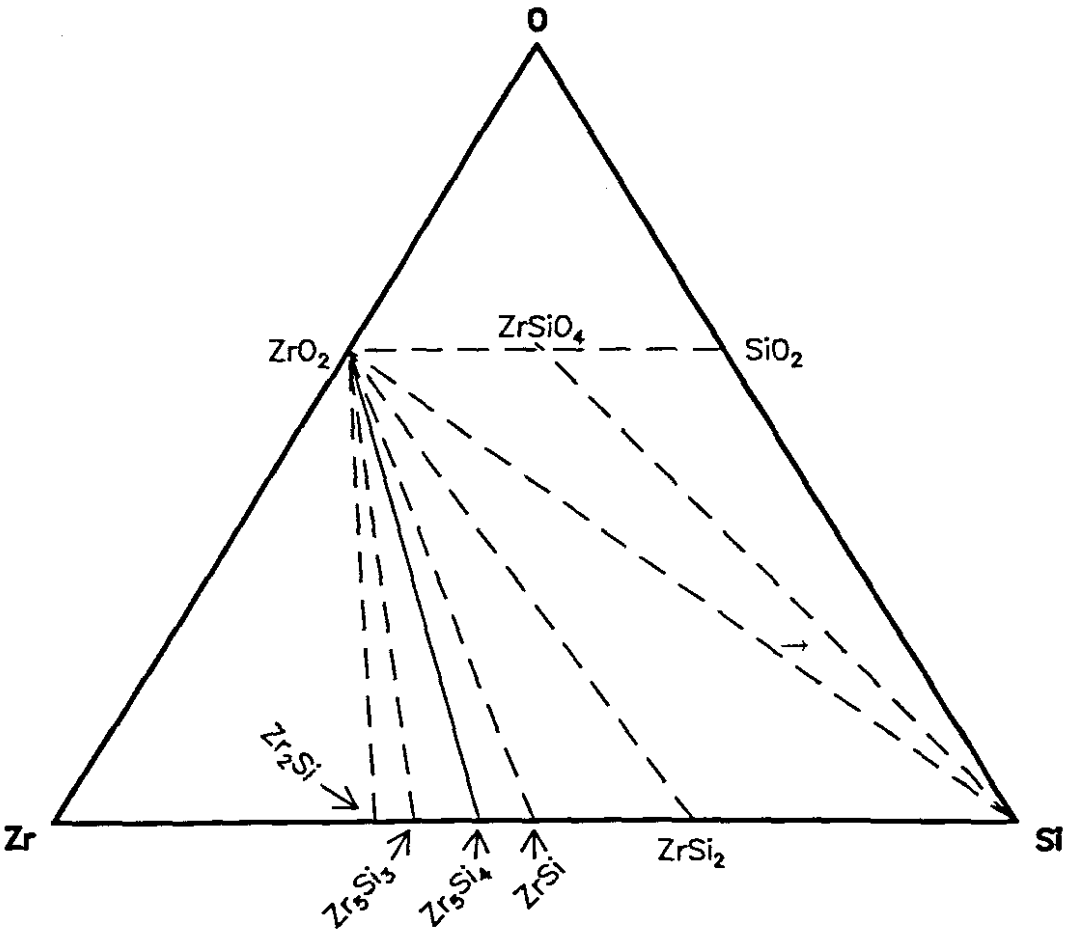

FIGURE 6.7: Ternary stability phase diagram for the elements zirconium, silicon and oxygen. The solid tie line (or tie line) within the triangle shows that ZrO_2 is stable in contact with Zr_5Si_3. The broken lines (also suggesting stability) have been inferred from thermodynamic calculations. Adapted from Wang [15].

and Mo. A tie line exists between Mo and SiO_2 indicating that SiO_2 is stable in contact with Mo. In the experimental investigation, stability was confirmed up to a temperature of 900°C (see **Fig. 3.3**). From thermodynamics, the tie line can be established by calculating the heat of reaction corresponding to the point where two possible tie lines would cross (see **Table 6.5**). Since the values of heats of reaction are negative, the reactions as written will tend to proceed to the right, thereby confirming that SiO_2 is stable in contact with Mo. Similarly, SiO_2 is stable in contact with the silicides of molybdenum viz Mo_3Si, Mo_5Si_3 and $MoSi_2$ as well as with the oxides of molybdenum viz MoO_2 and MoO_3.

Cu-SiO_2

A ternary phase diagram for the Si-O-Cu sysytem is shown in **Fig. 6.9**. SiO_2 is stable in contact with Cu as indicated by the tie line between Cu and SiO_2. In the experimental investigation, the stability of SiO_2 in contact with Cu was confirmed up to a temperature of 800°C. Above this temperature, the copper film was lost as can be seen in the RBS spectrum (see **Fig 5.1**). From thermodynamics, the tie line can be established by calculating the heat of reaction corresponding to the point where two possible tie lines would cross (see **Table 6.6**). The negative values of the heats of reaction are an indication that the reactions will tend to proceed to the right as written, thereby confirming that SiO_2 is stable in contact with Cu. Similarly, SiO_2 should be stable when in contact with the silicides of copper viz. $Cu_{55}Si_{11}$, Cu_4Si and $Cu_{19}Si_6$ and with the oxides of copper viz CuO and Cu_2O. These tie lines are

TABLE 6.5: Heat of reaction calculations to show the presence of a tie line between Mo and SiO_2

Tie line reactions	ΔH_R kJ/(mol.at)
$3Si + 2MoO_3 \rightarrow 2Mo + 3SiO_2$	-110.9
$Si + MoO_2 \rightarrow Mo + SiO_2$	-78.7

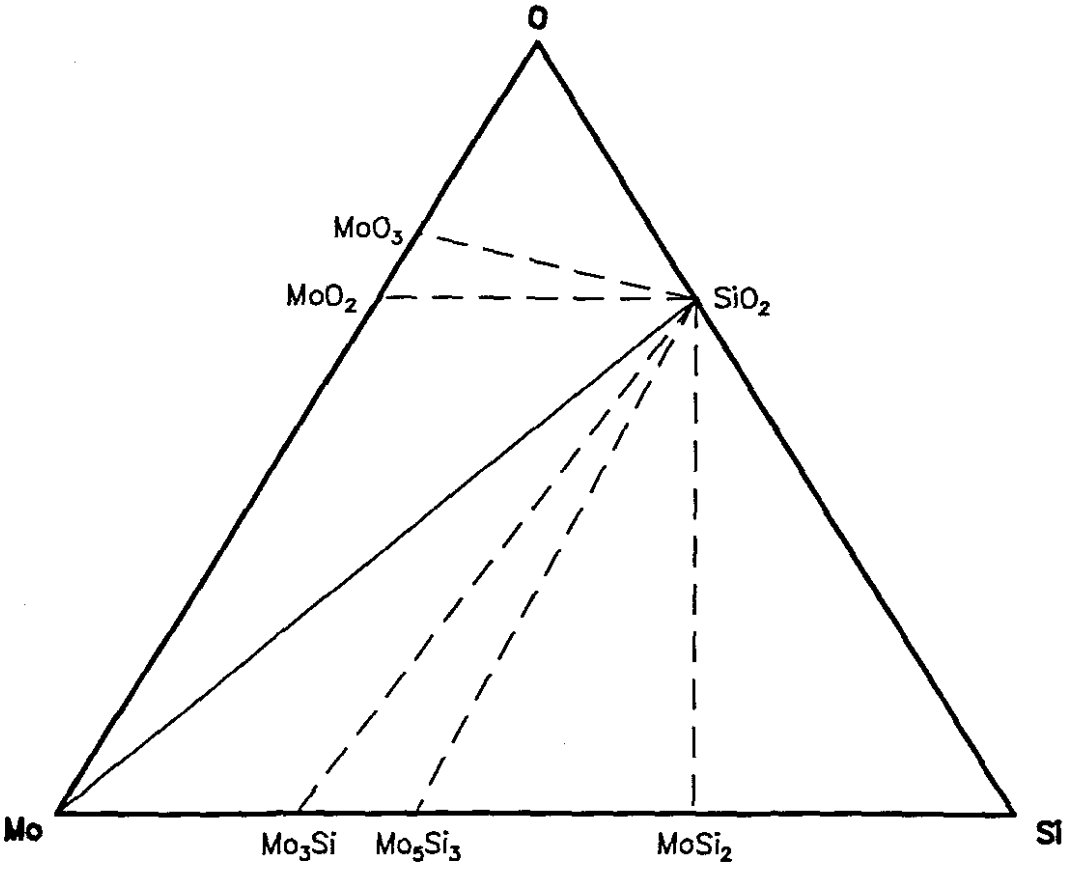

FIGURE 6.8: Ternary stability phase diagram for the elements molybdenum, silicon and oxygen. The solid line (or tie line) between the molybdenum (Mo) and SiO_2 is based on experimental investigations. The broken lines (also suggesting stability) are inferred from thermodynamic calculations. Adapted from Beyers [12].

TABLE 6.6: Heat of reaction calculations to show the presence of a tie line between Cu and SiO_2

Tie line reactions	ΔH_R kJ/(mol.at)
$Si + 2\,CuO \longrightarrow 2\,Cu + SiO_2$	-117.8
$Si + 2Cu_2O \longrightarrow 4Cu + SiO_2$	-80.9

shown by means of dotted lines because they are inferred.

Pt-SiO_2

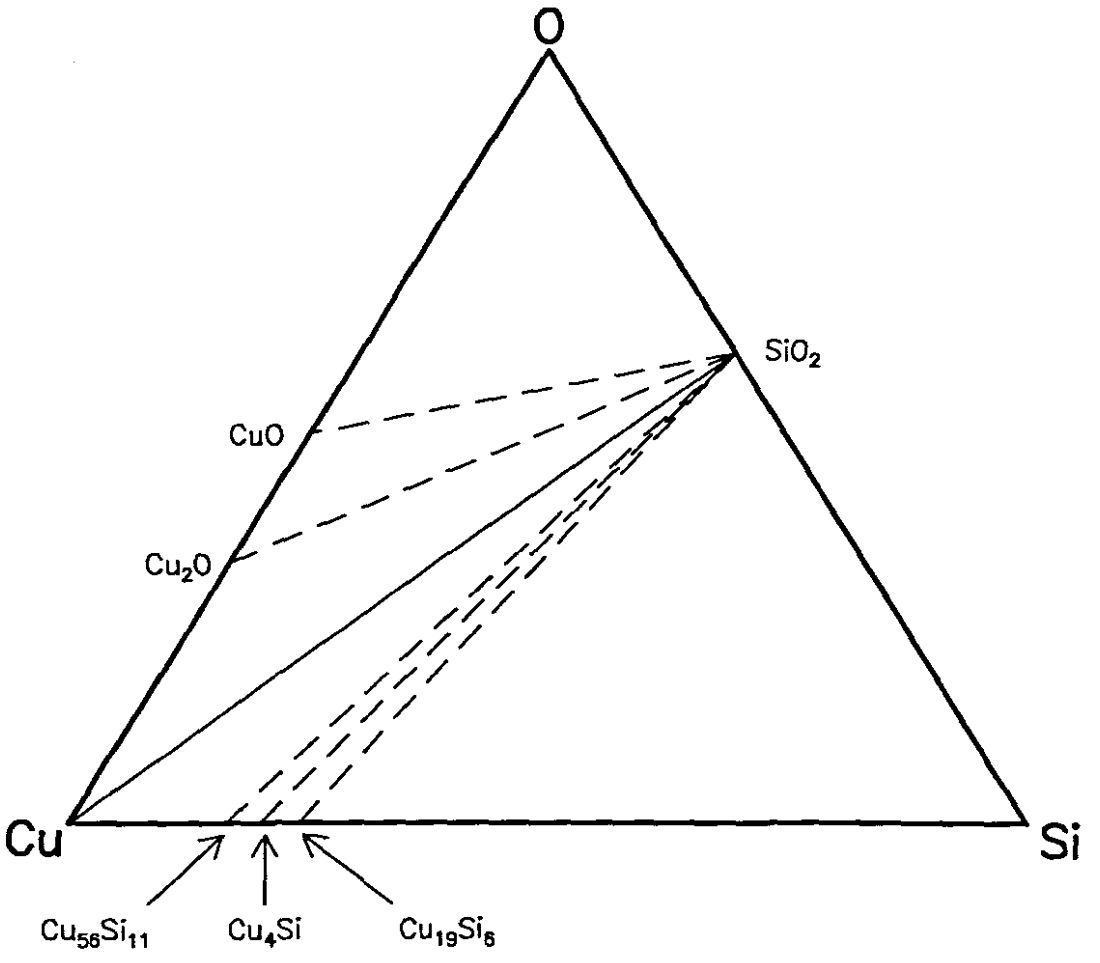

FIGURE 6.9: Ternary stability phase diagram for the elements copper, silicon and oxygen. The solid line (or tie line) within the triangle shows that copper is stable in contact with SiO_2. The broken lines (also suggesting stability) have been inferred from thermodynamic calculations.

TABLE 6.7: Heat of reaction calculations to show the presence of a tie line between Pt and SiO_2

Tie line reactions	ΔH_R kJ/(mol.at)
$Si + PtO_2 \longrightarrow Pt + SiO_2$	-192.3
$2Si + Pt_3O_4 \longrightarrow 3Pt + 2SiO_2$	-182.7
$Si + 2PtO \longrightarrow 2Pt + SiO_2$	-152.24

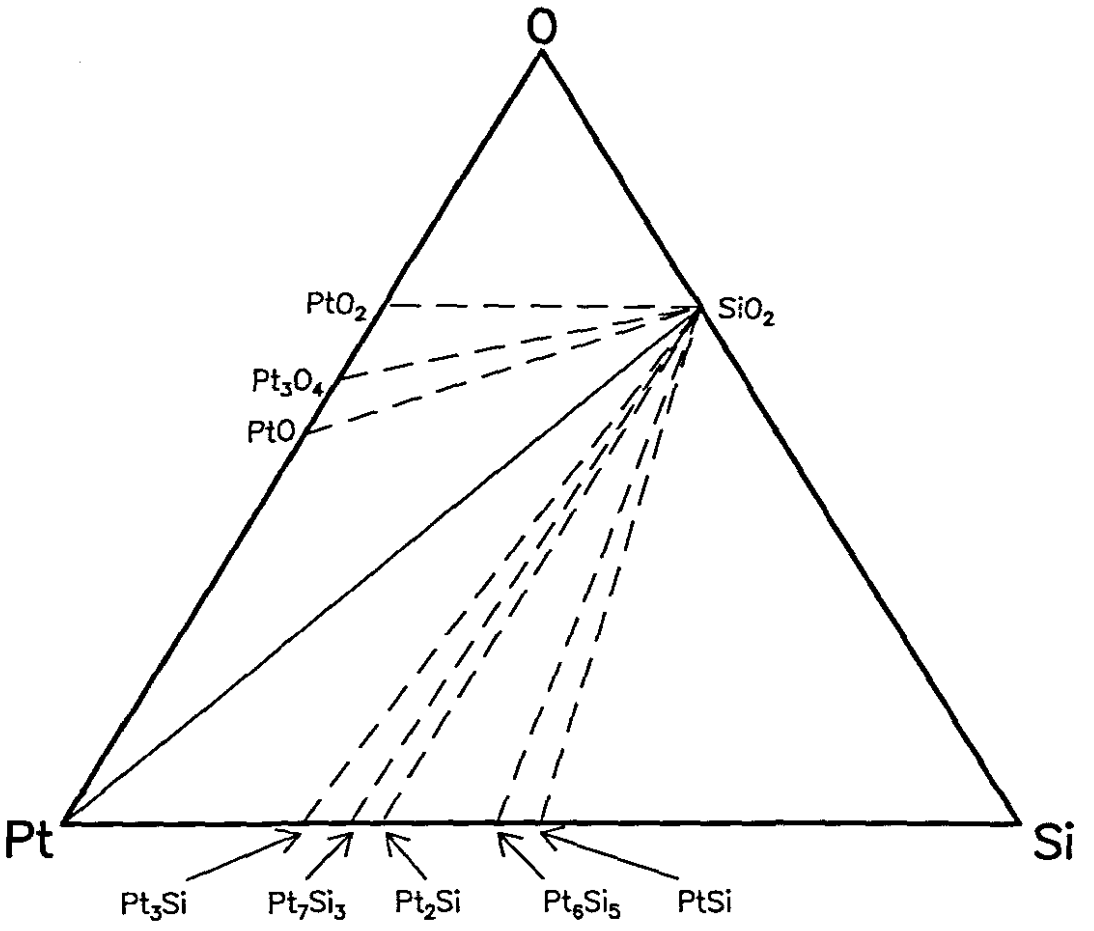

FIGURE 6.10: Ternary stability phase diagram for the elements platinum, silicon and oxygen. The solid line (or tie line) within the triangle shows that platinum is stable in contact with SiO_2. The broken lines (also suggesting stability) have been inferred from thermodynamic calculations.

A ternary stability phase diagram involving the elements Si, O and Pt is shown in **Fig. 6.10**. The tie line between Pt and SiO_2 indicates that SiO_2 is stable in contact with Pt. In the experimental investigation, stability of SiO_2 in contact with Pt was confirmed up to a temperature of 900°C (see **Fig. 5.2**). From thermodynamics, the tie line can be established by calculating the heat of reaction corresponding to the point where two possible tie lines would cross.

Table 6.7 gives the values of heats of reaction for reactions between Si and the oxides of platinum. Since the values of heats of reaction are negative, the reactions

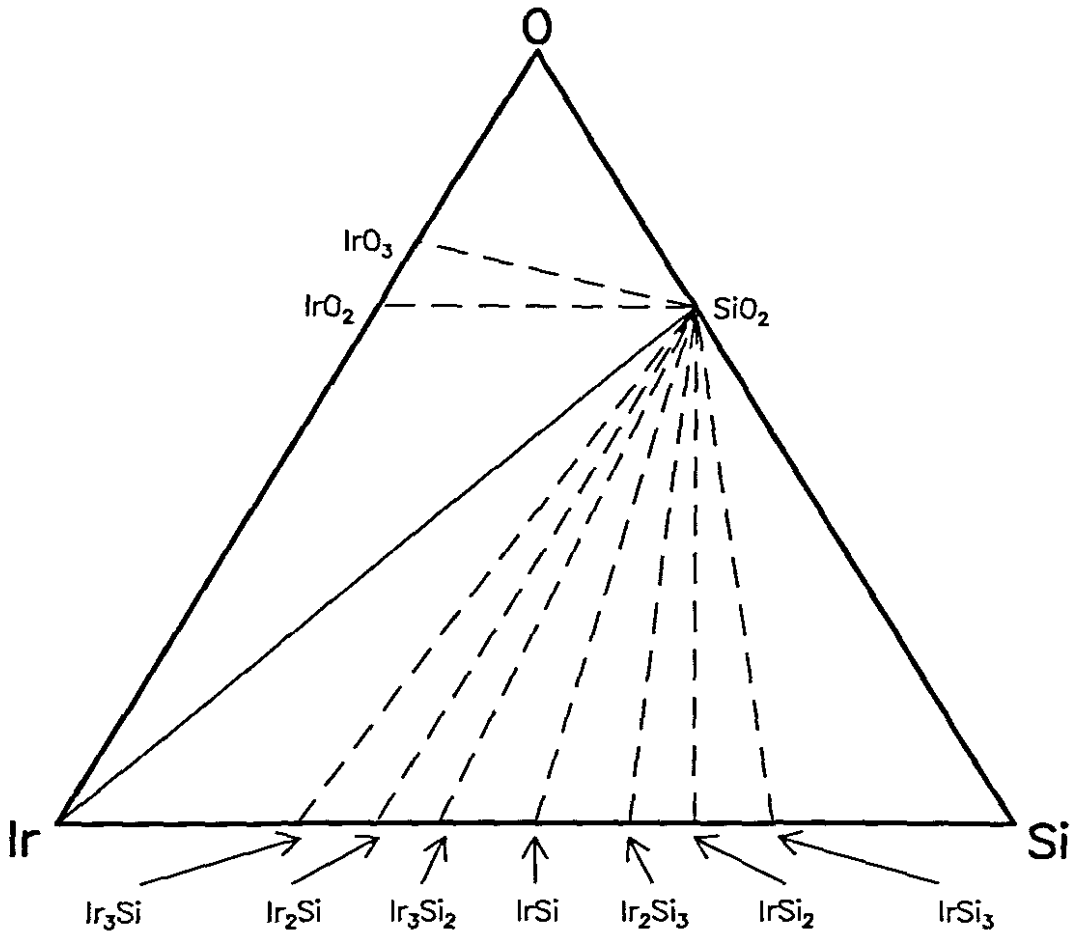

FIGURE 6.11: Ternary stability phase diagram for the elements iridium, silicon and oxygen. The solid line (or tie line) within the triangle shows that iridium is stable in contact with SiO_2. The broken lines (also suggesting stability) have been inferred from thermodynamic calculations.

will tend to proceed to the right as written, thereby confirming that SiO_2 is stable in contact with Pt. In the experimental investigation, stability of SiO_2 in contact with Pt was confirmed up to a temperature of 900°C (see **Fig. 5.2**).

Similarly, SiO_2 is stable in contact with the silicides of platinum viz Pt_3Si, Pt_7Si_3, Pt_2Si, Pt_6Si_5 and PtSi as well as with the oxides of platinum viz PtO_2, Pt_3O_4 and PtO as indicated by the inferred tie lines.

Ir-SiO_2

TABLE 6.8: Heat of reaction calculations to show the presence of a tie line between Ir and SiO_2

Tie line reactions	ΔH_R kJ/(mol.at)
$3\,Si + 2IrO_3 \longrightarrow 2\,Ir + 3SiO_2$	-247.9
$Si + IrO_2 \longrightarrow Ir + SiO_2$	-157.4

Fig. 6.11 shows a ternary stability phase diagram involving the elements Si, O and Ir. A tie line exists between Ir and SiO_2 indicating that SiO_2 is stable in contact with Ir. In the experimental investigation, stability of SiO_2 in contact with Ir was confirmed up to a temperature of 900°C (see **Fig. 5.3**). A calculation of the heat of reaction corresponding to the point where two possible tie lines would cross is used to establish the actual tie line (see **Table 6.8**). The values of the heats of reaction are negative for both reactions. The reaction will therefore proceed in the specified direction, indicating that SiO_2 is stable in contact with Ir.

Similarly, SiO_2 is stable in contact with the silicides of iridium viz Ir_3Si, Ir_2Si, Ir_3Si_2, IrSi, Ir_2Si_3, $IrSi_2$ and $IrSi_3$ as well as with the oxides of iridium viz IrO_2 and IrO_3.

Re-SiO_2

A ternary stability phase diagram involving the elements Si, O and Re is shown in **Fig. 6.12**. A tie line exists between Re and SiO_2 indicating that SiO_2 is stable in

TABLE 6.9: Heat of reaction calculations to show the presence of a tie line between Re and SiO_2

Tie line reactions	ΔH_R kJ/(mol.at)
$4\,Si + Re_2O_8 \longrightarrow 2\,Re + 4\,SiO_2$	-166.1
$7\,Si + 2\,Re_2O_7 \longrightarrow 4\,Re + 7\,SiO_2$	-153.1
$3\,Si + 2\,ReO_3 \longrightarrow 2\,Re + 3\,SiO_2$	-136.5
$Si + ReO_2 \longrightarrow Re + SiO_2$	-117.8

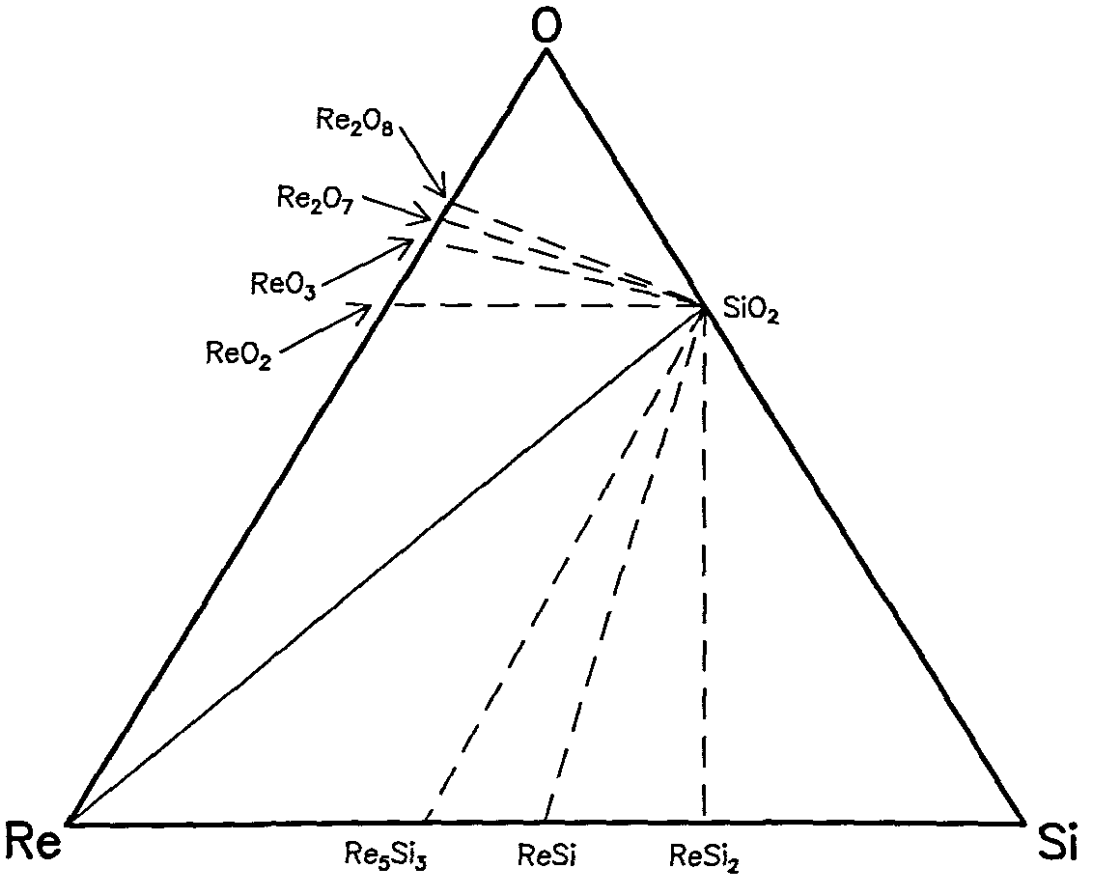

FIGURE 6.12: Ternary stability phase diagram for the elements rhenium, silicon and oxygen. The solid line (or tie line) within the triangle shows that rhenium is stable in contact with SiO_2. The broken lines (also suggesting stability) have been inferred from thermodynamic calculations.

contact with Re. In the experimental investigation, stability of SiO_2 in contact with Re was confirmed up to a temperature of 900°C (see **Fig. 5.4**). Thermodynamics allows us to establish the tie lines by calculating the heat of reaction corresponding to the point where two possible tie lines would cross.

The heats of reaction of each of the reactions where Si reacts with an oxide of Re to give SiO_2 and Re are negative indicating that these reactions will proceed in the given direction (see **Table 6.9**). We therefore conclude that SiO_2 is stable in contact with Re i.e. thermodynamics would not favour the reverse reaction. Since the values of heats of reaction are negative, the reactions as written will tend to proceed to the right, thereby confirming that SiO_2 is stable in contact with Re.

Similarly, SiO_2 is stable in contact with the silicides of rhenium viz Re_5Si_3, ReSi and $ReSi_2$ as well as with the oxides of rhenium viz ReO_2, ReO_3, Re_2O_7 and Re_2O_8 as can be seen from the inferred tie lines in **Fig. 6.12**.

6.7 Summary and conclusion.

Much work has been performed on silicon dioxide/metal systems. Systems most studied are the SiO_2/refractory metal and the SiO_2/noble metal systems. Lately some work has been done on SiO_2/rare earth metal systems. In the case of refractory metals, there may or may not be a reaction between the SiO_2 and the refractory metal. Some of the cases studied here and by other workers have been found not to react for temperatures of up to 900°C when annealed in vacuum for up to three hours. In cases where a reaction takes place in a refractory metal/SiO_2 system, an easily recognisable structure is formed. It has the form SiO_2/metal silicide/metal oxide for cases where SiO_2 is much thicker than the metal (thus leaving some unreacted SiO_2). All noble metals studied in this investigation and by other workers were found not to react when annealed for three hours at temperatures of up to 900°C. Both rare earth metals studied (Y and Yb) were found to react with SiO_2. Reactions between rare earth metals and SiO_2 can happen at low temperatures e.g. 320°C in the case of Yb, as shown in **Fig. 4.1**. This is in contrast to refractory metal/SiO_2 systems where reactions only tend to start above 500°C. The resulting structure after a reaction

in rare earth metal/SiO_2 systems is RSi_xO_y, where R stands for a rare earth metal. A ternary mixture whose composition varies throughout the reacted region is found i.e. x and y are not constants.

Thermodynamic data has been shown to be useful in predicting whether a reaction in a metal/SiO_2 system wil take place or not. In this study it has been found that predictions based on heats of reaction and average electronegativities worked very well. In cases where calculated heats of reaction were negative, a reaction took place in those systems studied. The reaction products identified corresponded to those cases with a negative heat of reaction. Metals with an average electronegativity (based on the Allred-Rochow, Pauling and relative compactness electronegativities) of less than 1.45 on the Pauling scale were found to react, with the exception of W (see **Table 6.3**). The electronegativity parameter ϕ^* as defined in the Miedema model can also be used to predict whether a reaction will take place or not. Metals with ϕ^* of less than 4.45 were found to react (see **Table 6.4**). It was found that ϕ^* is a better parameter than average electronegativity in predicting whether a reaction in the solid state will take place or not.

Beyers *et al.* showed that ternary phase diagrams can be used as an aid in predicting results of thin-film reactions [**13**]. We have, in cases where these ternary phase diagrams have been drawn, correlated them with our own experimental results and have found good agreement. In cases where the diagrams do not exist, we have developed them and correlated calculated ternary diagrams to experimental results. Good agreement between predictions of ternary phase diagrams and experimental results was also found in all cases studied.

CHAPTER 7

SUMMARY AND CONCLUSION.

7.1 Introduction.

The fabrication of microstructures on silicon with SiO_2 used as an insulating layer results in various metals coming into contact with SiO_2. This presents both opportunities and challenges for the manufacturer of microelectronic devices. This is the case not only for the traditional microelectronic device (e.g. integrated circuit) but for new devices incorporating new structures like quantum dots. In a quantum dot a metal cluster is imbedded in an insulating or semiconducting layer (e.g. Ag clusters in SiO_2).

The knowledge gained from studying the reaction of SiO_2 in contact with metals advances not only the general scientific knowledge for this particular combination but may also be used to infer the expected behaviour and method of analysing other combinations e.g. metals embedded in other insulators - Au clusters embedded in MgO.

This work adresses the issue of a chemical reaction between SiO_2 and metals. An attempt has been made to identify the resulting reaction products i.e. the compound phases. The identification methods used were Rutherford Backscattering Spectromery (RBS) and X-Ray Diffraction Spectrometry (XRD). A summary of compound phases identified is given in the next section.

A theoretical explanation of results found, based on existing methods has also been attempted. The EHF model which could have been used to predict resulting compound phases could not be used because of a lack of ternary phase diagrams [6]. An easier approach was therefore attempted, the one of predicting whether a chemical reaction would take place or not. Phrased differently it means whether SiO_2 in contact with a particular metal is stable or not. Two methods were used to make a prediction on whether a reaction was possible. We used heats of reaction, average electronegativities [3], electronegativities as defined in the Miedema model [5] , as well as the method developed by Beyers [12] which relies on the Gibbs phase rule and changes in G (Gibbs free energy) to draw a ternary phase diagram.

7.2 Summary.

Zr thin films were found to react with SiO_2. The reaction was seen to start at 640°C for samples annealed for 30 minutes. The RBS spectrum of the sample annealed at 690°C for 30 minutes developed a shoulder on the Zr signal which showed the presence of Zr_5Si_4. It also showed a shoulder on the surface of Zr which was midway between the oxides ZrO and ZrO_2. The unannealed sample showed no reaction. The resulting final structure was $SiO_2/Zr_5Si_4/ZrO_2$. The XRD spectrum confirmed the RBS results that no interaction was present in the unannealed sample. It showed that Zr had already crystallized. The XRD spectrum of the sample annealed at 690°C showed the presence of ZrO_2 and ZrO. The presence of Zr_5Si_4 could not be confirmed because of an overlap of the ZrO_2 and Zr_5Si_4 signals on the spectrum. At 720°C the signal corresponding to ZrO had disappeared. This sample could therefore only be containing ZrO_2 (and possibly Zr_5Si_4).

Presented with the same problem of identifying ZrO_2 and Zr_5Si_4 signals on the spectrum, Wang and Mayer [15] overcame it by first obtaining an X-ray spectrum of the $Si< 100 >/SiO_2/Zr$ sample annealed at 750°C. Thereafter they milled the sample using a beam of Ar^+ ions to remove the top layer of ZrO_2. The X-ray diffraction spectrum of the milled sample revealed that some lines were now missing. The remaining lines corresponded to the phase Zr_5Si_4.

The results obtained in the case of Zr could be expected because the electronegativity of Zr is less than 1.45 on the Pauling scale *viz.* 1.21. The heat of reaction between Zr and SiO_2 when the resulting products are ZrO_2 and Zr_5Si_4 is negative. Zr is therefore predicted to react with SiO_2.

According to the ternary phase diagram SiO_2 is not stable when in contact with Zr, i.e. Zr should react with SiO_2. This was found to be the case experimentally. Mo thin films (1500Å) on SiO_2 substrates were annealed at temperatures of up to 900°C over three hours. RBS analysis using 2MeV alpha particles was carried out on the samples. The RBS spectra revealed a perfect overlap, i.e. those of the as deposited and the annealed samples, an indication that no interaction had taken place between the Mo film and the SiO_2. The heats of reaction in all reactions involving SiO_2 and Mo are positive (see **Table 7.1**), an indication that such a reaction is thermodynamically unfavourable. Mo has an average electronegativity of 1.45 (Pauling scale) and would therefore be expected not to react with SiO_2. Metals with an average value of electronegativity of equal to or greater than 1.45 on the Pauling scale, were found in this study not to react. The ternary stability phase diagram involving Mo, Si and O (see **Fig. 6.8**) has a tie line between Mo and SiO_2, an indication that Mo is stable in contact with SiO_2. We conclude therefore that Mo is a refractory metal that does not react with SiO_2 for tempertures of up to 900°C.

The electronegativity parameter ϕ^* as defined in the Miedema semi-empirical model was found to correlate well with heats of reaction. It was found that metals with a value of ϕ^* of less than 4.45 V reacted with SiO_2 whereas those with values of ϕ^* of equal to or more than 4.45 V did not. Zr has a value of ϕ^* equal to 3.45 V and our experiments as well as those of others have shown that it reacts with SiO_2. Mo on the other hand whose value of ϕ^* is 4.65 V does not react with SiO_2.

Refractory metals may or may not react with SiO_2. Those with an average electronegativity equal to or greater than 1.45 on the Pauling scale react whereas those with an electronegativity of more than 1.45 generally do not react. Where there is a reaction, for the case of refractory metals, the silicide formed is found next

to the SiO_2 and the oxide is near the surface. The oxygen which results from the decomposition of the SiO_2 diffuses through the metal silicide and reaches the metal to form a metal oxide. The diffusion has been explained as due to the solubility of oxygen in the metal. The metal atoms next to the SiO_2/metal interface move into the near interface region of the SiO_2 substrate where only the silicon remains after decomposition of the SiO_2 and the subsequent diffusion of the oxygen. With the temperature being sufficiently high, the metal and the silicon react to form a silicide. While the oxidation and silicidation proceed, more oxygen will be released from further decomposition of the SiO_2. The oxygen will diffuse through the intermediate silicide layer into the surface (metal-oxygen) region where formation of the oxide will continue. Metal atoms next to the (metal-oxygen)/silicide interface will on the other hand move across the intermediate silicide layer into the SiO_2 layer and combine with the freed silicon. The oxide and silicide layer will hence continue to grow until all metal is consumed, since the investigations focus on thin metal films which therefore makes the metal to be the limiting reagent as opposed to the substantially thick SiO_2.

The RBS spectra of annealed Si< 100 >/SiO_2/refractory-metal samples in which metal-SiO_2 interaction occured show the oxygen signal to be occupying the surface position. The signal of the metal is seen to grow broader (towards lower energy values) and shorter as the metal is "consumed" in the course of oxidation and silicidation. **Fig. 6.1** summarises the two cases that have been observed in refractory metals.

Thin films of the noble metals Pt, Re, Ir and Cu on SiO_2 substrates were annealed under vacuum at temperatures of up to 900°C for 3 hours. RBS analysis using 2MeV alpha particles was then carried out on the samples. in vacuum. The RBS spectra of the as deposited samples and the annealed samples were found to coincide at all points for all annealing temperatures. This was found to be the case for each noble metal. The conclusion drawn is that no interaction occured between the noble metal thin films and the SiO_2 substrates.

The heats of reaction for the interaction of these metals with SiO_2 were found to positive without exception (see **Table 7.1**). Thus, thermodynamics does not favour

interaction between between noble metals and SiO_2.
The average electronegativity (Pauling scale) of each of these metals is greater than 1.5. This is further confirmation that each of these metals will not interact with SiO_2 [3].

Thin film interaction of each of the rare earth metals Y and Yb with SiO_2 substrates was investigated for cases where the metal film was the surface layer and cases where the metal film was covered with SiO_2. The samples were annealed at temperatures of up to 490°C, for periods ranging between 15 and 90 minutes. RBS analysis using a 2 MeV beam of alpha particles was carried out on the samples. Analysis of the RBS spectra revealed that the rare earth metal signal in cases where the annealed samples had not been covered diminished with time, suggesting that the interaction between the rare earth metal and the SiO_2 may have led to formation of volatile phases. The simulation fit on the RBS spectra of the Si<>/SiO_2/metal/SiO_2 annealed samples suggested the existance of ternary phases. The XRD spectra however revealed the presence of a mixture of metal oxides and metal silicides for the Y, whereas the Yb showed some ternary phases to be also present.

The average electronegativity (Pauling scale) for both Y and Yb is less than 1.45 (see **Table 6.3**), an indication that these metals will interact with SiO_2.
Because of a lack of published thermodynamic data on the heats of formation of all the silicides and oxides of the rare earth metals, ternary phase diagrams for the metals could not be drawn.

The work done in this study is shown in **Table 7.1**. The table shows that for refractory metals there may or may not be a reaction (cases of Zr and Mo). For rare earth metals there is a reaction for the cases studied, Yb and Y. For noble metals no reaction could be detected.

7.3 Conclusion.

Solid state interaction between thin metal films and SiO_2 was carried out by depositing thin films of the refractory metals Zr and Mo, the rare-earth metals Yb

TABLE 7.1: A summary of metal-SiO_2 interactions studied in this investigation.

Metal classification	Metal	observed phases	resulting structure	reaction ?
refractory metals	Zr	Zr_5Si_4 ZrO_2 ZrO	SiO_2/M−silicide/M−oxide	Yes
	Mo	–	SiO_2/Metal	No
rare earth metals	Yb	Yb_5Si_3 Yb_3Si_5 Yb_3O_4 Yb_2O_3	SiO_2/mixture of silicides /SiO_2 and oxides	Yes
	Y	$YO_{1.335}$ $\gamma-Y_2Si_2O_7$ $\alpha-Y_2Si_2O_7$ Y_2SiO_5	SiO_2/ternary mixture/SiO_2	Yes
noble metals	Cu	–	SiO_2/Metal	No
	Pt	–	SiO_2/Metal	No
	Ir	–	SiO_2/Metal	No
	Re	–	SiO_2/Metal	No

and Y as well as the noble metals Cu, Pt, Ir and Re onto SiO_2 substrates thermally grown on Si< 100 > wafers. In the case of Yb and Y, a thin evaporated layer of SiO_2 was deposited on top of the metals in order to minimize oxidation. The thicknesses of the metal films ranged from 600 to 4500Å. Deposition was carried out under high vacuum conditions, better than 10^{-7}kPa. The samples were then annealed in a vacuum tube furnace at pre-set temperatures for specific time intervals. The samples were characterised firstly by Rutherford Backscattering Spectrometry (RBS) to determine whether solid state reaction had occurred, by comparing the RBS spectra of the annealed samples with those of the virgin samples. Thereafter the samples were analyzed by X-Ray Diffraction (XRD) to identify which compound phases had formed. It was found that Zr, Yb and Y reacted with the SiO_2 whereas

none of the other metals reacted at temperatures of up to 900°C maintained for 3 hours. These results and other metal-SiO_2 interaction studies that could be found in the literature were summarized and extensively analyzed. In the case of those refractory metals which reacted with the SiO_2 e.g. Zr, Hf, Nb, Ta, Ti and V it was found that a thin layer of metal silicide formed and that in all cases the metal silicide was found to be sandwiched between the SiO_2 substrate and a top layer of metal oxide.

The following model explains the formation of the above configuration. Atoms of the metal diffuse through the thin metal silicide layer until they reach the SiO_2/metal silicide interface where they interact with the SiO_2 substrate which leads to dissociation of the SiO_2. The released oxygen atoms diffuse through the thin metal silicide layer and form a metal oxide on top of the silicide. The resulting configuration is of the form $SiO_2/MSi_y/MO_x$. It could therefore be concluded that the oxygen diffuses more readily through the metal silicide than the silicon does. If silicon were more rapid in diffusing through the silicide than oxygen, the sample configuration after the reaction would have been $SiO_2/MO_x/MSi_y$ (see **Fig 7.1**).

In the case of the rare earth metals, solid state reaction always occured. RBS results indicated that all three elements M, Si and O were present throughout the reaction region. XRD results indicated that for Yttrium ternary phases were present whereas for Ytterbium a mixture of oxides and silicides were identified.

In this study, an extensive table of standard heats of formation in units of kJ/(mol.at) for various metal silicides and metal oxides was compiled (see **Appendix A**). Using this table, heats of reaction for the interaction of SiO_2 with various metals were calculated and the results summarized (see **Table 6.2**). The values of the heats of reaction were found to be negative in cases where the elements reacted with the SiO_2 substrate and positive where no reaction occurrred. These results proved to be consistent with theoretical thermodynamic considerations.

From the results of this study, a correlation could be established with the values of the average electronegativity of the different metals as a means of establishing whether an interaction between the SiO_2 and the metal would occur or not. Metals

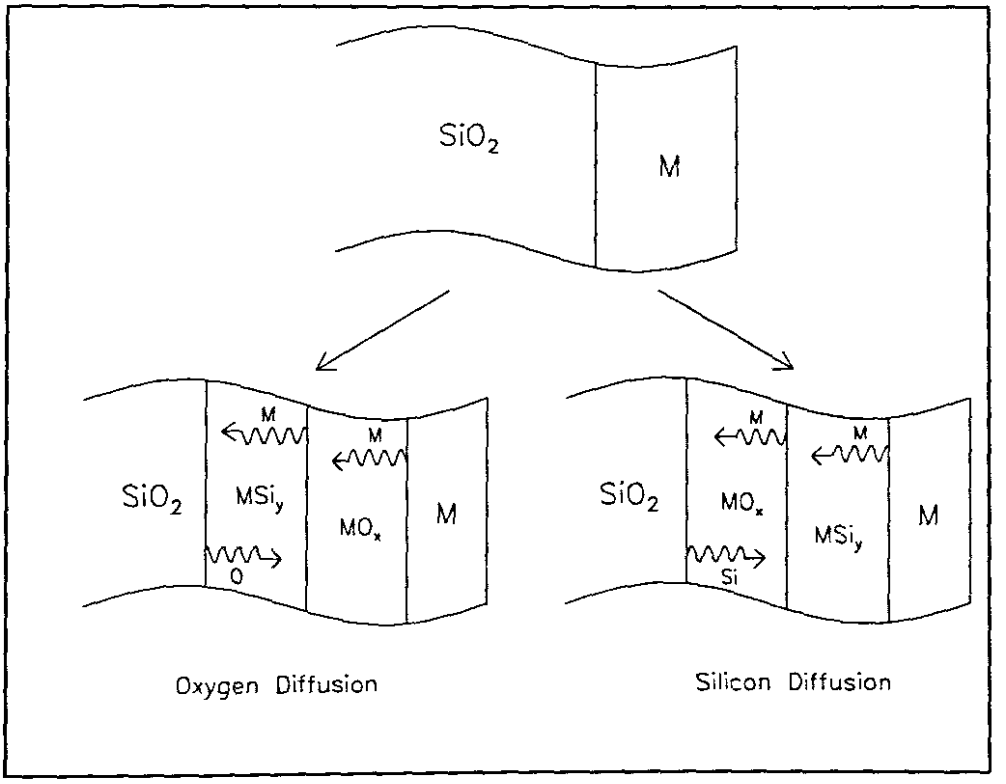

FIGURE 7.1: The two possible configurations of the layers resulting from the solid state reaction of SiO_2 with a thin refractory metal film. Rutherford Backscattering Spectrometry Results (RBS) showed that the metal oxide layer was closer to the sample surface than the metal silicide layer indicating that oxygen diffuses more readily through the metal silicide than silicon through the metal oxide.

with an average electronegativity (average of Allred-Rochow, relative compactness and Pauling electronegativities) of less than 1.45 on the Pauling scale were found to react with SiO_2 (see **Table 6.3**). An even better correlation was obtained using the Miedema electronegativity parameter (ϕ^*). Metals with (ϕ^*) values less than 4.45V were found to react with SiO_2 while those with values equal to or greater than 4.45V did not (see **Table 6.4**).

It has also been shown that ternary phase diagrams can be used to predict solid state interaction between metal films and SiO_2. Consider the following reaction (unbalanced) between a metal film M and SiO_2 to form a metal silicide MSi_y and a metal oxide MO_x i.e.

$$M + SiO_2 \longrightarrow MSi_y + MO_x$$

. If the free energy change of the reaction, ΔG of the reaction is negative, then the products are stable with respect to the reactants and a tie line can be drawn between MO_x and MSi_y. We can construct a ternary phase diagram as shown in **Fig 7.2**. Only one of the possible tie lines has been shown. If however the free energy change of the reaction is positive, then the reactants are stable with respect to the products and a tie line would thus exist between M and SiO_2. Construction of phase diagrams must comply with the Gibbs phase rule which states that *there is a maximum number of three phases in mutual equilibrium for an arbitrary composition.* Regions of three phase equilibrium form triangles (tie triangles) the corners of which identify the chemically compatible phases, i.e. phases which are thermodynamically stable in contact with each other. The tie lines connect two phases which are in equilibrium with each other. Two tie lines can therefore not cross since the point of intersection of the two tie lines would imply the coexistance of four phases in mutual equilibrium, contrary to Gibbs phase rule.

Based on the results of our experimental investigations and on the Gibb's phase rule, phase diagrams for the refractory elements Mo and Zr, the noble elements Pt, Re and Ir as well as the near noble element Cu interacting with SiO_2 were constructed. In each case (except for Zr), a tie line was drawn from the metal to the SiO_2 indicating stability of each of these metals in contact with SiO_2 for

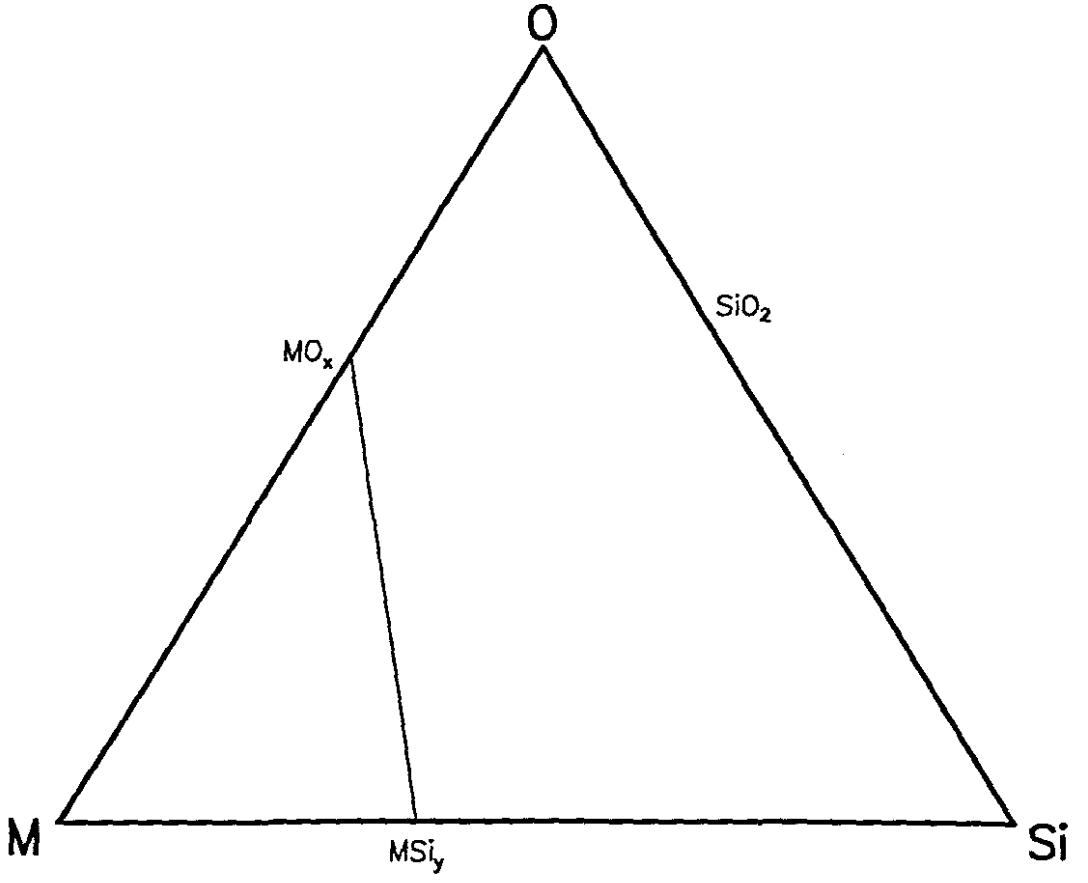

FIGURE 7.2: A ternary phase diagram illustrating a metal (M)–SiO_2 type interaction yielding a metal oxide (MO_x) and a metal silicide (MSi_y). The presence of a tie line between MO_x and MSi_y indicates that the two are stable in contact with each another while the lack of a tie line between M and SiO_2 suggests that the latter pair is unstable when in contact. This is in agreement with Gibb's phase rule which forbids the crossing of tie lines.

temperatures of up to 900°C, with the remainder of the tie lines inferred. Our phase diagram for Mo was comparable with that of R. Beyers [**12**]. Our phase diagram for Zr confirmed the existence of a tie line between Zr_5Si_4 and ZrO_2 as in that of S.Q. Wang and J.W. Mayer [15].

APPENDIX A

Standard heats of formation of metal silicides and oxides

Element	Silicides	ΔH_f° kJ/(mol.at)	Ref	Oxides	ΔH_f° kJ/(mol.at)	Ref
Ca	Ca_2Si	−69.7	[30]	CaO	−317.1	[30]
	CaSi	−75.3	[30]	CaO_2	−219.7	[30]
	$CaSi_2$	−50.2	[30]			
	Ce_5Si_4	−68.7	[31]			
	CeSi	−74.1	[31]			
	Ce_3Si_5	−74.9	[31]			
	$CeSi_2$	−70.4	[31]			
Co	Co_2Si	−38.5	[3,32]	CoO	−119.5	[30]
	CoSi	−50.2	[3,32]	Co_3O_4	−129.3	[30]
	$CoSi_2$	−34.3	[32]			
Cr	Cr_3Si	−34.4	[32]	Cr_3O_4	−218.8	[33]
	Cr_5Si_3	−35.0	[32]	Cr_2O_3	−225.9	[30]
	CrSi	−30.2	[32]	CrO_2	−194.1	[30]
	$CrSi_2$	−25.8	[32]	CrO_3	−144.9	[30]
Cu	$Cu_{56}Si_{11}$	−2.8	[31]	Cu_2O	−55.8	[30]
	Cu_4Si	−3.4	[31]	CuO	−77.6	[30]
	$Cu_{19}Si_6$	−4.0	[31]			
Dy	Dy_5Si_3	−62.2	[31]	Dy_2O_3	−372.6	[30]
	Dy_5Si_4	−77.8	[31]			

Cont...

Element	Silicides	ΔH_f° kJ/(mol.at)	Ref	Oxides	ΔH_f° kJ/(mol.at)	Ref
Dy	DySi	−76.0	[31]	Dy_2O_3	−372.6	[30]
	Dy_2Si_3	−76.5	[31]			
	Dy_3Si_5	−74.6	[31]			
	$DySi_2$	−69.4	[31]			
Er	Er_5Si_3	−63.0	[31]	Er_2O_3	−379.6	[33]
	ErSi	−76.6	[31]			
	Er_3Si_5	−74.5	[31]			
Fe	Fe_3Si	−25.8	[32]	FeO	−135.6	[30]
	FeSi	−39.3	[32]	Fe_3O_4	−159.5	[30]
	$FeSi_2$	−30.6	[32]	Fe_2O_3	−164.3	[30]
Gd	Gd_5Si_3	−61.4	[31]	Gd_2O_3	−363.2	[30]
	Gd_5Si_4	−71.1	[31]			
	GdSi	−75.5	[31]			
	Gd_2Si_3	−76.6	[31]			
	$GdSi_2$	−69.8	[31]			
Hf	Hf_3Si	−53.0	[31]	HfO_2	−371.0	[30]
	Hf_2Si	−69.8	[31]			
	Hf_5Si_3	−77.2	[31]			
	Hf_3Si_2	−81.0	[31]			
	Hf_5Si_4	−86.3	[31]			
	HfSi	−90.1	[31]			
	$HfSi_2$	−75.1	[31]			
Ho	Ho_5Si_3	−61.4	[31]	Ho_2O_3	−376.2	[30]
	Ho_5Si_4	−70.1	[31]			
	HoSi	−74.9	[31]			
	$HoSi_2$	−68.0	[31]			
Ir	Ir_3Si	−28.1	[31]	IrO_2	−64.0	[3]
	Ir_2Si	−35.9	[31]	IrO_2	−80.5	[30]
	Ir_3Si_2	−40.0	[31]	IrO_2	−91.4	[33]
	IrSi	−40.5	[31]			
	Ir_2Si_3	−33.5	[31]			
	$IrSi_2$	−25.1	[31]			
	$IrSi_3$	−11.6	[31]			
La	LaSi	−62.8	[3]	La_2O_3	−358.7	[30]
	$LaSi_2$	−61.9	[3]			
Lu	Lu_5Si_3	−64.5	[31]	Lu_2O_3	−376.4	[30]
	LuSi	−78.0	[31]			
	Lu_3Si_5	−75.5	[31]			

Cont...

Element	Silicides	ΔH_f° kJ/(mol.at)	Ref	Oxides	ΔH_f° kJ/(mol.at)	Ref
Mg	Mg_2Si	−26.4	[30]	MgO	−300.6	[30]
				MgO_2	−207.5	[3]
Mn	Mn_6Si	−17.9	[31]	MnO	−192.5	[30]
	Mn_9Si_2	−22.9	[31]	Mn_3O_4	−198.1	[30]
	Mn_3Si	−31.1	[31]	Mn_2O_3	−191.4	[30]
	Mn_5Si_2	−34.9	[31]	MnO_2	−173.4	[30]
	Mn_5Si_3	−41.6	[31]	Mn_2O_7	80.9	[30]
	MnSi	−41.5	[31]			
	$Mn_{11}Si_{19}$	−28.7	[31]			
Mo	Mo_3Si	−29.1	[30]	MoO_2	−196.0	[30]
	Mo_5Si_3	−38.8	[30]	MoO_3	−186.3	[30,33]
	$MoSi_2$	−43.9	[30]			
Nb	Nb_5Si_3	−60.7	[32]	NbO	−209.8	[30]
	$NbSi_2$	−46.0	[32]	NbO_2	−265.4	[33]
				Nb_2O_5	−271.4	[30]
Nd	Nd_5Si_3	−60.5	[31]	Nd_2O_3	−361.6	[30,33]
	Nd_5Si_4	−69.6	[31]			
	NdSi	−74.7	[31]			
	Nd_3Si_4	−77.0	[31]			
	Nd_2Si_3	−76.3	[31]			
	Nd_5Si_9	−72.9	[31]			
Ni	Ni_3Si	−37.2	[32]	NiO	−120.3	[30]
	Ni_5Si_2	−42.3	[32]	Ni_2O_3	−97.9	[3,33]
	Ni_2Si	−46.9	[32]			
	Ni_3Si_2	−45.2	[32]			
	NiSi	−42.4	[32]			
	$NiSi_2$	−29.3	[32]			
Os	OsSi	−29.1	[31]	OsO_2	−98.2	[30]
	Os_2Si_3	−22.7	[31]	OsO_3	−47.7	[3]
	$OsSi_3$	−15.5	[31]	OsO_4	−78.7	[30]
Pd	Pd_5Si	−29.2	[34]	PdO	−42.7	[33]
	Pd_9Si_2	−31.3	[34]			
	Pd_3Si	−38.5	[34]			
	Pd_2Si	−43.0	[34]			
	PdSi	−26.2	[34]			
Pr	Pr_5Si_3	−60.5	[31]	Pr_2O_3	−365.1	[30]
	Pr_5Si_4	−69.6	[31]	PrO_2	−324.8	[30]
	PrSi	−74.9	[31]			

Cont...

Element	Silicides	ΔH_f° kJ/(mol.at)	Ref	Oxides	ΔH_f° kJ/(mol.at)	Ref
Pr	Pr_3Si_4	−77.2	[31]	Pr_2O_3	−365.1	[30]
	$PrSi_2$	−70.3	[31]	PrO_2	−324.8	[30]
Pt	Pt_3Si	−36.9	[31]	PtO	−35.6	[3]
	Pt_7Si_3	−43.8	[31]	Pt_3O_4	−23.3	[33]
	Pt_2Si	−47.7	[31]	PtO_2	−44.8	[3]
	Pt_6Si_5	−56.1	[31]			
	PtSi	−56.0	[31]			
Pu	Pu_5Si_3	−64.8	[31]	PuO_2	−352.0	[30]
	Pu_3Si_2	−67.8	[31]			
	PuSi	−73.8	[31]			
	Pu_3Si_5	−65.4	[31]			
	$PuSi_2$	−58.3	[31]			
Re	Re_5Si_3	−19.7	[30]	ReO_2	−144.2	[30]
	ReSi	−26.4	[30]	ReO_3	−152.7	[30]
	$ReSi_2$	−30.1	[30]	Re_2O_7	−138.7	[30]
				Re_2O_8	−128.9	[3]
Rh	Rh_2Si	−39.0	[31]	Rh_2O	−31.8	[3]
	Rh_5Si_3	−42.1	[31]	RhO	−45.2	[3]
	Rh_3Si_2	−43.4	[31]	Rh_2O_3	−76.6	[30]
	RhSi	−43.8	[31]			
	Rh_4Si_5	−40.6	[31]			
	Rh_3Si_4	−39.3	[31]			
Ru	Ru_2Si	−29.7	[31]	RuO_2	−101.5	[30]
	RuSi	−32.4	[31]	RuO_4	−61.0	[33]
	Ru_2Si_3	−25.6	[31]			
Sc	Sc_5Si_3	−69.0	[31]	Sc_2O_3	−381.2	[30]
	ScSi	−77.7	[31]			
	Sc_3Si_5	−72.2	[31]			
Si				SiO_2	−301.2	[33]
Ta	Ta_9Si_2	−27.1	[32]	Ta_2O_5	−292.3	[30]
	Ta_2Si	−40.9	[32]			
	Ta_5Si_3	−41.8	[32]			
	$TaSi_2$	−32.4	[32]			
Tb	Tb_5Si_3	−62.2	[31]	TbO_2	−323.8	[33]
	Tb_5Si_4	−71.3	[31]	Tb_2O_3	−365.5	[30]
	TbSi	−76.2	[31]			
	Tb_3Si_5	−75.2	[31]			
	$TbSi_2$	−69.5	[31]			
Th	Th_3Si_2	−55.9	[30]	ThO	−303.3	[3]
	ThSi	−63.0	[30]	ThO_2	−408.9	[30]

Cont...

Element	Silicides	ΔH_f° kJ/(mol.at)	Ref	Oxides	ΔH_f° kJ/(mol.at)	Ref
Th	Th_3Si_5	−59.7	[30]	ThO	−303.3	[3]
	$ThSi_2$	−56.9	[30]	ThO_2	−408.9	[30]
Ti	Ti_3Si	−53.0	[32]	TiO	−271.3	[30]
	Ti_5Si_3	−72.4	[32]	Ti_2O_3	−304.2	[30, 33]
	Ti_5Si_4	−81.0	[32]	Ti_3O_5	−307.4	[30]
	TiSi	−78.6	[32]	TiO_2	−314.9	[33]
	$TiSi_2$	−57.0	[32]			
Tm	Tm_5Si_3	−62.9	[31]	Tm_2O_3	−377.7	[33]
	TmSi	−76.4	[31]			
	Tm_3Si_5	−74.2	[31]			
U	U_3Si	−23.0	[30]	UO_2	−361.2	[30]
	U_3Si_2	−34.1	[30]	U_4O_9	−34.7	[30]
	USi	−42.3	[30]	U_3O_7	−342.7	[33]
	U_3Si_5	−44.3	[30]	U_3O_8	−324.9	[30]
	USi_2	−43.2	[30]	UO_3	−307.5	[30]
	USi_3	−32.6	[30]			
V	V_3Si	−45.2	[32]	VO	−215.9	[30]
	V_5Si_3	−58.0	[32]	V_2O_3	−243.8	[30]
	VSi_2	−40.2	[32]	V_3O_5	−241.6	[33]
				V_4O_7	−240.0	[33]
				VO_2	−237.8	[30]
				V_2O_5	−221.5	[30]
W	W_5Si_3	−16.9	[30]	WO_2	−196.6	[30]
	WSi_2	−31.0	[30]	W_2O_5	−202.1	[3]
				WO_3	−210.7	[30]
Y	Y_5Si_3	−61.4	[31]	Y_2O_3	−381.1	[30]
	Y_5Si_4	−70.4	[31]			
	YSi	−75.5	[31]			
	Y_3Si_5	−74.9	[31]			
Yb	Yb_5Si_3	−34.2	[31]	Yb_2O_3	−362.9	[30]
	YbSi	−42.3	[31]			
	Yb_3Si_5	−42.1	[31]			
	$YbSi_2$	−38.9	[31]			
Zr	Zr_3Si	−54.4	[3]	ZrO	−365.3	[3]
	Zr_2Si	−69.8	[3]	ZrO_2	−366.9	[30]
	Zr_5Si_3	−72.0	[3]	ZrO_3	−252.1	[33]
	Zr_3Si_2	−77.0	[3]			
	Zr_5Si_4	−77.8	[3]			
	ZrSi	−77.4	[3]			
	$ZrSi_2$	−53.1	[3]			

References

[1] S. P. Muraka, J. Vac. Sci. Technol. **17**, 775 (1980).

[2] C.R.M. Grovenor, *Micro Electronic Materials* (Adam-Hilger, Briston, Philadelphia, 1989).

[3] R. Pretorius, J.M. Harris, and M.-A. Nicolet, Solid State Electron. **21**, 667 (1978).

[4] R. Pretorius, T.K. Marais, and C.C. Theron, Mater. Sci. Eng. R **10**, 1 (1993).

[5] A. R. Miedema F. R. de Boer and A. K. Niessen, *COHESION IN METALS. transitin metal alloys* (Elsevier Science Publishers, The Netherlands).

[6] R. Pretorius, MRS Proc. **25**, 15 (1984).

[7] R.M. Walser and R.W. Bené, Appl. Phys. Lett. **28**, 624 (1976).

[8] B.Y. Tsaur, S.S. Lau, J.W. Mayer, and M.-A. Nicolet, Appl. Phys. Lett. **38**, 922 (1981).

[9] T. K. Marais, *Phase Formation Sequence in Metal-Semiconductor and Metal-Metal Binary Thin Film Systems* PhD Thesis. (University of Western Cape), 1993.

[10] U. Gösele and K.N. Tu, J. Appl. Phys. **53**, 3252 (1982).

[11] S.Q. Wang and J.W. Mayer, J. Appl. Phys. **67**, 2932 (1989).

[12] R. Beyers, J. Appl. Phys. **56**, 147 (1984).

[13] R. Sinclair R. Beyers and M. E. Thomas, J. Vac. Sci. Technol. B **2**, 781 (1984).

[14] D. M. Brown W. E. Engeler M. Garfinkel and P. V. Gray, Solid-State Electron **11**, 1105 (1968).

[15] S.Q. Wang and J.W. Mayer, J. Appl. Phys. **64**, 4711 (1988).

[16] S-Q. Wang and J.W. Mayer, Thin Solid Films. **202**, 105 (1991).

[17] J. Osterwalder P. Grönig, T. Greber and L. Schlapbach, Vacuum **41**, 1439 (1990).

[18] R. Hofman and W. A. Henle, Physical Review B **47**, 10407 (1993).

[19] R. E. Hummel J. Y. Kim and R. T. DeHoff, J. Vac. Sci. Technol. A **7**, 1273 (1989).

[20] R. R. Rye and A. J. Ricco, J. Vac. Sci. Technol. A **5**, 2755 (1987).

[21] N. M. Davey andR. J. Seymour, Platinum Metals Rev. **29**, 2 (1985).

[22] H. Kräutle W. K. Chu M. -A. Nicolet J W. Mayer and K N. Tu, in *Proceedings of the International Conference on Applications of Ion Beams to Metals*, edited by E. P. Eernisse S. T. Picraux and F. L. Vook (Plenum, New York).

[23] G. L. P. Berning and H. C. Swart, Surface and Interface Analysis **26**, 420 (1998).

[24] H. Kräutle, M-A. Nicolet, and J.W. Mayer, J. Appl. Phys. **45**, 3304 (1974).

[25] H. Kräutle, M-A. Nicolet, and J.W. Mayer, Phys. Stat. Sol. **20**, 33 (1973).

[26] J.W. Mayer S.W. Russell, J.W. Strane and S.Q. Wang, J. Appl. Phys. **76**, 257 (1994).

[27] S.S. Iyer C.Y. Ting, M. Wittmer and S.B. Brodsky, J Electrochem. Soc. **131**, 2934 (1984).

[28] S.Q. Wang and J.W. Mayer, J. Appl. Phys. **65**, 4774 (1989).

[29] R. Beyers, *PhD Thesis* (Stanford University), U.S.A., 1989.

[30] O. Kubaschewski and C.B. Alcock, *Metallurgical Thermochemistry* (Pergamon Press, Oxford, 1979), p. 268.

[31] A.K. Niessan, F.R. de Boer, R. Boom, P.F. de Châtel, W.C.M. Mattens, and A.R. Miedema, CALPHAD **7**, 51 (1983).

[32] M.E. Schlesinger, Chem. Rev. **90**, 607 (1990).

[33] R.C. Weast, D.R. Lide, M.J. Astle, and W.H. Beyer, *CRC Handbook of Chemistry and Physics* (Chemical Rubber Publishing Company, 1989).

[34] H.C. Baxi and T.B. Massalski, Journal of Phase Equilibria **12**, 349 (1991).